The Operating Features of a Stoichiometric, Ammonia and
Gasoline Dual Fueled Spark Ignition Engine.

by

Shawn Grannell

A dissertation submitted in partial fulfillment
of the requirements for the degree of
Doctor of Philosophy
(Applied Physics)
in The University of Michigan
2008

Doctoral Committee:

    Professor Dionissios N. Assanis, Co-Chair
    Assistant Research Scientist Stani V. Bohac, Co-Chair
    Professor Roy Clarke
    Professor Bradford G. Orr
    Professor Emeritus Marc H. Ross
    Don Gillespie, El Don Engineering

This photo was taken on August 17, 2007 at the south end of the Golden Gate Bridge. This test vehicle was used for a cross country trip from Ann Arbor to San Francisco demonstrating the use of ammonia with gasoline. The vehicle uses nearly 100% gasoline at idle and approximately 70% ammonia/30% gasoline on a lower heating value energy basis at normally aspirated, wide open throttle. During the 3740 kilometers of dual fueled operation the test vehicle consumed 183 liters of gasoline and 295 kilograms of ammonia. The average fuel mix was approximately 50% ammonia/50% gasoline on a lower heating value energy basis.

This vehicle was made substantially operational on ammonia promoted with propane in February 2003 and on ammonia with gasoline in March 2003. From this result it was understood at the start of the dissertation work that a stoichiometric, ammonia and hydrocarbon dual fueled engine would operate acceptably well on ammonia promoted with a relatively small, nearly constant, minimum required hydrocarbon input per cycle.

TABLE OF CONTENTS

LIST OF TABLES

LIST OF FIGURES

x

LIST OF ABBREVIATIONS

Acronyms:

BMEP...................Brake Mean Effective Pressure
BTC......................Before Top Center
COV(IMEP$_n$)........Coefficient of Variation of the Net Indicated Mean Effective Pressure
CFR.....................Cooperative Fuel Research (Engine)
EGR.....................Exhaust Gas Recirculation
FMEP...................Friction Mean Effective Pressure
FTIR....................Fourier Transform Infrared
IMEP$_g$...................Gross Indicated Mean Effective Pressure
IMEP$_n$...................Net Indicated Mean Effective Pressure
KLSA...................Knock Limited Spark Advance
LHV.....................Lower Heating Value
LPG.....................Liquid Petroleum Gas (mostly propane and butane)
MAPP$^®$ gas.........Methylacetylene-Propadiene in LPG mixture
MBT.....................Maximum Brake Torque
MFB$_a$...................Apparent Mass Fraction Burned
NDIR...................Nondispersive Infrared
NO$_x$.......................Nitric Oxide (NO) + Nitrogen Dioxide (NO$_2$)
PMEP...................Pumping Mean Effective Pressure.
PPM.....................Parts Per Million (by volume in a gas)
RPM.....................Revolutions Per Minute
TC........................Top Center: Crank angle = 0° at Top Center
WOT....................Wide Open Throttle (Normally Aspirated)

Other Abbreviations:

Cat........................Catalyst
Cyl.......................Cylinder
Exh.......................Exhaust
Gas.......................Gasoline
kHz.......................kilohertz
T-couple...............Thermocouple
Vol.......................Volume

LIST OF SYMBOLS

Constants:

Q_{LHVg} .... Gasoline Lower Heating Value $\quad$ = 42450 Joules per gram

Q_{LHVa} .... Ammonia Lower Heating Value $\quad$ = 18600 Joules per gram

V_d .... Displaced Volume of the engine $\quad$ = 0.625 Liters

Variables:

b_c .... Gasoline fraction on a chemical equivalence basis $\ 0 \le b_c \le 1$

b_e .... Gasoline fraction on a lower heating value energy basis $\ (\%)\ \ 0\% \le b_e \le 100\%$

f_{rpm} .... Engine crankshaft rotation frequency $\ $ (Revolutions per minute)

γ ....Effective ratio of specific heats evaluated from pressure data $\ $ (Typically $\gamma = 1.3$)

$\dot{m}_g$ ....Gasoline Mass Flow $\ $ (Grams per minute)

$\dot{m}_a$ ....Ammonia Mass Flow $\ $ (Grams per minute)

N ....Ammonia/Gasoline cost ratio, on a lower heating value energy basis

η_b ....Brake thermal efficiency $\ $ (%)

η_{ig} .... Gross indicated thermal efficiency $\ $ (%)

η_{in} .... Net indicated thermal efficiency $\ $ (%)

P .... Cylinder pressure $\ $ (Kilopascals)

Q .... Accumulated apparent heat release $\ $ (Joules)

Q_t .... Total fuel lower heating value energy input per cycle $\ $ (Joules)

r_c ....Compression ratio

τ .... Crankshaft torque $\ $ (Newton×meters)

θ .... Crank angle $\ $ (Degrees) $\ \theta = 0$ at the end of compression, at top center

θ_{spark} ......Crank angle at the spark $\ $ (Degrees)

V .... Cylinder volume $\ $ (Liters)

Other Symbols:

{} .... Function brackets. Shows functional dependence one variable on another. For example, $V\{\theta\}$ show the cylinder volume V as a function of crank angle θ.

d ....The differential operator. For example, dV is a differential change in V.

GLOSSARY

Apparent Mass Fraction Burned: This is the total apparent heat released at a given point, inferred from the cylinder pressure and volume data, divided by the total fuel energy input per cycle.

Bark: A verb referring to how the engine qualitatively behaves when it is run without the benefit of any of the various noise and pollution abatement devices and exhaust pipe, normally positioned downstream of the exhaust manifold and/or turbocharger.

Bottom Center: This is the crankshaft position for which the piston is furthest from the cylinder head, at ±180 degrees crank angle.

Brake Mean Effective Pressure: (kPa) This is the useful crankshaft work obtained per cycle, divided by the displaced volume.

Burn Duration: (degrees) The burn duration is the crank angle width of the burn interval.

Burn Interval: The burn interval is the crank angle region bounded by the 10% and 90% burn angles (degrees) of the 60-cycle average MFB_a curve.

Coefficient of Variation of the Net Indicated Mean Effective Pressure: (%) This is the standard deviation of the $IMEP_n$ divided by the mean $IMEP_n$ for a set of 60 individual cycles. It is a measure of the cycle-to-cycle indicated work yield variation, and it is used to define operation at the rough limit.

Compression Ratio: The ratio of the cylinder volume at bottom center, to that at top center. It is expressed as N:1, for example 12:1. The expression N:1 is used as an abbreviated way to refer specifically to compression ratio. For example, 12:1 compression ratio is sometimes simply called 12:1.

Displaced Volume: (Liters) This is the volume swept by the piston with each stroke.

Dual Fuel(ed): Adjective referring to operating points and data for which ammonia is used with one other fuel. Unless otherwise noted, the other fuel is gasoline.

Exhaust Gas Recirculation: This method involves directing a portion of the engine-out exhaust gas back into the intake, for the purpose of introducing a controlled residual fraction. Exhaust gas recirculation is not used in this study.

Fourier Transform Infrared: The Nicolet FTIR records an interference pattern generated by a translating interferometer whose optical path passes through a cell through which the exhaust sample also passes. The Fourier transform of the interference pattern is used to calculate what parts of the broad infrared spectrum are being absorbed by the exhaust sample, and the concentration of various pollutants.

Friction Mean Effective Pressure: (kPa) This is the portion of the work available per cycle at the piston crown that doesn't show up at the crankshaft, divided by the displaced volume. The formula $FMEP = IMEP_n - BMEP$ is used to find the FMEP. FMEP is a loss term and it is always positive.

Gross Indicated Mean Effective Pressure: (kPa) This is the work available per cycle at the piston crown for the compression-expansion process only, divided by the displaced volume, and it excludes the intake/exhaust pumping loop.

Idle: This the engine load at which the crankshaft torque is zero, at any given engine speed.

Ignition Delay: (degrees) The ignition delay is the crank angle width of the ignition interval.

Ignition Interval: The ignition interval is the crank angle region bounded by the spark (degrees) and the 10% burn angle (degrees) of the 60-cycle average MFB_a curve.

Knock-Free: Knock free operation occurs when the knock signal amplitude remains below 10 kPa, which is the threshold for a knock signal that is sufficiently distinguished from noise.

Knock Limited Spark Advance: For most points of operation on gasoline it was not possible to use MBT spark advance without causing knock. Whenever knock limited spark advance was used, the spark timing was retarded away from MBT just far enough to avoid knock.

Lower Heating Value: (Joules per gram) This is the enthalpy of combustion of a fuel per unit of fuel mass. It is the energy yield obtained from combustion without condensing any of the water formed in the combustion reaction. This term is also used as an adjective to refer to the energy basis by which the total and partial fuel energy inputs per cycle, and fuel input ratios, are calculated.

Maximum Brake Torque (Spark Timing): This refers to the spark timing for which the engine torque and efficiency are maximized. It also refers to an operating condition in which the optimal spark advance can be maintained and is maintained.

Mean Effective Pressure: (kPa) This is a generic terms referring nonspecifically to the gross and net indicated mean effective pressures and brake mean effective pressure. It's another term for load. The mean effective pressures track together, and increase with increasing fuel energy input per cycle.

Net Indicated Mean Effective Pressure: (kPa) This is the work available per cycle at the piston crown for the entire cycle, divided by the displaced volume, and it includes the intake/exhaust pumping loop.

Nondispersive Infrared: The Horiba NDIR looks at the absorbance of an exhaust sample, within a specific infrared range, to calculate the total hydrocarbon count.

Pumping Mean Effective Pressure: (kPa) The formula $PMEP = IMEP_g - IMEP_n$ describes the pumping mean effective pressure. PMEP is a positive quantity for throttled operation, so it is a loss term. Like the FMEP, the PMEP reduces the work yield.

Revolutions Per Minute (RPM): The engine speed. The acronym RPM is used as an abbreviated way to refer specifically to engine speed. For example, 1600 RPM engine speed is sometimes simply called 1600 RPM.

Road Load: This is a set of operating conditions such as mean effective pressures, fuel mix, efficiencies, speed, etc. at which an engine is designed to operate most of the time, and which characterizes the average behavior of the engine.

Smooth Firing: Smooth firing occurs when the $COV(IMEP_n) \leq 3\%$.

Specific Ammonia Input: (Joules per liter) This is the ammonia lower heating value energy input per cycle, divided by the displaced volume. It is calculated from the ammonia mass flow, ammonia lower heating value, engine speed, and displaced volume.

Specific Gasoline Input: (Joules per liter) This is the gasoline lower heating value energy input per cycle, divided by the displaced volume. It is calculated from the gasoline mass flow, gasoline lower heating value, engine speed, and displaced volume.

Top Center: This is the crankshaft position for which the piston is closest to the cylinder head, at zero degrees crank angle.

Total Specific Fuel Input: (Joules per liter) This is the total lower heating value energy input per cycle, divided by the displaced volume. It is calculated from the gasoline and ammonia mass flows and lower heating values, engine speed, and displaced volume. Total specific fuel input = specific gasoline input + specific ammonia input.

Wide Open Throttle (Normally Aspirated): This term refers to loads which correspond to intake pressure = 1 bar. The engine runs as it would if it were allowed to breath freely without any restriction by the throttle and without the application of supercharge pressure.

ABSTRACT

An overall stoichiometric mixture of air, gaseous ammonia and gasoline was metered into a single cylinder, variable compression ratio, supercharged CFR engine at varying ratios of gasoline to ammonia. For each combination of load, speed, and compression ratio there is a range of ratios of gasoline to ammonia for which knock-free, smooth firing was obtained. This range was investigated at its rough limit and also at its MBT knock limit. If too much ammonia is used, then the engine fires with an excessive roughness. If too much gasoline is used, then knock-free combustion can't be obtained while MBT spark timing is maintained. Stoichiometric operation on gasoline alone is also presented, for comparison.

It was found that a significant fraction of the gasoline used in spark ignition engines can be replaced with ammonia. Operation on about 100% gasoline is required at idle. However, a fuel mix comprising 70% ammonia/30% gasoline on a LHV energy basis can be used at WOT. Even greater ammonia to gasoline ratios are permitted for supercharged operation.

The use of ammonia with gasoline allows knock-free operation with MBT spark timing at combinations of load and compression ratio which are inaccessible to gasoline. The thermal efficiencies obtained for operation on ammonia with gasoline are as good, or better, than those obtained with gasoline alone, where comparable. The maximum brake thermal efficiency achieved during operation on ammonia with gasoline was 32.0% at 10:1 compression ratio and BMEP = 1025 kPa. The maximum brake thermal efficiency obtained during operation on gasoline alone was 24.6% at 9:1 compression ratio and BMEP = 570 kPa.

Engine-out and post-catalyst emissions results are also presented. Engine-out emissions of hydrocarbons and carbon monoxide are replaced with emissions of ammonia when ammonia is used. The harmful emissions produced by an ammonia and gasoline fueled engine can be made to clean up with the same catalytic converter already

in use for engines fueled by gasoline alone. The emissions clean-up window is between stoichiometric and 0.2% rich for all ratios of gasoline to ammonia.

CHAPTER 1
INTRODUCTION

1.1 Motivation and Overview

This study investigates the use of anhydrous ammonia as an engine fuel. The principal problem with the use of ammonia as an engine fuel is the slow flame speed of ammonia/air mixtures. Ammonia can also be difficult to ignite, and it has a long ignition delay, a high autoignition temperature and narrow flammability limits. The challenge of ammonia is to make it burn completely at the right time, so that efficient engine operation can be achieved without the emission of large quantities of ammonia in the exhaust. The demonstration of post-catalyst emissions clean-up is also required for ammonia to be considered a practical engine fuel. These challenges have caused ammonia to be overlooked as a solution to the problem of storing the energy obtained from nuclear power and renewable sources, and making it available at reasonable energy/volume and energy/mass densities for use in mobile applications, such as automobiles.

This study is the first to use $COV(IMEP_n)$ and knock detection to define and comprehensively map the fuel mix limits of an engine, fueled by ammonia and a combustion promoter. It is also the first to demonstrate successful post-catalyst emissions clean-up and stoichiometric operation on ammonia and a combustion promoter, using closed loop fuel control. This study describes a means by which ammonia can be used as the principal fuel for an engine. The advantages that can be derived from using ammonia as an engine fuel are also explored.

1.2 Prior Literature

1.2.1 Diesel Engine Operation

Direct liquid injection of ammonia at 35:1 gives marginal performance, even with elevated water jacket and intake air temperatures of 300° F [Gray et al., 1966]. Thus it is likely impractical to operate engines at compression ratios that are high enough to autoignite ammonia by compression alone. A high temperature glow plug and/or an additive, such as dimethyl hydrazine, can be used to make ammonia burn with direct injection at 23:1, but the combustion is sensitive to various temperatures and also the position of the glow plug [Gray et al., 1966].

Fuels whose autoignition temperature is higher than is the maximum compression temperature can be inducted with the intake air, and ignited by a comparatively small pilot injection of diesel fuel, provided that the overall fuel/air equivalence ratio is not too far outside the normal flammable limits of the principal fuel. Methane, methanol, and ethanol begin to burn poorly when used in this manner if the overall fuel/air equivalence ratio drops below 0.4-0.5, and ammonia burns poorly when the overall fuel/air equivalence ratio drops below 0.7 [Bro and Pedersen, 1977]. The use of ammonia in an unthrottled diesel engine is potentially advantageous only when the engine is operating at nearly full load, because the partial ammonia/air equivalence ratio needs to be high enough to ensure flame propagation beyond the diesel spray region.

The pilot injected diesel engine can make efficient use of ammonia over a wider range of loads if the load is controlled by variation of intake pressure by means of throttling and/or turbocharging, such that the partial ammonia/air equivalence ratio is held constant. However, this engine is found to suffer degradation of combustion quality and an increasing ignition delay with decreasing intake pressures at loads corresponding to throttled operation. Misfire occurs at intake pressure ≤ 0.5 bars [Pearsall and Garabedian, 1967].

1.2.2 Spark Ignition Engine Operation

Efforts to improve the combustion of ammonia in diesel engines have produced recommendations for the use of spark ignition, elevated compression ratios, and gaseous ammonia induction with the intake air at a constant equivalence ratio [Pearsall and Garabedian, 1967]. Literature surveys by Mozafari (1988) and Cooper et al. (1991) give similar recommendations.

Liquid phase ammonia induction gives better volumetric efficiency than gaseous ammonia induction because liquid ammonia cools the intake mixture, and liquid ammonia does not displace as much air. However the theoretical efficiency gain for liquid induction is small [Starkman et al., 1966], and the resulting compression temperature reduction and mixture non-uniformity are counterproductive to the task of improving the combustibility of the ammonia [Mozafari, 1988]. Liquid ammonia induction is projected to result in 15% more power than gasoline for normally aspirated operation [Luthra et al., 1971], but the power difference between liquid and gaseous ammonia induction is easily made up with supercharge.

Although the use of high compression ratios and supercharge are known to improve the combustibility of ammonia in spark ignition engines [Cornelius et al., 1965], the engine must also be able to run at light loads, including idle. Something else is also needed, even for engines that include the supercharge regime in their range of operation, because a high compression ratio alone is not enough to make an ammonia fueled engine run smoothly at idle and at light loads.

1.2.3 Use of Combustion Promoters

The combustibility of ammonia can be improved with the use of combustion promoters. Combustion promoters are more reactive fuels which are used with the ammonia to improve the ignitability and flame speed. Hydrogen has been used as a combustion promoter for ammonia. Hydrogen can be obtained by decomposing a small fraction of the ammonia into hydrogen and nitrogen in a catalyst chamber heated by the

engine exhaust gases [Zavka and Massagno, 1938]. This decomposition system is specified to convert, in an uncontrolled way, about 3.4 to 18.2 percent of the ammonia into hydrogen and nitrogen. The use of this catalyst chamber, or cracker, would enable engine operation with ammonia as the only fuel. However, Smith and Starkman (1966), Starkman et al. (1966), and Starkman and Samuelsen (1967) found the decomposition yield from an ammonia cracker can be inadequate and difficult to control, and they also found that hydrogen concentrations corresponding to about 20% decomposition are required at intake pressure = 70-100 kPa. Cornelius et al. (1965), Kroch (1945), and Kroch and Restieau (1945) avoided the cracker problem by metering hydrogen-bearing gas mixtures into the engine separately from the ammonia.

Kroch (1945) describes the use of ammonia promoted with coal gas as a substitute for petroleum fuels during world war two, as wartime conditions made diesel fuel unavailable for Belgian mass transit vehicles during 1942 and 1943. The Belgian vehicles obtained about 40% of their energy from the ammonia and 60% from the coal gas, on average. The ratio of coal gas to ammonia was varied by the operator whose goal was to match the consumption of the fuels with their regional availability, and not necessarily to minimize the use of the coal gas. Kroch and Restieau (1945) specify that the operator manually sets the ratio of ammonia to coal gas consumed by these vehicles, and that, once set, this ratio remains constant for all engine speeds. No provision is described for automatically varying the ratio of ammonia to coal gas with engine load and/or speed.

Detailed work relating to the use of gasoline as a combustion promoter for an ammonia fueled spark ignition engine has not been found in the literature. None of the references describe a comprehensive engine operating map for using ammonia with a combustion promoter at any specific target combustion conditions.

1.2.4 Emissions

The principal exhaust emissions produced when burning ammonia are nitrogen oxides and ammonia. An ammonia-fueled spark ignition engine produces slightly less nitric

oxide under stoichiometric and fuel rich conditions than does a gasoline-fueled engine. An ammonia fueled engine produces more nitric oxide than does its gasoline fueled counterpart under fuel lean conditions [Sawyer et al., 1968].

Nitric oxide emissions from an ammonia fueled engine are found not to vary if the intake manifold pressure of a throttled spark ignition engine is varied between 70 and 100 kPa, and nitric oxide emissions are found to decrease very slightly with increasing spark advance [Graves and Hodgson, 1975]. The in-cylinder concentrations of nitric oxide during the combustion and expansion processes were found to be about 10 times the exhaust concentration, and it is believed that the process by which ammonia is oxidized is largely responsible for the formation of nitric oxide [Sawyer et al., 1968].

Ammonia in the exhaust was observed in many of the studies. As much as 20% of the ammonia escapes in the exhaust when no combustion promoter is used [Mozafari, 1988]. A combustion promoter must be used in order to achieve acceptable combustion efficiency and thus minimize the engine-out emission of ammonia. The successful use of closed loop fuel control for efficiency and total emissions clean up, using oxygen sensors and a standard three-way catalyst, remains to be demonstrated [Shand et al., 1985].

1.3 Research Objectives of Thesis

1.3.1 Gasoline as a Combustion Promoter

In this study, ammonia is used as the principal fuel without decomposing any of it into hydrogen and nitrogen. Gasoline is used as the combustion promoter, and ammonia is used up to the maximum extent practical at each combination of load, speed, and compression ratio. The main goal of this study is to define and map the fuel mix limits for an ammonia and gasoline dual fueled spark ignition engine, within which the engine will operate acceptably well. The effect of compression ratio on the fuel mix limits is of particular interest.

The use of ammonia promoted with gasoline avoids the problems of storing large quantities of a high pressure gas and/or obtaining a sufficient ammonia cracking yield. The flammability of the intake mixture is tuned by controlling the ratio of fuel mass flows. The use of gasoline as a combustion promoter also retains the possibility of running the same engine on gasoline alone when ammonia is not available.

1.3.2 COV(IMEP$_n$)

This study seeks to be the first to characterize the usability of (COV(IMEP$_n$)) as a sensitive indicator of combustion stability for an engine fueled by ammonia and a combustion promoter. Excessively high (COV(IMEP$_n$)) must be avoided whether accompanied by a loss of efficiency and power, or not. However, a significant loss of efficiency and power is anticipated only when the COV(IMEP$_n$) is excessive. Acceptable operation is therefore assured when the COV(IMEP$_n$) remains below a particular value yet to be determined. Also, unlike efficiencies which are usually calculated after the fact, the COV(IMEP$_n$) is easy to monitor in real time while adjustments are made. For these reasons, COV(IMEP$_n$) is used in this study to detect the point at which the replacement of gasoline with ammonia should be taken no further as the fuel mix is varied.

1.3.3 Emissions Characterization and Cleanup

It is important to remember that in many of the exhaust emissions tests disclosed in the literature, the engine was probably running badly. If the engine is misfiring, for example, one should expect to find large amounts of fuel in the exhaust. Any useful measurement of the engine's operating characteristics, including exhaust emissions, must be done in an operating regime in which the engine is running well in order for a proper characterization to be achieved.

The other main goal of this study is to obtain engine-out exhaust emissions measurements from an ammonia and gasoline dual fueled engine during operation which

is acceptable from the standpoint of efficiency and combustion stability. The exhaust emissions to be measured include hydrocarbons, ammonia, oxides of nitrogen, and carbon monoxide. An attempt at achieving post-catalyst exhaust emissions clean-up is also made, and the features of the emissions clean-up point are characterized.

1.4 Fuel Properties and Equation of Combustion

Table 1.1 summarizes the properties of ammonia and gasoline. Ammonia is stored as a liquid at a modest pressure near 10 bars at room temperature. For the same LHV energy content, liquid ammonia has 2.6 times the volume, and 2.3 times the mass of gasoline. Ammonia is characterized by a higher knock resistance, lower flame speed, and narrower flammable equivalence ratio range than hydrocarbon fuels. The flame speed results and equivalence ratio range are for pressure = 1 bar, temperature = 300º F. The octane rating for ammonia is an estimate, because ammonia is unlikely to burn well under the standard conditions used for research and motor octane tests.

Property	Ammonia	Gasoline
Lower heating value	18.6 MJ/kg (calculated)	42.45 MJ/kg (analyzed)
Octane rating	>130 RON [Hodgeson, 1973]	92.4 (R+M)/2 (analyzed)
Specific gravity of fuel in liquid form	0.64 g/cm^3 (15º C)	0.73 g/cm^3 (analyzed, 21º C)
Stoichiometric air/fuel mass ratio for single fuel	6.1	14.5
Flammable equivalence ratio range [Verkamp et al., 1967]	0.72-1.46	0.55-4.24 (JP-4)
Flame speed at stoichiometric [Verkamp et al., 1967]	12 cm/s	62 cm/s (JP-4)

Table 1.1. The properties of ammonia and gasoline.

Stoichiometric operation is used for all points in this study. Stoichiometric operation gives the best compromise between power density and efficiency, and it is also near the

flame speed maximum for ammonia [Verkamp et al., 1967]. The post-catalyst exhaust emissions clean-up point for ammonia also occurs at stoichiometric, just as it does for gasoline. Stoichiometric operation is the best match for the overlap of these criteria.

All dual fueled operation in this study involves using ammonia with gasoline, except for the results and discussion for Figures 3.12 and 3.19, which describe how E85 (85% ethanol, 15% gasoline) behaves as a combustion promoter for ammonia. Equation set 1.1 describes the stoichiometric combustion of gasoline and ammonia in 1 mole of air. The equation reduces to the combustion of gasoline when $b_c = 1$, and that of ammonia when $b_c = 0$. b_c is the gasoline fraction, on a chemical equivalence basis. It is the fraction of the oxygen consumed by the gasoline. The formula C_6H_{11} is used to represent gasoline because the H/C atomic ratio of the gasoline used in this study was $1.834 \approx {}^{11}/_6$.

$$(0.790 \; N_2 + 0.210 \; O_2) + 0.024 \times b_c \; C_6H_{11} + 0.280 \times (1-b_c) \; NH_3 \Rightarrow$$
$$(0.930 - 0.140 \times b_c) \; N_2 + (0.420 - 0.288 \times b_c) \; H_2O + 0.144 \times b_c \; CO_2 \qquad \text{Eq. set 1.1}$$
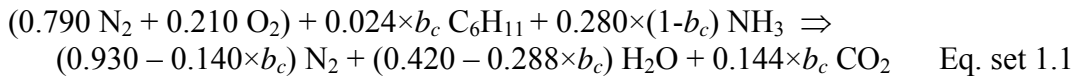
LHV energy yield per mole of air: $(88.7 - 4.0 \times b_c)$ kJ

The energy yield per mole of both the intake mixture and exhaust products for the stoichiometric gaseous ammonia/air mixture is about 83% of those for the stoichiometric vaporized gasoline/air mixture. At WOT, normally aspirated operation on ammonia with gasoline, instead of only gasoline, might involve a slight power loss, except that there are other effects which contribute to the power output, such as the ability to use MBT spark timing with ammonia. The exhaust gas temperatures are also expected to be lower when some ammonia is used because the energy of combustion is distributed over more moles of gas.

The gasoline fraction on a chemical equivalence basis and LHV energy basis are very nearly the same. Equation 1.2 describes the gasoline fraction on a LHV energy basis b_e, expressed as a percent.

$$b_e = \frac{84.7 \times b_c}{88.7 - 4.0 \times b_c} \times 100\% = \frac{\dot{m}_g Q_{LHVg}}{\dot{m}_g Q_{LHVg} + \dot{m}_a Q_{LHVa}} x100\% \qquad \text{Eq. 1.2}$$

CHAPTER 2
EQUIPMENT, CALIBRATION, AND METHODS

2.1 Engine

2.1.1 CFR engine

This study uses a cooperative fuel research (CFR) engine [ASTM, 1956], shown in Figure 2.1, which has an 83.4 mm cylinder bore diameter, 114.3 mm stroke, and 625 cm^3 displaced volume. The engine's "split cylinder" configuration features a separable cylinder and cylinder head, which when assembled act as one solid piece. The cylinder is moved in the clamping sleeve to vary the compression ratio. The cylinder head features two diametrically opposed ports at the edge of the combustion chamber. One port was used for the single Champion 3405-2 spark plug, and the other was used for the 7061B Kistler cylinder pressure transducer. The piston and cylinder head are flat, which gives the combustion chamber a pancake shape. This configuration is expected to be somewhat more knock-prone and characterized by a longer burn duration and exaggerated heat loss than those which might be achieved with a centrally located igniter and hemispherical combustion chamber.

Supercharged operation was achieved with the use of compressed air. An actual intake compressor would have required a power take-off, thus lowering the brake thermal efficiency. A turbocharger would have recovered some of the energy in the exhaust pressure pulse from the elevated cylinder pressure at the exhaust valve opening. However, a turbocharger would also have raised the cylinder pressure during the exhaust stroke [Hu and Lawless, 2001], thus lowering the brake and net indicated thermal efficiencies slightly. No effort was made to correct for either the supercharge work or the exhaust pressure pulse recovery.

Intake Plenum

Clamping Sleeve

Spark Advance Dial

Crank Angle Encoder

Exhaust Line

Movable Cylinder Assembly

Compression Ratio Crank

Capacitive Signal Pick-up on Ignition Wire
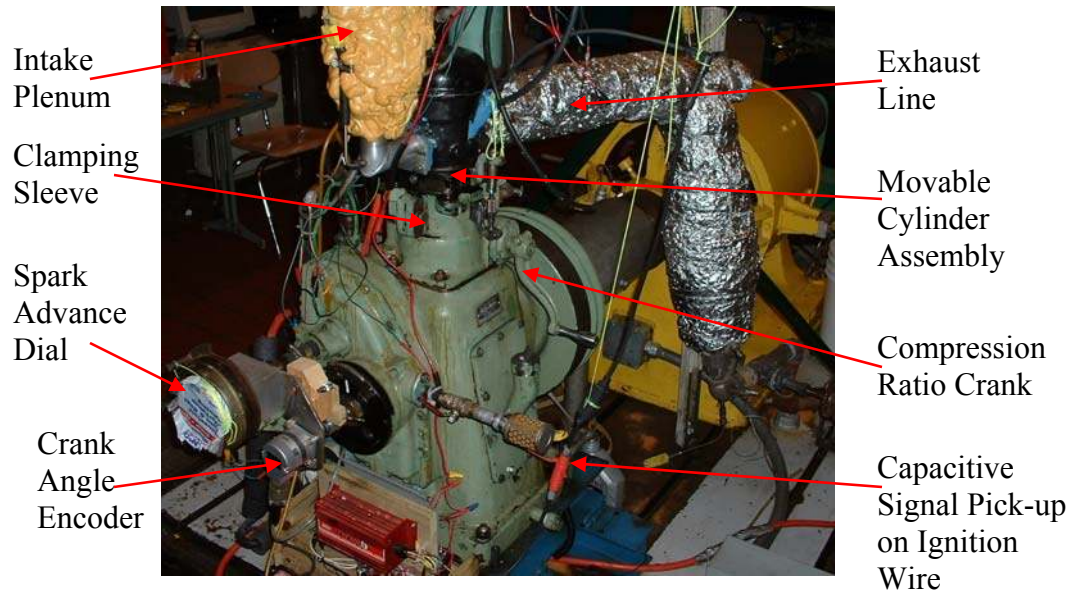
Figure 2.1. The CFR engine.

A CFR engine is usually equipped with a shrouded intake valve which is intended to induce swirl and turbulence, and promote mixing, and thus facilitate operation at 600 and 900 RPM. However, an intake valve without a shroud was used in this study, because the shroud would have reduced the volumetric efficiency for speeds between 1000 and 1600 RPM. Moderate swirl is of little value when ammonia is used, and combustion is adversely affected when too much swirl is used, probably because the slowly propagating ammonia flame is blown out by the use of high swirl [Pearsall and Garabedian, 1967]. No effort is made to induce any more swirl or turbulence than necessary in this study.

The CFR engine has no valve overlap. Although the exhaust valve opening and closing and intake valve closing occur effectively at the ends of the piston's range of travel, the intake valve does not open substantially until the piston is about $^1/_3$ to $^1/_2$ of the way down. This intake behavior causes a large additional pumping loss that would not be present with standard valve timing. The loss associated with the late intake valve opening is proportional to the intake pressure. No effort is made to correct for this loss, which goes up with increasing speed.

Figure 2.2 shows the PMEP as a function of load for all points, grouped by speed. At low load, the PMEP is due to the low intake pressure. Even for supercharged operation

the PMEP is mostly positive because of the late intake valve opening. The effect of late intake valve opening on PMEP becomes more exaggerated with increasing speed.
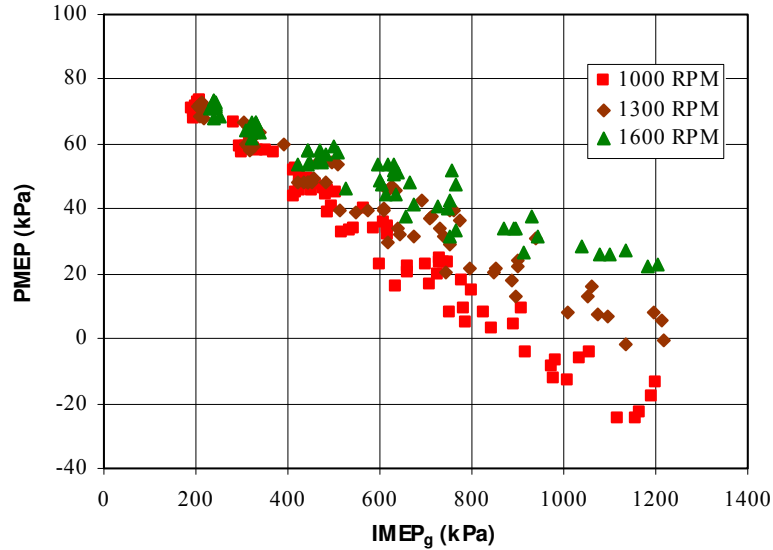
Figure 2.2. The pumping mean effective pressure.

Figure 2.3 shows the FMEP as a function of load for all points, grouped by speed. The CFR engine has a high FMEP because it has a single cylinder. The FMEP has no significant compression ratio dependence. The friction changes little with load, so the BMEP/$IMEP_n$ ratio increases with increasing load. A substantial efficiency gain can be achieved by downsizing a throttled engine and rescaling its operating profile to higher load, possibly to the extent that the engine operates mostly in the supercharge regime, where the total of pumping and friction losses are a smaller fraction of the gross indicated work. Such an engine would convert a greater average percentage of the gross indicated work into work available at the crankshaft.

The engine coolant remains at its boiling temperature because it transfers heat to an external water loop by boiling and condensing. A mixture of antifreeze and water is used as the coolant, which has an apparent boiling point between 102 and 105° C. The engine is lubricated with Mobil 1 synthetic 0W-40 oil. The crankcase temperature was maintained between 84 and 96° C.

No exhaust gas recirculation (EGR) is used. No other effort is made to increase the residual fraction. It is understood that marginal combustion occurs at the rough limit. The use of EGR or other means of obtaining a substantial residual fraction would have increased the combustion promoter requirement at the rough limit.
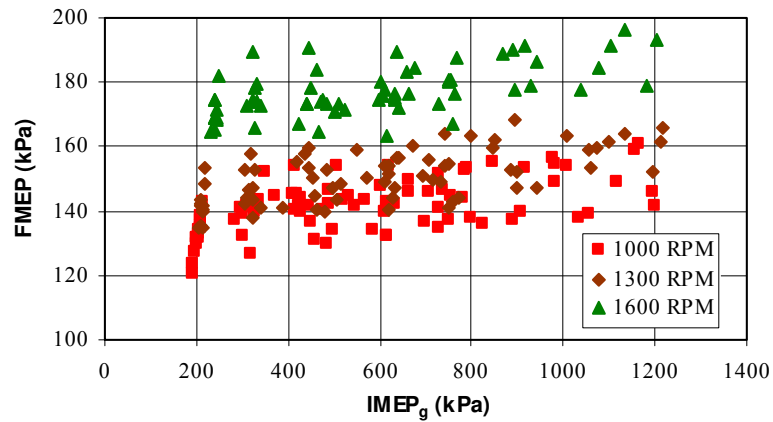
Figure 2.3. The friction mean effective pressure.

2.1.2 Compression Ratio Calibration

The engine flywheel has degree markings, and there is a crank angle pointer above the flywheel. The crank angle pointer is aligned so that the piston is in the same position when the pointer reads $\pm$ 90 degrees on the flywheel.

The average distance between the flat piston crown and the top edge of the cylinder at TC was measured with a 1 inch micrometer calibration block inserted with a catching fit in an accessible measurement transfer gap between the fixed cylinder clamping sleeve and movable cylinder block. This gap was used to transfer the piston height measurement after the cylinder head was installed. The average piston crown position below the top edge of the cylinder at TC is 0.180 inches plus the width of the transfer gap shown in Figure 2.4.
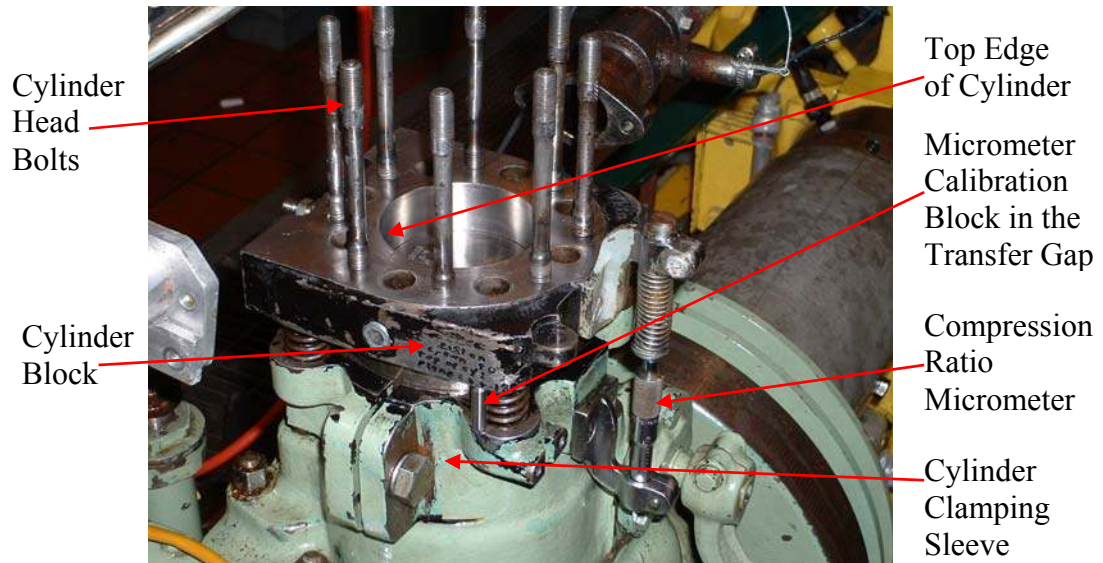
Figure 2.4. The cylinder block without the cylinder head.

The cylinder head gasket's contribution to the clearance volume was calculated from the gasket's inner diameter and its average compressed thickness. Figure 2.5 shows the four equidistant notches which were cut into the outer edge of the head gasket, so that its average compressed thickness could be measured by inserting a feeler gauge between the cylinder head and cylinder block. The inside head gasket and cylinder diameters were 3.261 and 3.2845 inches, respectively. The head gasket's average compressed thickness was 0.054 inches after tightening the cylinder head bolts, and this value did not drift.

The additions to the clearance volume due to the spark plug and pressure transducer ports were measured, with the spark plug and pressure transducer installed, by filling the ports with water from a marked syringe until the water was flush with the head plane. The addition due to the crevice volume between the uppermost compression ring and piston crown was also counted, and this was calculated from the piston, ring, and cylinder dimensions. The subtraction from the clearance volume due to the intake and exhaust valves was calculated from the dimensions of the valves, and the measurement of how far they stick out from the head plane. The total of the additions minus the subtractions is 0.153 cubic inches. The head plane itself is ground flat, and the valve seats are flush with the head plane.
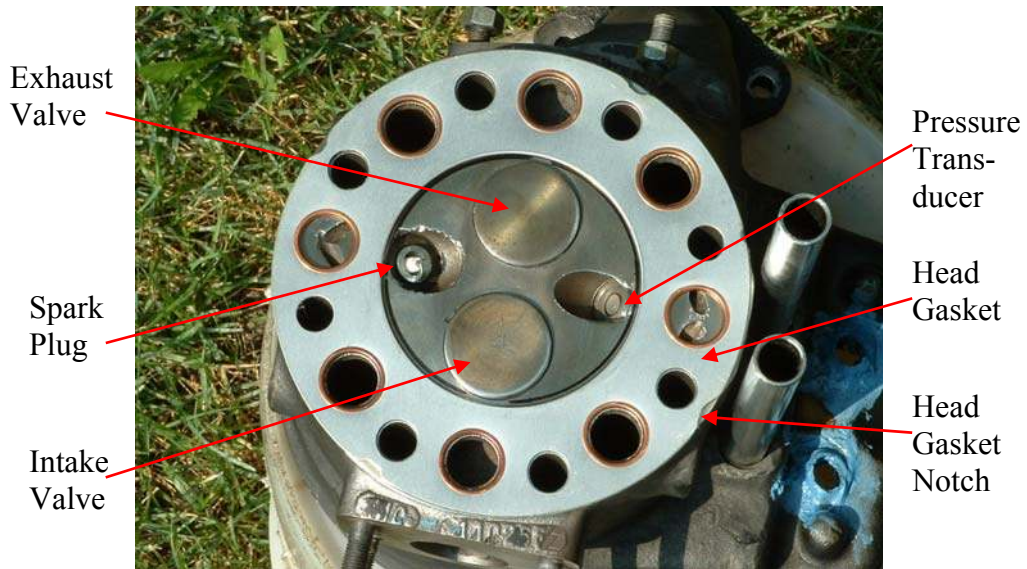
Figure 2.5. The cylinder head and gasket.

The clearance volume measurement was transferred outside the cylinder using the transfer gap shown in Figure 2.4. 16:1 occurs when the cylinder volume at TC is $^1/_{15}$ of the displaced volume. The stroke is 4.5 inches. The compression ratio micrometer mount height was adjusted to make its reading 0.000 when the transfer gap is 0.049 inches, which occurs at 16:1. 14:1, 12:1, 10:1, and 8:1 occur at compression ratio micrometer readings of 0.046, 0.109, 0.200, and 0.343 inches, respectively.

2.1.3 Limits of Operation

For gasoline, an increasing spark retard from MBT is required to avoid knock as the load is increased. The load was increased until the KLSA reached TC, or until the exhaust gas temperature became hazardous for the exhaust components (about 900° C), whichever occurred first. In either case, further attempts to increase the load beyond that point produce a diminished return on power output, rapidly decreasing efficiency and increasing exhaust gas temperatures.

For operation on ammonia with gasoline, the CFR engine was run at loads ranging from idle up to loads at which the peak firing pressures approach 100 bars, or the intake

pressure reaches 160 kPa, whichever occurs first. No firing pressure limit was specified for this engine, but a 100 bar limit was judged reasonable for the engine design. The firing pressure limit is reached at progressively lower loads as the compression ratio is raised above 12:1. The intake pressure was limited to a maximum of 160 kPa for 8:1 and 10:1 to avoid breaking any of the intake path components, especially the intake air heater. The maximum load for dual fueled operation was not limited by knock or any other consideration besides firing pressure and intake pressure. Speeds of 1000, 1300, and 1600 RPM were used for all fuels.

2.1.4 Load characteristics

In certain load regions the engine runs throttled, while in others it is supercharged. WOT occurs at 1 bar intake pressure and $IMEP_n \approx 700$ kPa. At idle the engine produces zero torque. Idle occurs at $IMEP_n \approx 150$ kPa. The engine was not throttled below idle. Supercharged operation involves intake pressures greater than ambient, and is represented by points where $IMEP_n > 700$ kPa.

Many of the charts are plotted as a function of load. Load is represented by the intake pressure, total specific fuel input, $IMEP_g$, $IMEP_n$, and BMEP axes. The total specific fuel input is the total fuel LHV energy input per cycle, divided by the displaced cylinder volume. Tables 2.1 and 2.2 show the approximate relationship between the load axes, for dual fueled operation and for operation on gasoline, respectively.

Intake pressure, (kPa)	Total Specific Fuel Input (Joules/Liter)	$IMEP_g$ (kPa)	$IMEP_n$ (kPa)	BMEP (kPa)
30, Idle	600	210	150	0
65	1350	450	400	250
100, WOT	2100	730	700	550
130	2700	970	960	810
160	3300	1200	1200	1050

**Table 2.1. The approximate relationship between
load axes for dual fueled operation.**

15

Intake Pressure, (kPa)	Specific Gasoline Input (Joules/Liter)	$IMEP_g$ (kPa)	$IMEP_n$ (kPa)	BMEP (kPa)
30, Idle	600	210	150	0
65	1450	500	450	300
100, WOT	2300	750	720	570
130	3100	930	920	770

Table 2.2. The approximate relationship between load axes for operation on gasoline.

2.2 Cylinder Pressure Transducer and Calibration

A water-cooled 7061B Kistler piezoelectric cylinder pressure transducer is used for cylinder pressure measurement. This pressure transducer is rated to output 79.9 picocoulombs per bar. The Kistler charge amplifier used with the pressure transducer was set to output 5 volts per 100 bar, 1 bar per 79.9 pC. The expected response constant of the pressure transducer and charge amplifier combination is 2000 kPa per volt with this procedure, according to the amplifier's calibration instructions.

The pressure transducer was placed in a dead weight tester which applies and releases a known pressure. The voltage response of the charge amplifier/transducer combination is characterized by a nearly constant ratio of applied pressure to amplifier output voltage change. This ratio of applied pressure to voltage change is shown in Figure 2.6 for different applied pressures. A weighted average response constant of 2023 kPa per volt was found, in close agreement with the expected 2000 kPa per volt, the latter value being the nominal value when the charge amplifier is set up according to the manufacturer's instructions. The constant 2023 kPa per volt was programmed into the data acquisition system.
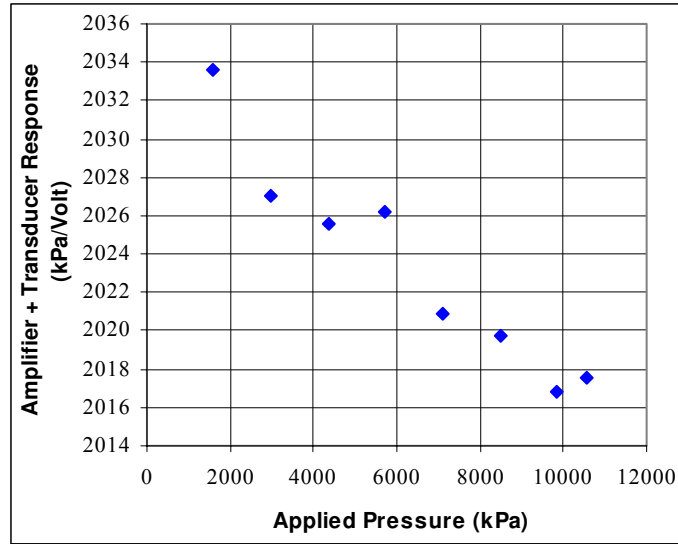
Figure 2.6. The response constant for the pressure transducer/charge amplifier combination.

2.3 Data Acquisition System

A data acquisition system and Combust2 software, made by Electro-Mechanical Associates, are used to acquire the cylinder pressure signal, a spark timing signal from a diode-clamped capacitive pick-up placed on the spark plug wire (see Figure 2.1), and the ammonia mass flow controller output voltage. The signals are recorded as a function of crank angle at 5 points per degree, and 60 cycles per set. The DC voltage readings of the data acquisition system agree within 0.5% of simultaneous readings taken with the same voltmeter used to calibrate the ammonia mass flow controller and the pressure transducer/charge amplifier combination.

The data acquisition system uses the crank angle encoder pictured in Figure 2.1. This device is connected to the crankshaft with a flexible coupling. It produces one pulse of 0.1 degrees duration per revolution, aligned at TC, and another signal consisting of a square wave with 1800 periods per revolution. This crank angle encoder was chosen because a data rate of 5 points per degree was required to reliably detect knock. At 5 points per degree, 1000 RPM, a knock signal at 6 kHz would have about 5 data points per period. The data acquisition system calculates crank angle from the crank angle encoder

signals. It also uses the pressure signal to distinguish the end of compression from the end of exhaust.

2.4 Pressure Signal Analysis

2.4.1 Features of the Pressure Trace

Figure 2.7 shows the basic features of a recorded pressure trace, plotted in a base 10 log-log space. This is the 60-cycle average pressure trace for dual fueled operation at the MBT knock limit, 10:1, 1300 RPM, intake pressure = 160 kPa. Appropriate constants P_o and V_o were chosen for this plot, such that $Log_{10}(P/P_o) = 1$ at $P = 1$ bar, and $Log_{10}(V/V_o) = 1$ at $V = 0.5$ liters. Note how the intake pressure is greater than the exhaust pressure near the end of the intake stroke. The exhaust valve opening and closing and intake valve closing occur effectively at the ends of the piston's range of travel. However, the intake pressure is less than the exhaust pressure near the beginning of the intake stroke, despite supercharging, because the intake valve opens late. The blue arrows indicate the direction of movement.
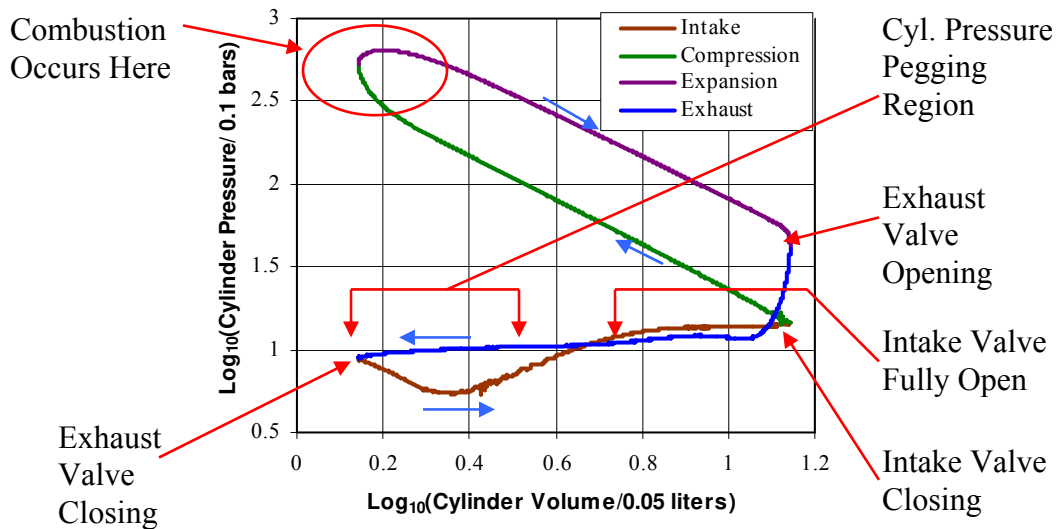
Figure 2.7. The basic features of a recorded pressure trace.

18

The cylinder pressure signal is relative because the piezoelectric pressure transducer gives an AC signal. To get the absolute pressure, a portion of the pressure trace must be pegged to a particular value. The portion at the end of the exhaust stroke from 315 degrees to 360 degrees is chosen as the pegging region, because in that region the cylinder pressure is known more closely than it is anywhere else in the cycle. The average cylinder pressure within the pegging region was set equal to 1 bar.

The cylinder pressure at the exhaust valve opening was about 5 bars for the pressure trace in Figure 2.7. A significant amount of blow down energy could be recovered at high load if the cylinder contents were expanded to ambient pressure through a work recovery device placed in the exhaust, such as a turbine. An operating cycle that recovers the blow down energy would be more efficient than the Otto cycle, because the Otto cycle only recovers the work available at the piston.

The recovery of blow down energy, as a feature possibly integrated into turbocharged operation, is not covered in this study. The use of electric-assist turbochargers is recognized as a viable solution to the problem of turbo lag at low engine speeds and during transients [Kattwinkel et al., 2003]. A turbocharger designed for unsteady flow should be able to capture some of the blow down energy at the exhaust valve opening, after which the average backpressure during the exhaust stroke is less than the peak blow down pressure [Hu and Lawless, 2001]. An engine designed to operate turbocharged most of the time could use an electric assist turbo for load control by varying the turbine speed. Any work recovered at the exhaust turbine in excess of the work consumed at the compressor turbine could be added to the shaft output of the engine, as an alternative to wastegating.

The effective ratio of specific heats for 10:1 is evaluated from the negative slope of the compression line between 0.38 and 0.61 on the horizontal axis, and for this example $\gamma = 1.32$. This region is well outside of the rounded portions of the curve, where the combustion occurs.

2.4.2 Apparent Mass Fraction Burned, Ignition Delay, and Burn Duration

Equation 2.1 describes the differential apparent heat release dQ, which is calculated from cylinder pressure P and instantaneous volume V. The units are Joules. The effective ratio of specific heats γ is calculated for each operating point from cylinder pressure and volume during compression between 50 and 30 degrees BTC, and its typical value is 1.3.

$$dQ = \frac{\gamma}{\gamma-1}PdV + \frac{1}{\gamma-1}VdP \qquad \text{Eq. 2.1}$$

Equation 2.2 describes the dimensionless apparent mass fraction burned (MFB_a), which is calculated from the apparent heat release. The integral starts at 30 degrees BTC, where none of the operating points showed significant combustion despite a spark advance of often more than 30 degrees. The total heat release is normalized to the total fuel LHV energy input per cycle Q_t, which is described by Equation 2.3. The units of Q_t are Joules per cycle.

$$\text{MFB}_a(\theta) = \frac{1}{Q_t}\int_{-30°}^{\theta} dQ \qquad \text{Eq. 2.2}$$

$$Q_t = (\dot{m}_g Q_{LHVg} + \dot{m}_a Q_{LHVa}) \times \frac{2}{f_{rpm}} \qquad \text{Eq. 2.3}$$

The MFB_a curves asymptote to an end value less than 1, typically 0.7, mostly because of the heat irreversibly lost to the combustion chamber boundaries. The 10% burn angle is the crank angle at which an MFB_a curve reaches 10% of its end value, typically 0.07,

near the lower corner of the curve. 90% burn occurs where the curve reaches 90% of its end value, typically 0.63, near the upper corner of the curve.

60 cycles were acquired for each operating point. The burn interval is the crank angle region bounded by the 10% and 90% burn angles of the 60-cycle average MFB_a curve. The burn duration is the crank angle width of the burn interval. The ignition interval is the crank angle region bounded by the spark and the 10% burn angle of the 60-cycle average MFB_a curve. The ignition delay is the crank angle width of the ignition interval.

2.4.3 COV($IMEP_n$)

The COV($IMEP_n$) is the standard deviation of the $IMEP_n$ divided by the mean $IMEP_n$ for a set of 60 cycles. The COV($IMEP_n$) is a measure of the cycle-to-cycle net indicated work yield variation, and it is used to define roughness. An engine would appear to be running "rough" when the COV($IMEP_n$) is high, whether this is accompanied by an efficiency loss or not. Excessive roughness is defined as having a COV($IMEP_n$) in excess of 3%. Smooth firing occurs when the COV($IMEP_n$) $\leq$ 3%.

2.4.4 Knock

Knock is detected in the pressure signal with a knock filter which is an included feature of the Combust2 software. The knock filter is a high pass filter with unity gain in the pass band. The cutoff frequency corresponds to a period of 12 points, or 2.5 kHz, 3.25 kHz, and 4 kHz at 1000 RPM, 1300 RPM, and 1600 RPM, respectively.

Figure 2.8 shows a comparison of the pressure signal and the knock signal for an individual knocking cycle with peak firing pressure = 29 bars, 10:1, 100% gasoline, and 1600 RPM. The pass band gain is one, or very nearly so. Note how the knock signal follows the high frequency components of the raw pressure signal.
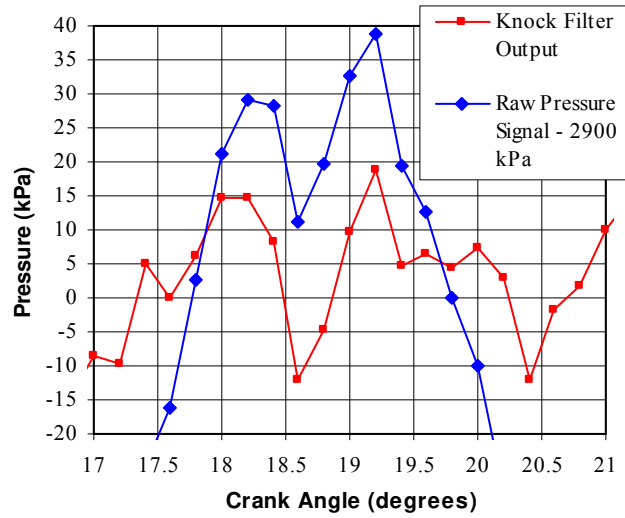
**Figure 2.8. A comparison of the pressure signal
and the knock signal for a knocking cycle.**

Figure 2.9 shows the same knock signal which is used in Figure 2.8. Stoichiometric gasoline/air mixtures were usually found to knock when the average peak firing pressure reached 20-30 bars.
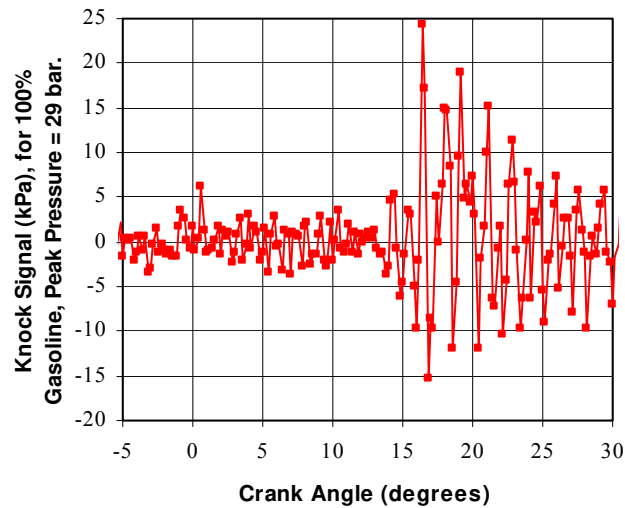
**Figure 2.9. The knock filter output for operation
on 100% gasoline, peak pressure = 29 bars.**

Figure 2.10 shows the knock filter output for an individual cycle with peak firing pressure = 100 bars, 12:1, 100% ammonia, and 1000 RPM. The knock filter had some response to the pressure rise rate at this high combination of load and compression ratio. However, there is no ringing above noise level which would have been indicative of knock. Ammonia tolerates much higher firing pressures without knock than gasoline does.
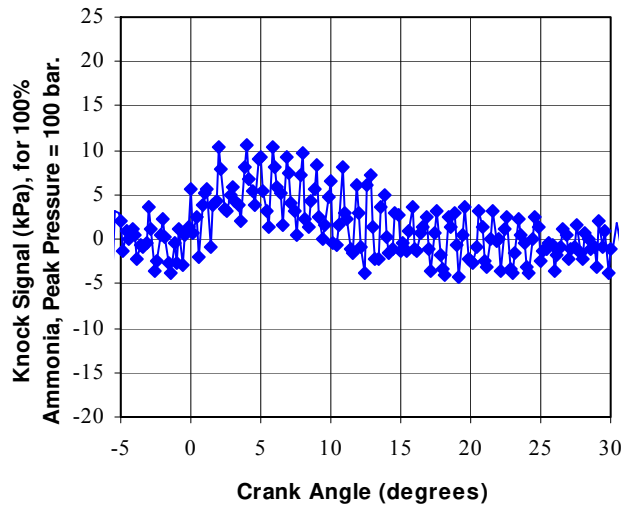
**Figure 2.10. The knock filter output for operation
on 100% ammonia, peak pressure = 100 bars.**

The condition for incipient knock is a knock signal amplitude of 10-50 kPa for one or more cycles in a set of 60. Knock-free operation occurs when the knock signal amplitude remains below 10 kPa, which is the threshold for a knock signal that is sufficiently distinguished from noise. A knock signal amplitude of more than 50 kPa was judged to be excessive. Excessive knock was corrected by retarding the spark for operation on gasoline, or by using more ammonia and less gasoline for dual fueled operation.

Figure 2.11 shows Fourier transforms of the knock signals from Figures 2.9 and 2.10. The gasoline knock signal has frequency peaks at 6 kHz and 10.3 kHz. These are most likely the first two modes of a circular disk acoustic cavity. The ammonia knock signal has frequency peaks near 0 kHz and 6 kHz. The rapid pressure rise to 100 bars excited only the first cavity mode, and the event was not sharp enough to be characterized as

23

knock. The 0 kHz peak, which would normally be suppressed by the knock filter, is an artifact in the knock filter's response to rapid pressure rise.
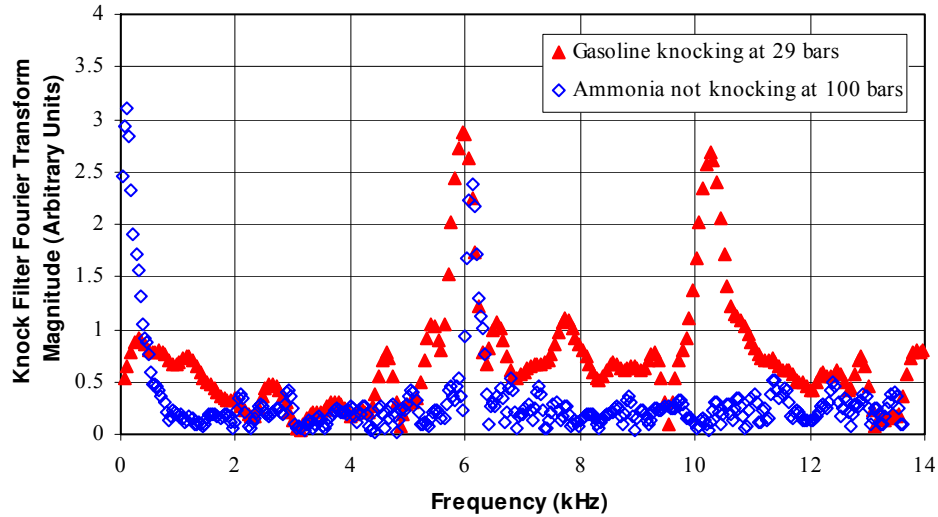
Figure 2.11. Fourier transforms of the knock signals from Figures 2.9 and 2.10.

It appears that knock involves excitement of the first and second cavity modes, which are near 6 kHz and 10.3 kHz, respectively. No significant response was found in the gasoline knock signal above 11 kHz, despite the 48 kHz sampling frequency at 1600 RPM, which should have permitted some detection up to 24 kHz. The 6 kHz and 10.3 kHz modes clear the knock filter's 4 kHz high pass cutoff at 1600 RPM, and both mode frequencies are less than half of the 30 kHz sampling frequency at 1000 RPM. The choice of equipment was indeed suitable for detecting the knock signal.

2.5 Engine Intake Path

Figure 2.12 shows the intake path, which consists of these items, starting at the shop air line and working downstream: two single stage air pressure regulators, a supercharge hose, an intake air heater through which the engine coolant is circulated, a throttle body with manual throttle adjustment, gasoline injector, and ammonia gas inlet port, and

24

finally, a 3.5 liter intake plenum at the cylinder head inlet. The ammonia inlet port is adjacent to the gasoline injector. Both the gaseous ammonia and liquid gasoline are metered vertically onto the upstream side of the throttle plate, which facilitates mixing of the fuels and air. A pressure drop of at least 10 kPa is maintained across the throttle plate for all operating points, even during supercharged operation.
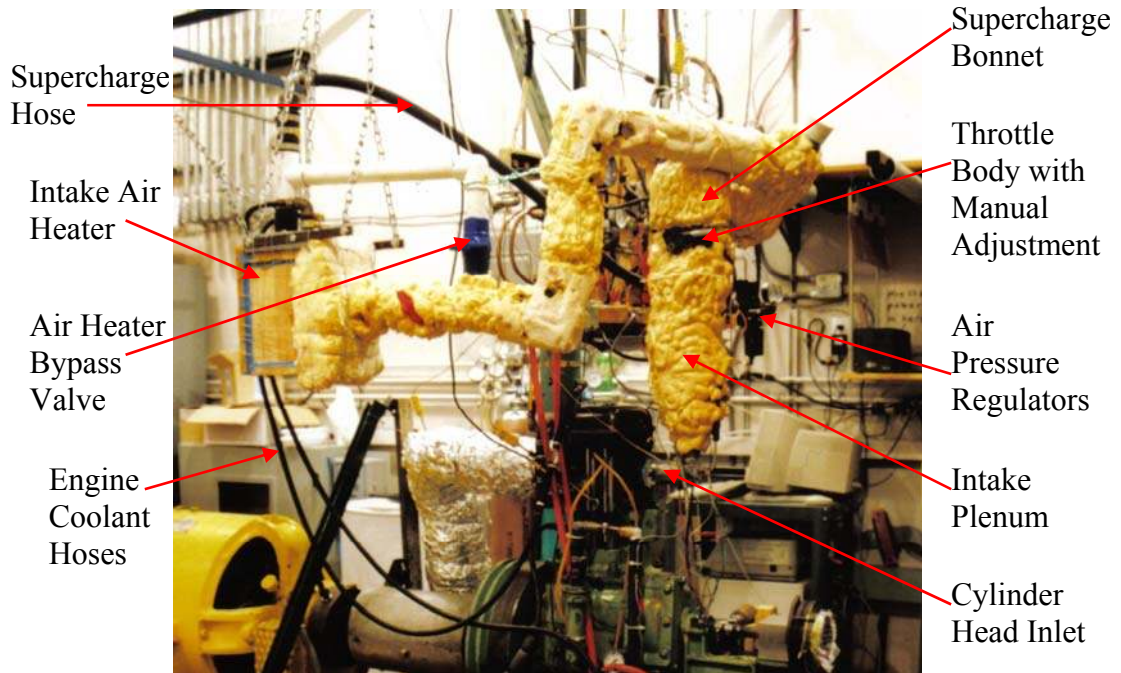
Figure 2.12. The intake path.

The intake plenum is used to dampen the pulsations from the engine intake process. It also provides a large volume within which the air, gasoline, and ammonia can mix, with the goal of maximizing the homogeneity of the mixture. Any change in either the gasoline input or the ammonia input is accompanied by a change in the air input to maintain the stoichiometry at all operating points. Load is controlled by varying the intake pressure. Any reported intake pressures refer to the average pressure in the intake plenum, which is varied through a combination of throttle and air pressure regulator adjustment.

An elevated intake air temperature was used to vaporize the gasoline, thereby making the intake mixture more uniform. The air heater bypass valve was adjusted to maintain

the supercharge bonnet air temperature between 55 and 60º C for all operating points. The intake mixture temperature near the cylinder head inlet port remained between 41-53° C. Substantial quantities of liquid gasoline were found upon momentary removal of the thermocouple near the cylinder head inlet port only when the temperature there was less than 20-25° C.

The intake air humidity was low because compressed air was used from a shop line, which is equipped with a water separator. The absence of condensation in the 700 kPa shop line indicates that the relative humidity must have been 14% or less at room temperature = 20-27° C.

2.6 Fuel Delivery and Mass Flow Measurement

The gasoline and ammonia are stored in separate tanks, and their mass flows into the engine are controlled and measured independently. Stoichiometric operation is achieved with the use of a standard automotive exhaust gas oxygen sensor, the characteristics of which are similar to the one used by Camp and Rachel (1975). The engine-out oxygen sensor was used, and the reference voltage was set at 0.45 volts for the performance results and engine-out exhaust emissions results. The engine-out and post-catalyst oxygen sensor voltages were measured at small deviations from stoichiometric for the post-catalyst exhaust emissions results.

For operation on gasoline, the gasoline mass flow is adjusted by a control loop that responds to the oxygen sensor signal. The gasoline input is increased very slowly if a lean condition was sensed, and vice versa. The ramp rate was made slow enough such that the output fluctuation is less than 1% during steady state operation.

For dual fueled operation, the gasoline mass flow was set manually and adjusted to achieve a particular combustion condition. The gasoline input is less than that required for stoichiometric operation on gasoline alone, and the ammonia fills in for the remaining fueling requirement. The gaseous ammonia mass flow is slowly and automatically adjusted in response to the oxygen sensor signal to maintain stoichiometric combustion. The ammonia fuel ramp rate was made slow enough such that the ammonia mass flow

fluctuation is due almost entirely to hunting within the ammonia mass flow controller's internal servo loop. The ammonia mass flow controller input pressure was adjusted at each operating point to minimize that fluctuation. The resulting overall peak-to-peak equivalence ratio variation is about 1%.

The gasoline delivery system consists of a supply tank, a circulating loop through which the gasoline is pumped continuously, and a gasoline injector which is run synchronous with the engine. There is one gasoline injection per revolution, two per cycle. The circulating gasoline loop is regulated to hold the pressure drop across the gasoline injector at 280 kPa. The gasoline input per cycle is controlled by the gasoline injector pulse width. Figure 2.13 shows the throttle body/intake plenum/fuel delivery assembly.
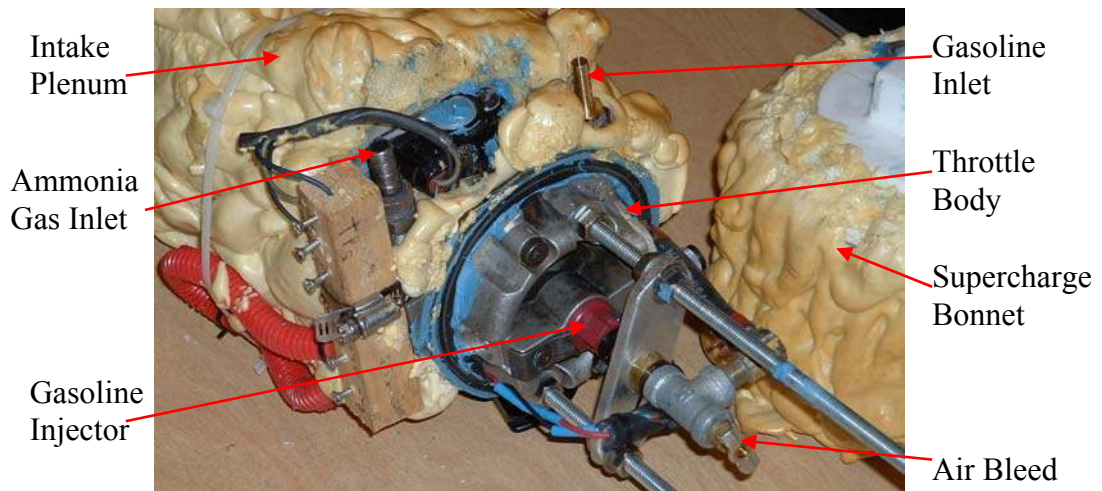
Figure 2.13. The throttle body/intake plenum/fuel delivery assembly.

The gasoline mass flow is measured with a flask on a scale, from which the fuel delivery system draws gasoline during timed measurements after steady state operation is achieved. The fuel supply is set up so that fuel can be drawn from the supply tank or from the flask. The flask can also be filled from the supply tank. The flask is filled and emptied through a dip tube which does not touch the flask. The flask's opening for the dip tube has minimal clearance for the dip tube to minimize evaporation. The flask was filled and emptied several times during each engine warm-up period to ensure uniform

fuel composition throughout the entire delivery system during experimental measurements. The scale was calibrated periodically with a 500 gram calibration weight. Figure 2.14 shows the flask, scale, and other equipment used for measuring the gasoline mass flow.
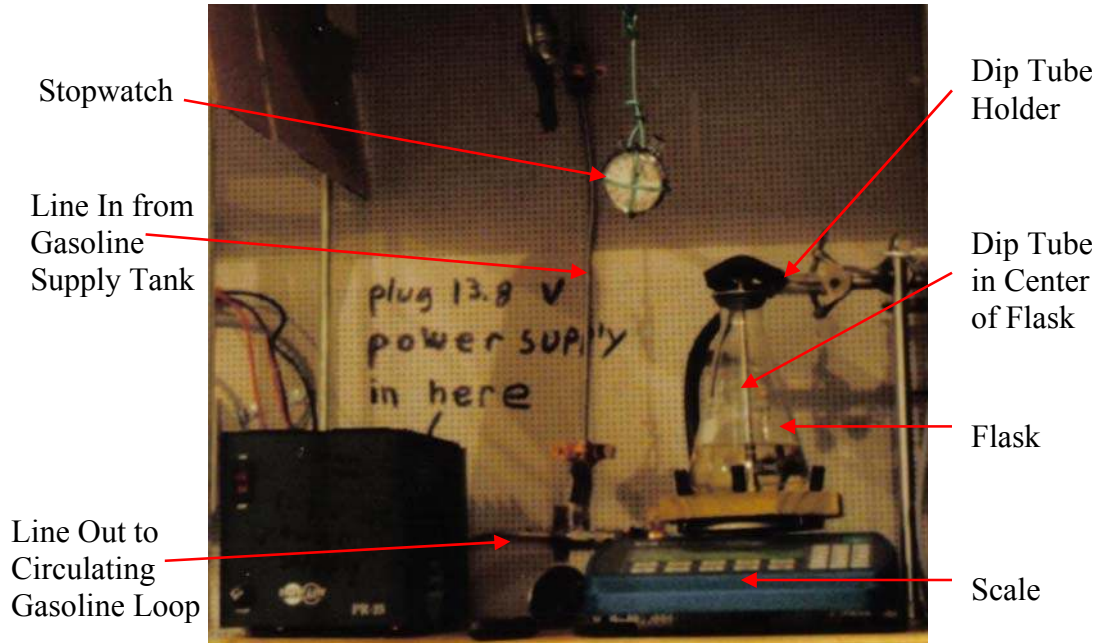
Figure 2.14. The equipment used for measuring the gasoline mass flow.

The ammonia delivery system consists of a supply tank, a pressure regulator for ammonia, and an ammonia mass flow controller made by Aalborg which also measures the ammonia mass flow. The ammonia is directed into the throttle body upon leaving the mass flow controller.

Figure 2.15 shows the ammonia tank and pressure regulator. The ammonia is allowed to vaporize in the tank and it is taken from the tank in gaseous form. No effort was made to heat the tank. The tank chilled slightly for the quantities of ammonia required to get data, but this did not cause any problems. The gaseous ammonia reached room temperature (20-27° C) upon reaching the mass flow controller.
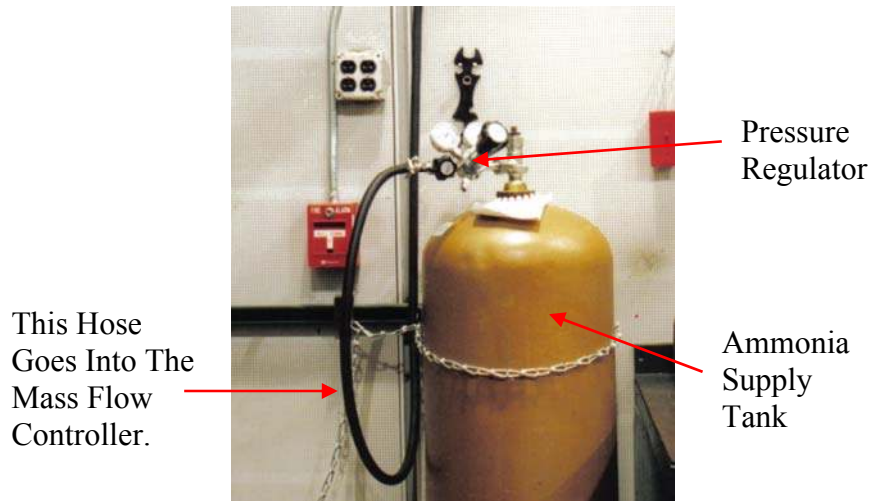
Figure 2.15. The ammonia tank and pressure regulator.

Figure 2.16 shows the ammonia mass flow controller and other items related to fuel control. The ammonia hose is shown disconnected from the throttle body for the purpose of calibrating the ammonia mass flow controller.
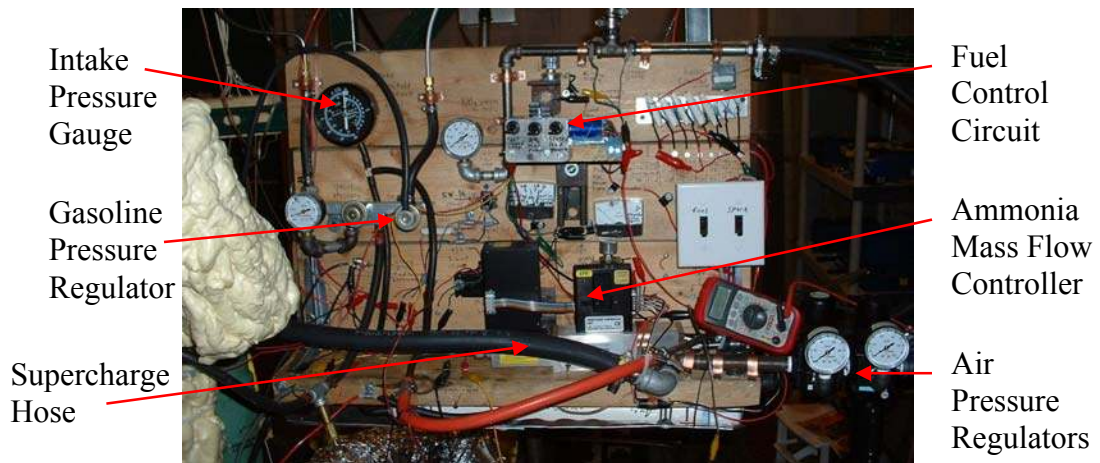
**Figure 2.16. The ammonia mass flow controller
and other items related to fuel control.**

The ammonia flow is controlled and measured by the ammonia mass flow controller. The ammonia mass flow controller receives a 0-5 volt DC signal from the fuel control circuit. The fuel control circuit also responds to the oxygen sensor signal, receives

manual input settings, and operates the gasoline injector. The ammonia mass flow controller sets the mass flow in response to the signal it receives, and it also outputs a 0-5 volt DC signal which corresponds to a measurement of the ammonia mass flow. The ammonia mass flow controller's internal servo loop seeks to keep the input and output voltages nearly the same. The ammonia output fluctuates slightly because the servo loop hunts about the target value, which is set by the input voltage.

Figure 2.17 shows the method for calibrating the ammonia mass flow controller. Ammonia is buoyant in air. A calibration bag was weighted with a large nut for easy placement on the scale, and for each measurement the bag was filled to buoyancy. The molecular weights of air and ammonia are approximately 29 and 17 grams per mole, respectively. The apparent weight change of a bag filled with gaseous ammonia is thus approximately -12 grams per 17 grams of ammonia contained in the bag.
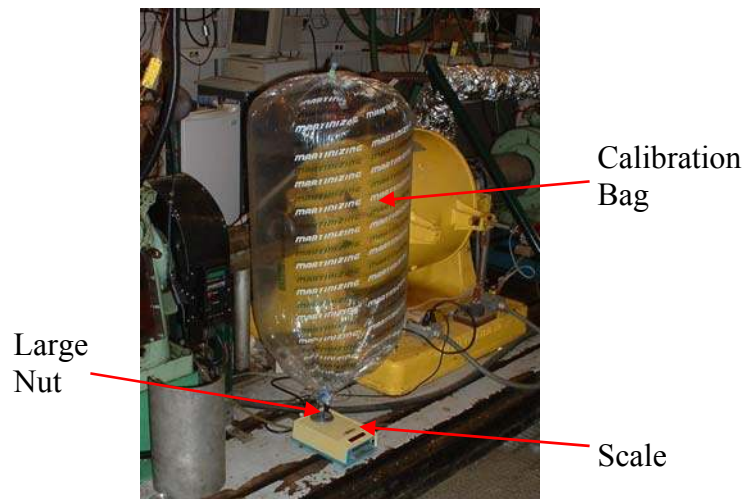
Figure 2.17. The ammonia calibration bag.

For each of the calibration measurements the output of the ammonia mass flow controller was allowed to reach steady state. The ammonia flow was then directed into the calibration bag. The average output voltage was measured during a timed period of filling the bag. The apparent weight change of the bag was measured at timed intervals after filling the bag. The timed weight measurements were used to correct for the leakage of ammonia out of the bag up to the start of fill. To get accurate bag weight

measurements it was necessary to turn the room ventilation off for several minutes and leave the room while weighing the bag. The room was momentarily re-entered for scale readings, and care was taken to avoid disturbing the bag during each measurement. The Van der Waals corrections, corrections for moisture, and the actual molecular weights of air and ammonia, altogether amounted to 2-3% of the total measurement. For very small ammonia flow rates, the same method was used except a balloon was used instead of a weighted bag.

Figure 2.18 shows the ratio of ammonia mass flow to ammonia mass flow controller output voltage. This ratio is a piecewise linear function. This measured calibration function was used to calculate the ammonia mass flow from the ammonia mass flow controller output voltage. For medium to high ammonia mass flow, the ratio is constant, and it is 16.28 grams per minute per volt. This response constant differs from the manufacturer's specification of 100 standard liters (21° C) per minute at 5 volts by a factor of 1.15. Oh well, at least they got the medium-high range linearity right. The features below 1 volt are important, too, and these are not disclosed.
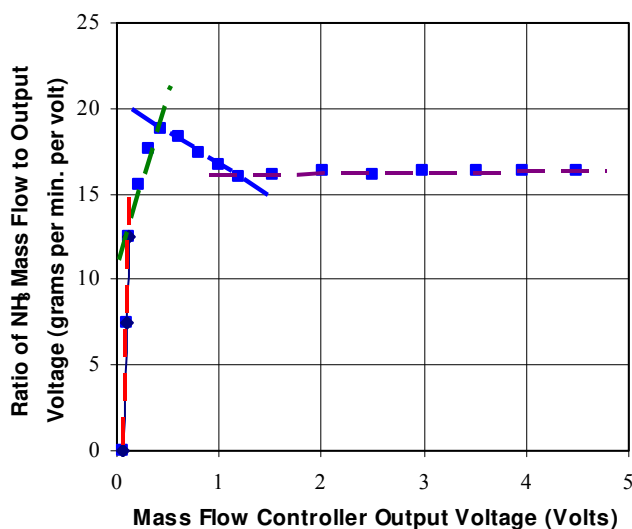
Figure 2.18. The ratio of ammonia mass flow to ammonia mass flow controller output voltage.

31

2.7 Ignition

2.7.1 Ignition System

A HyFire 6A capacitive discharge coil driver and Mallory ignition coil are used for ignition. The spark plug gap was set to 0.040" and left there for all operating points. This is the maximum spark plug gap for which the ignition system can fire the spark plug reliably for all operating points within the limits of this study.

The HyFire 6A coil driver and Mallory coil deliver 6 sparks when triggered. These 6 sparks are evenly distributed over a crank angle interval of about 90 degrees at 1600 RPM, or 55 degrees at 1000 RPM, between the first and last spark. In this study, "spark" refers to the first spark, and "spark timing" and "spark advance" refer to the crank angle location of the first spark in degrees BTC. The energy delivered by the coil driver to the ignition coil for each of the 6 sparks is nominally 135 millijoules, according to the manufacturer.

2.7.2 Spark timing methods

MBT spark timing is achieved by manually turning the spark advance dial while monitoring the torque. An advanced torque roll-off is reached when the spark is advanced of MBT and the torque is reduced by a small amount from the maximum torque. A retarded roll-off is reached at the same torque on the retarded side of MBT. The MBT spark advance is set halfway between the advanced and retarded torque roll-offs.

For dual fueled operation, sometimes the advanced torque roll-off is weak and difficult to find when the $COV(IMEP_n)$ exceeds 5%. Typically, the advanced torque roll-off disappears completely when the $COV(IMEP_n)$ reaches 10%. Whenever the advanced torque roll-off cannot be found, then the combination of fuel mix and compressed charge density at the initial spark must be either inadequate or marginal for ignition, and the combustion may begin at one of the later sparks, at which the charge is more fully

compressed. In that case, the effect of increasing the spark advance only places more of the sparks into the misfire region while leaving the actual start of combustion essentially unchanged. If the misfire limit with respect to spark advance occurs on the retarded side of MBT, then the overall combustion timing should be retarded from the optimum. Retarded combustion was routinely observed when the advanced torque roll-off could not be found. The advanced torque roll-off is always strong and easy to find when the $COV(IMEP_n) \leq 3\%$.

For KLSA, the spark advance is set to the maximum permitted while avoiding knock. The final spark setting is always on the retarded side of MBT whenever MBT spark timing cannot be used because of knock.

Figure 2.19 shows the relationship between spark advance, ignition delay, and burn duration. The horizontal axis is the ignition delay plus a burn duration constant times the burn duration. The vertical axis is the actual spark advance. The burn duration constant was adjusted to make the slope = 1 for the best fit line for all MBT results for 7:1 through 12:1. The resultant best fit line happens to pass very close to the origin. The typical MBT timing uncertainty, found by the spread of the MBT points about both sides of this line, is ±3 degrees. Equation 2.4, which is derived from the results in Figure 2.19, describes the MBT spark advance.

$$\text{MBT spark advance} = \text{Ignition delay} + {}^1\!/_4 \times \text{Burn duration} \qquad \text{Eq. 2.4}$$

The 14:1 and 16:1 points feature slightly delayed combustion because of a combination of heat loss effects which retard the optimum combustion phasing at compression ratios greater than 12:1 [Caris and Nelson, 1959], and also the misfire effect which was explained earlier in this section.

For KLSA, the spark is retarded of MBT, and a point's distance below the MBT line is an indication of how far the spark is retarded from MBT for that point. Equation 2.5 describes how far the spark is retarded from MBT, for KLSA results. This relation is approximate, but it works well even when the spark is significantly retarded from MBT.

Spark retard from MBT = Ignition delay + 1/4×Burn duration - Spark advance.   Eq. 2.5
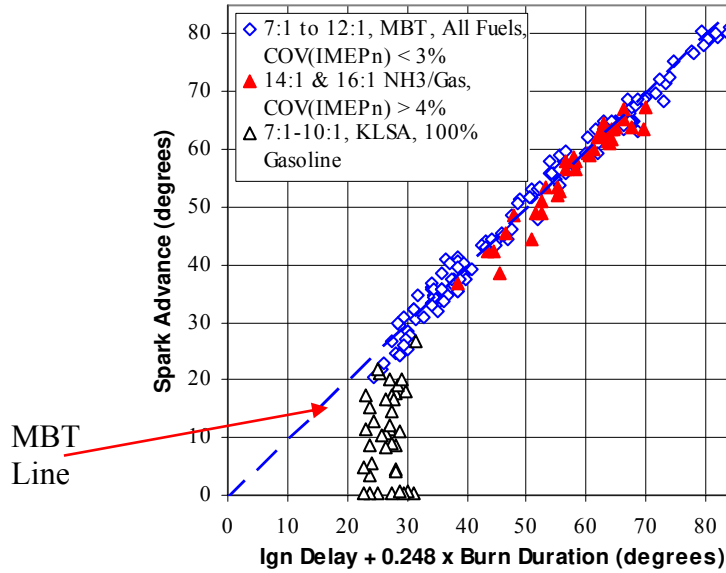
**Figure 2.19. The relationship between spark
advance, ignition delay, and burn duration.**

2.8 Torque Measurement and Calibration

The CFR engine is started and run with the use of a dynamometer, which holds the engine at a fixed speed chosen by the operator. The electric motor can act as both a motor and a generator, meaning that it can supply power, and also absorb any power that the CFR engine produces.

The dynamometer is equipped with a load cell to measure the torque. Figure 2.20 shows the dynamometer with the span calibration weight in place. A 25-pound weight produces 44.5 Newton-meters of torque when hung from the 40-centimeter moment arm of the dynamometer, and this known torque is used to calibrate the span. The universal coupling, which connects the engine and dynamometer, is positioned at the center of its lash whenever either the zero or the span is reset.

CFR Engine Flywheel

Dynamometer Motor/ Generator

Span Calibration Weight

Load Cell
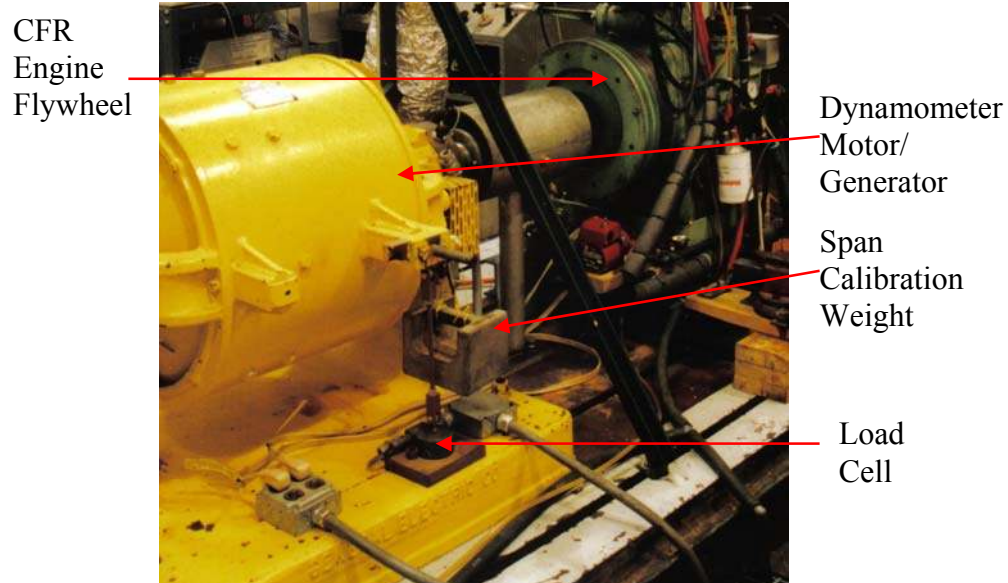
Figure 2.20. The dynamometer with span calibration weight.

Torque is an averaged quantity, and it is taken over a time window of 8 seconds. For that reason, the cylinder pressure data are better suited for characterizing individual cycles and cycle-to-cycle variations.

2.9 Thermocouple Calibration

Type K thermocouples are used to measure various temperatures throughout the engine, and also in the exhaust line. The Omega "Air Probes" used in the exhaust line feature a bare junction in a perforated cage, which is less prone to inaccuracies due to thermal conduction at high temperature. The thermocouple meter was calibrated by placing one of the thermocouples in a test oven: a Hot Point Cell made by Omega. The zero and gain on the thermocouple meter were adjusted such that the readings on the thermocouple meter and Hot Point Cell agree within 1° C over a range of 55 to 480° C. The Hot Point Cell was not operable above 480° C. All thermocouples agreed with each other to a precision better than 3° C.

2.10 Exhaust Line

Figures 2.21 and 2.22 show the exhaust line, which consists of a flexible pipe bolted to the cylinder head exhaust port, a catalytic converter, and pipes to carry the exhaust gas into a building ventilation system specially designed to handle engine exhaust. The pipe is fitted with one oxygen sensor near the engine (the engine-out oxygen sensor), and another after the catalytic converter (the post-catalyst oxygen sensor). There are also type K thermocouples inserted near the engine and also before and after the catalytic converter. The exhaust line was insulated from the engine to the catalytic converter so that the catalyst would get hot enough to work. The insulation consists of a thick aluminum oxide/silicon dioxide ceramic fiber inner layer, and an aluminum foil outer layer.
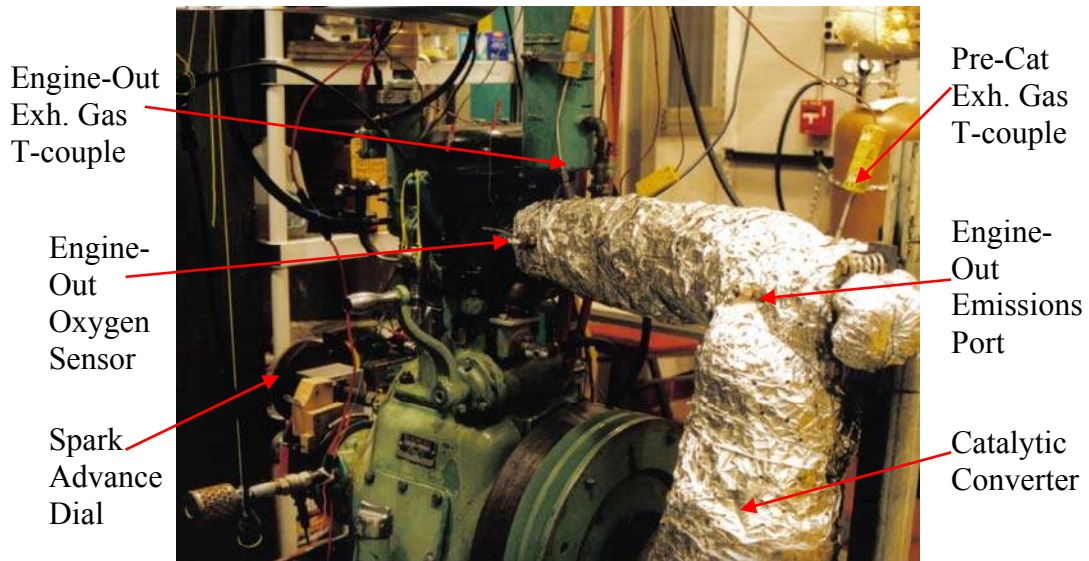
Figure 2.21. The upper portion of the exhaust line.

The catalytic converter is a standard three-way catalyst, similar to others that are commonly used to clean up the exhaust emissions from stoichiometric gasoline fueled engines. This catalyst was designed for a 1995 4-cylinder Chevrolet S-10 pickup. No air or any other materials are injected into the exhaust pipe after the engine. The catalyst comes into contact with only the exhaust from the engine. The portion of the exhaust line

from the engine to the catalyst was periodically tested for leaks to ensure that there were no gases leaking in and out, as this could affect the emissions results.

Exhaust gas is continuously sampled from the emissions ports during emissions measurements. These ports are closed off when not in use. The exhaust gas temperature results in chapter 3 were taken with the engine-out exhaust gas thermocouple shown in Figure 2.21.

Figure 2.22 shows the lower end of the exhaust line. It also shows how the hoses, which are used for extracting exhaust gas for analysis, are connected to the post-catalyst emissions port.
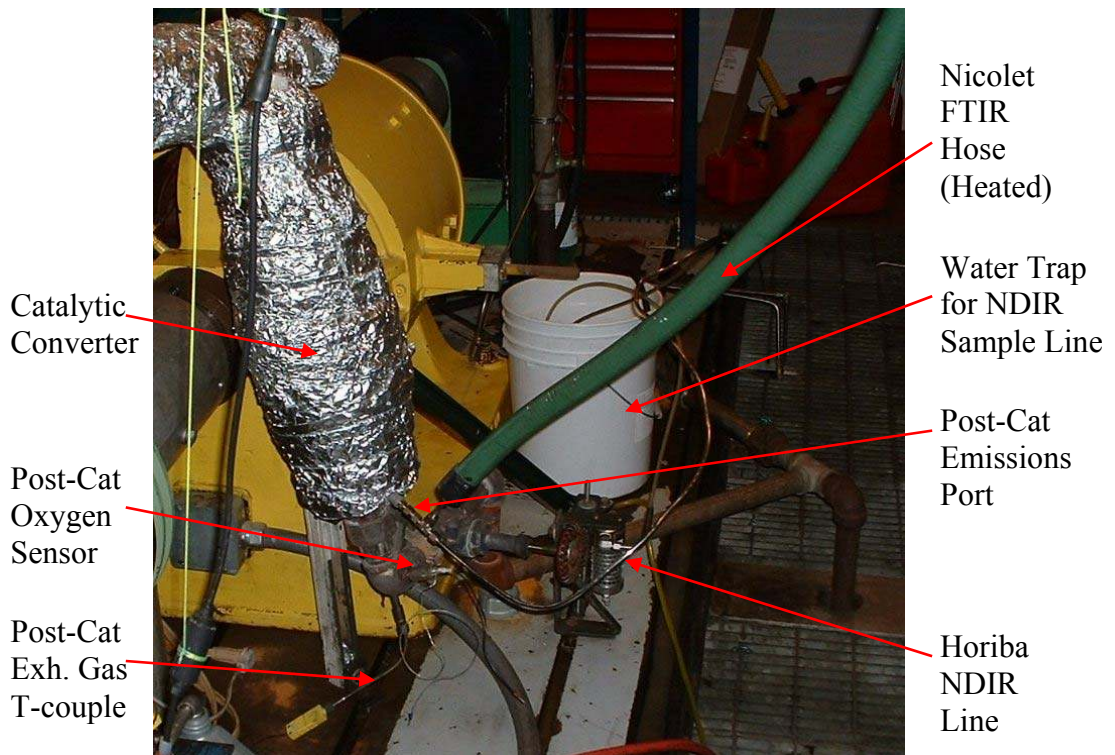
Figure 2.22. The lower portion of the exhaust line.

2.11 Emissions Measurement Equipment

2.11.1 Nicolet FTIR

An FTIR unit made by Nicolet is used to characterize NH_3, NO, N_2O, and CO emissions in the exhaust. This unit uses a heated sample line (100°C), and the gas cell and filter chambers are maintained at 160° C, so wet measurements are permitted. Wet measurements are required to accurately measure NH_3.

The FTIR total hydrocarbon reading was found to be unreliable on the first attempt to calibrate, so it is not used. The calibration gains for the remaining exhaust components were difficult to adjust, so instead, a rescaling factor was used for each component. The calibration gases used to find these rescaling factors are 1000 PPM CO in nitrogen, 4000 PPM NO in nitrogen, and 940 PPM NH_3 in nitrogen. The rescaling factor for CO is 8. This means that when the calibration gas containing 1000 PPM CO is fed into the FTIR, the CO reading is about 8000 PPM. Therefore, the actual CO concentration equals the FTIR reading divided by 8. For NH_3 and NO the rescaling factors are 5.55 and 5.25, respectively. The rescaling factors for H_2O and CO_2 are estimated to be somewhere between 5 and 7. The FTIR was used for measurements at the same gas cell temperature and pressure for which the rescaling factors were found. The FTIR unit was found to have no significant cross response with any of the measured components.

Figure 2.23 shows the N_2O calibration curve for the FTIR. Normally, N_2O concentrations of less than 100 PPM are expected for engine exhaust. In this range the FTIR response is linear, and the rescaling factor is about 4. However, in this study some of the N_2O measurements occur in the nonlinear response region.

The FTIR response was taken at various concentrations of N_2O in fresh air. For each point, a bag was filled with enough fresh air to occupy a ~5 gallon bucket, the inner dimensions of which were measured. A balloon was filled with the N_2O propellant from a chilled (to minimize moisture error), fresh whipped cream canister that lists N_2O as the sole propellant in the ingredients. A syringe with milliliter markings was then filled from the balloon. The syringe was used to squirt a measured quantity of N_2O into the bag. The contents of the bag were then mixed and fed into the FTIR.

38
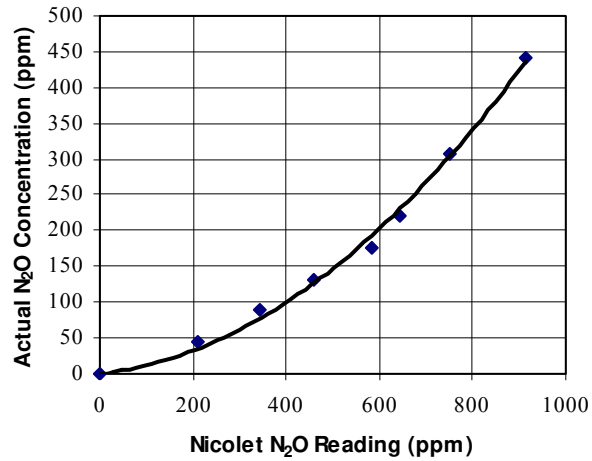
Figure 2.23. The FTIR's N_2O response.

Figure 2.24 shows the Nicolet FTIR. The FTIR uses a scanning interferometer which is sensitive to vibration. Vibration isolation was achieved by placing the FTIR onto aluminum slats. The slats were held up by bricks placed between the FTIR's points of contact on the slats.
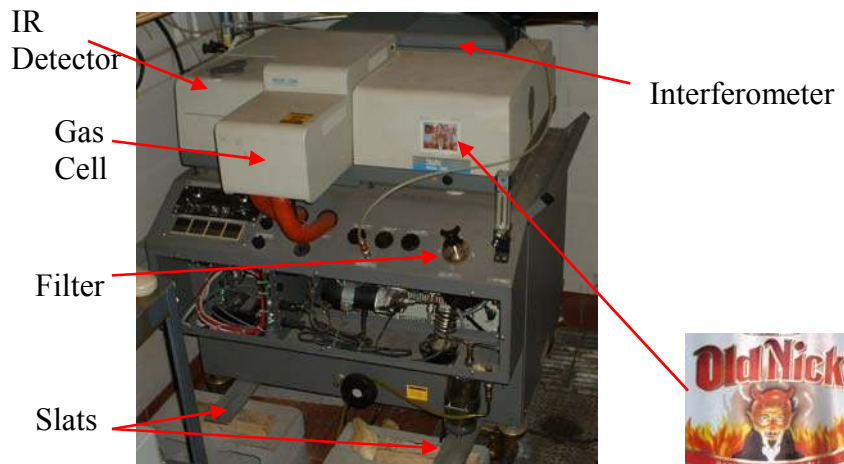
Figure 2.24. The Nicolet FTIR.

2.11.2 Horiba NDIR

An NDIR unit made by Horiba is used to measure hydrocarbon emissions in the exhaust. This unit is not heated and it does not tolerate liquid water, so a water trap was placed in the sample line for dry basis measurements. Figure 2.25 shows the water trap, which consists of a roll of metal tubing with a water collection chamber at the end, submerged in a bucket of ice water.

Figure 2.25. The water trap for the NDIR.

Figure 2.26 shows the Horiba NDIR, which reads hydrocarbon concentration in C_6 units to a resolution of 10 PPM. The NDIR unit was calibrated to read 290-300 PPM on a calibration gas consisting of 587 PPM propane in nitrogen. The NDIR's hydrocarbon reading has no cross response with NH_3, NO, N_2O, and CO.

Figure 2.26. The Horiba NDIR.

CHAPTER 3
PERFORMANCE RESULTS

3.1 Fuel Mix Map

3.1.1 Basic Features of the Fuel Mix Map

The CFR engine was run at fixed intake pressures, speeds and compression ratios as the fuel mix was varied, to demonstrate the basic features that emerge when gasoline is replaced with ammonia. For many combinations of load and compression ratio, MBT spark timing cannot be used with gasoline, because delayed combustion is required to avoid knock. When enough gasoline is replaced with ammonia, it becomes possible to use MBT spark timing. The MBT knock limit is the fuel mix at which the spark timing undergoes a transition from KLSA to MBT spark timing, as the replacement of gasoline with ammonia is increased. The replacement of gasoline with ammonia can be continued further until a rough limit is reached. A loss of combustion phasing controllability begins at the rough limit. A loss of efficiency can also occur if the replacement of gasoline with ammonia is taken beyond the rough limit. The fuel mix is expressed, as the fraction of gasoline's contribution to the total heat input, on a LHV energy basis. Equation 3.1 describes the gasoline fraction of the fuel mix b_e on a LHV energy basis, in %.

$$ b_e = \frac{\dot{m}_g Q_{LHVg}}{\dot{m}_g Q_{LHVg} + \dot{m}_a Q_{LHVa}} x100\% \quad \text{Eq. 3.1} $$

The COV(IMEPn) and net indicated thermal efficiency are plotted as a function of gasoline fraction in Figures 3.1, 3.2 and 3.3. The effect of fuel mix on the ignition delay, burn duration, and spark advance is also shown.

The fuel mix sweep shown in Figure 3.1 was obtained while running the CFR engine at 8:1, 1600 RPM and intake pressure = 80 kPa. Stoichiometric operation on 100% gasoline is featured in the rightmost data points. For operation on gasoline at this combination of load and compression ratio, MBT spark timing could not be maintained without causing knock. Note that the spark advance is less than the ignition delay for 100% gasoline, which shows that the spark timing is retarded of MBT. Whenever MBT spark timing is used, the spark advance is about 5-15 degrees greater than the ignition delay.

Figure 3.1. The effect of fuel mix on net indicated thermal efficiency, COV(IMEP_n), spark advance, ignition delay, and burn duration at 8:1, 1600 RPM, IMEP_n ~ 550 kPa.

The gasoline input was gradually replaced with ammonia until MBT spark timing could be maintained without knock, and this occurred at 87% gasoline/13% ammonia. This MBT knock limit is one of the two target combustion conditions, according to which the fuel mix was mapped as a function of load, speed, and compression ratio. The MBT

knock limit sets the upper limit on the gasoline input per cycle for knock-free, smooth firing with MBT spark timing.

The replacement of gasoline with ammonia was increased further, until an excessive roughness was observed. The $COV(IMEP_n)$ curve has a large, flat region, but the $COV(IMEP_n)$ increases rapidly with further replacement of gasoline with ammonia beyond the corner in the curve. The corner occurs where the $COV(IMEP_n)$ is about 3%. The rough limit is defined as the fuel mix at which the $COV(IMEP_n)$ reaches the chosen value of 3% in the region where further replacement of gasoline with ammonia causes the $COV(IMEP_n)$ to run away to higher values. The rough limit is the other target combustion condition, according to which the fuel mix was mapped as a function of load, speed and compression ratio. The rough limit sets the lower limit on the gasoline input per cycle for knock-free, smooth firing with MBT spark timing. The rough limit in Figure 3.1 was at 37% gasoline/63% ammonia.

The fuel mix sweep shown in Figure 3.2 was obtained at 12:1 compression ratio, 1600 RPM and intake pressure = 50 kPa. It is a lighter load and a higher compression ratio than that used in Figure 3.1. Operation on 100% gasoline at this light load is still possible at 12:1, but the spark must be retarded far from MBT to avoid knock. The fuel mix is 58% gasoline/42% ammonia at the MBT knock limit, and 53% gasoline/47% ammonia at the rough limit. The separation of the MBT knock limit and rough limit is much narrower at 12:1 than it is at 8:1.

The fuel mix sweep shown in Figure 3.3 was obtained at 9:1 compression ratio, 1000 RPM and WOT. It is a higher load and lower speed than that used in either Figure 3.1 or Figure 3.2. Operation on 100% gasoline required that the spark be retarded substantially from MBT to avoid knock. The fuel mix at the MBT knock limit was 57% gasoline/43% ammonia, and the fuel mix at the rough limit was 18% gasoline/82% ammonia. The $COV(IMEP_n)$ did not increase to large values with further fuel substitution beyond the rough limit but a leading edge could still be found. The rough limit is more difficult to find when the permitted substitution of gasoline with ammonia is high.
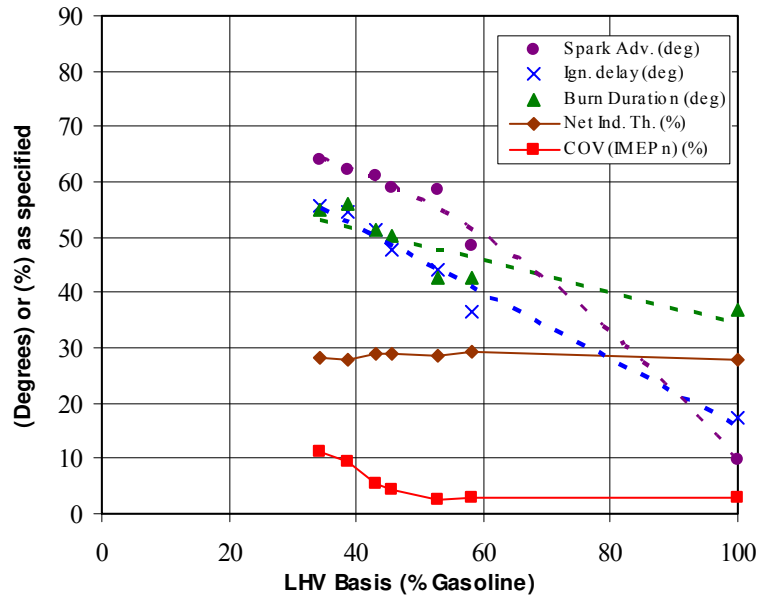
Figure 3.2. The effect of fuel mix on net indicated thermal efficiency, COV(IMEP$_n$), spark advance, ignition delay, and burn duration at 12:1, 1600 RPM, IMEP$_n$ ~ 260 kPa.
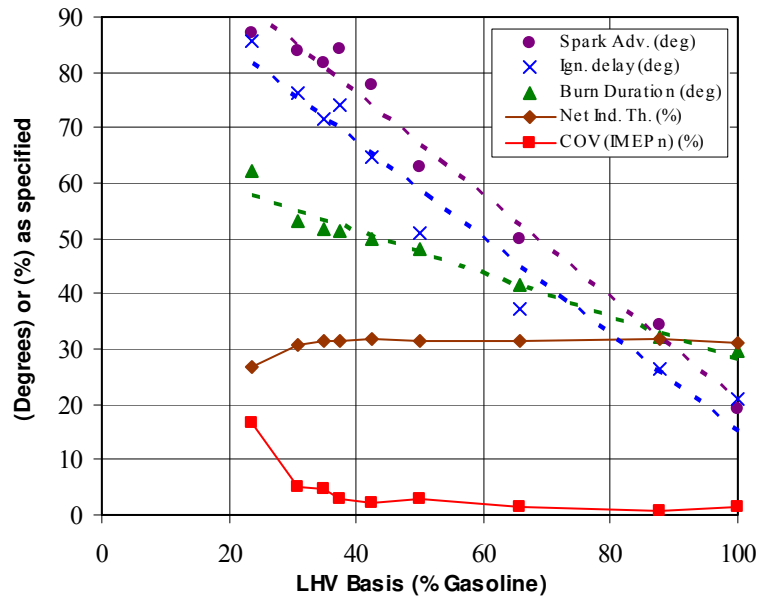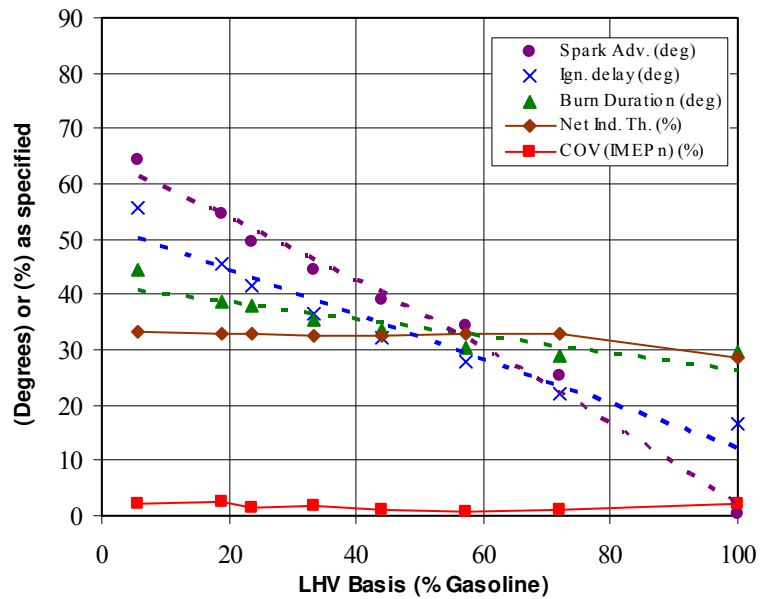

Figure 3.3. The effect of fuel mix on net indicated thermal efficiency, COV(IMEP$_n$), spark advance, ignition delay, and burn duration at 9:1, 1000 RPM, WOT, IMEP$_n$ ~ 700 kPa.

This leading edge could not always be found for supercharged operation at 1000 RPM and 1300 RPM. If the $COV(IMEP_n)$ remained at or below 2%, then the gasoline was turned off completely. Otherwise the engine was operated with a target $COV(IMEP_n)$ of 2.5% to 3% for all further results obtained at the rough limit.

Figures 3.1, 3.2, and 3.3 show that the burn duration and ignition delay depend linearly on the fuel mix, and that both become larger as more gasoline is replaced with ammonia while the load and speed are held constant. The burn duration and ignition delay get longer as more gasoline is replaced with ammonia, and this can be compensated with using more spark advance, up to the rough limit. When the replacement of gasoline with ammonia exceeds the rough limit, a loss of combustion phasing controllability and a loss of efficiency occur.

3.1.2 Relationship between Combustion Phasing, Fuel Mix Limits, and Efficiency

Figure 3.4 shows three sets of MFB_a curves. Each set consists of the first five individual cycles for an operating point. One set is shown for each: the 100% gasoline, MBT knock limit, and rough limit operating points from Figure 3.3. The 100% gasoline MFB_a curves show retarded combustion phasing because the spark had to be retarded from MBT to avoid knock. The MFB_a curves for the MBT knock limit are grouped tightly and show the optimum combustion phasing for best efficiency. Ammonia enables the use of MBT spark timing without knock, and this is why the ammonia is responsible for shifting the MFB_a curves back near TC for the MBT knock limit.

The net indicated thermal efficiency improved from 27.4% at 100% gasoline, to 32.7% at the MBT knock limit. If not enough ammonia is used to achieve knock-free combustion with MBT spark timing, then the efficiency goes down significantly whenever the spark must be retarded more than 10 degrees away from MBT. The net indicated thermal efficiency at the rough limit was 33.0%, which is not significantly different from the net indicated thermal efficiency at the MBT knock limit. The efficiencies are the same at the MBT knock limit, rough limit, and all points in between.
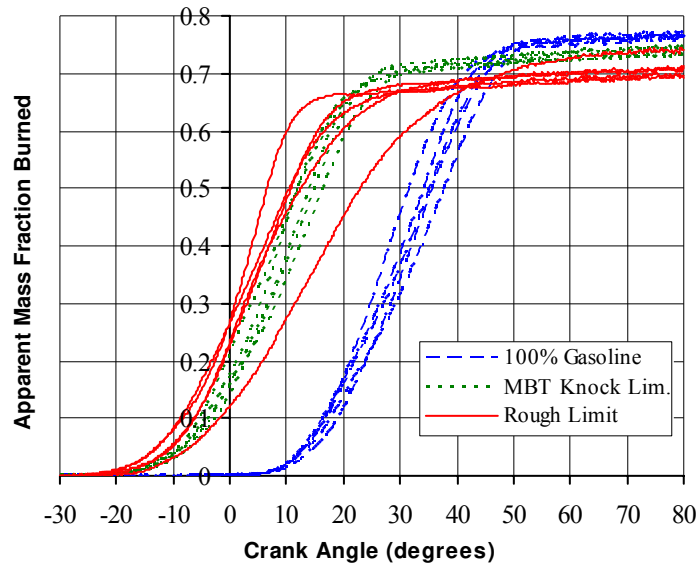
Figure 3.4. Sets of apparent mass fraction burned curves, showing the effect of ammonia on combustion phasing at 9:1, 1000 RPM, WOT.

The MFB_a curves for operation at the rough limit are grouped a bit loosely about both sides of the optimum placement. This combustion phasing variation causes the small cycle-to-cycle $IMEP_n$ variation at the rough limit. A small cycle-to-cycle ignition delay variation gets amplified into a larger combustion phasing variability as the burning progresses because the burn rate is affected by the expansion of the cylinder contents during combustion. An excessive cycle-to-cycle combustion phasing variability, which occurs when insufficient combustion promoter is used with ammonia, cannot be compensated by changing the spark advance. Figure 3.1 shows that a significant efficiency loss can occur if the $COV(IMEP_n)$ is allowed to exceed 5-10%.

Figure 3.5 shows three sets of pressure-volume curves. Each set consists of the first five individual cycles for an operating point. One set is shown for each: the 100% gasoline, MBT knock limit, and rough limit points from Figure 3.3. These pressure-volume curves correspond also to the 100% gasoline, MBT knock limit, and rough limit MFB_a curves in Figure 3.4.

The pressure-volume curves for 100% gasoline show the effect of retarded combustion phasing. The MBT knock limit curves show a more ideal shape that reflects the use of

MBT spark timing. The MBT knock limit curves are tightly grouped, and more closely approximate constant volume combustion, for which the work yield is maximized.
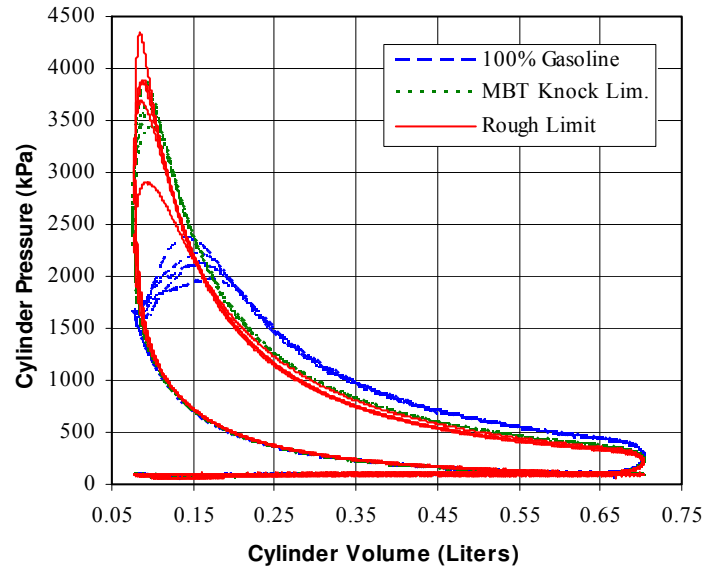
Figure 3.5. Sets of pressure-volume curves, showing the effect of ammonia on cylinder pressure at 9:1, 1000 RPM, WOT.

The rough limit curves are grouped more loosely about both sides of the optimum placement. The pressure variation from cycle to cycle is caused by the variation of combustion phasing at the rough limit. The $IMEP_n$ differed little among the individual cycles despite the large variation in the peak pressure above and below the optimum. The highest $IMEP_n$ yield for an individual cycle within the set of 60 cycles occurred for one cycle with a peak pressure near 3700 kPa.

3.1.3 Fuel Substitution at the Rough Limit

Operation at the rough limit maximizes the replacement of gasoline with ammonia. The rough limit is preferred when the goal is to maximize the displacement of liquid hydrocarbon fuels with ammonia when the production capacity for ammonia is unlimited. The rough limit would also be preferred when using combustion promoters that penalize

vehicle design excessively when stored on-board in large quantities, such as high pressure hydrogen gas.

The rough limit is a hard limit, which means that if not enough gasoline or other combustion promoter is used with ammonia, then the engine will operate in an undesirable way that cannot be corrected by changing the spark advance. Engine operation at a target COV(IMEP$_n$) ≈ 3% ensures acceptable combustion stability without loss of thermal efficiency or power, while minimizing the use of gasoline or other combustion promoter.

The total specific fuel input is used as the load axis when plotting things related to the properties of fuels. The total specific fuel input is the total (ammonia plus gasoline) fuel LHV energy per cycle, divided by the displaced volume. Equation 3.2 describes the total specific fuel input, and the units are Joules per liter.

$$\text{Total Specific Fuel Input} = \frac{\dot{m}_g Q_{LHVg} + \dot{m}_a Q_{LHVa}}{V_d} \times \frac{2}{f_{rpm}} \qquad \text{Eq. 3.2}$$

The usefulness of ammonia as a fuel was characterized by how compression ratio, speed, and load affect the fuel mix at the rough limit. The CFR engine was run at the rough limit for 8:1, 10:1 and 12:1, at speeds of 1000 RPM, 1300 RPM, and 1600 RPM. A load sweep was done for each of the 9 combinations of compression ratio and speed. Each load sweep started with marginal operation at idle with a fuel mix of nearly all gasoline. As the load was increased, the ammonia input was increased, and the gasoline input and spark advance required only small adjustments to maintain operation at the rough limit. The gasoline input per cycle for all points in a load sweep was not much larger, and often smaller, than that required at idle. The rough limit was not found for 14:1 and 16:1, for reasons that are explained later. With small corrections made to the gasoline input at each point, the engine could have been run at a constant MBT spark timing for each whole load sweep. The average spark advance for the load sweeps is shown in Table 3.1. All spark timing numbers are in degrees BTC.

	1000 RPM	1300 RPM	1600 RPM
8:1	62 degrees	70 degrees	76 degrees
10:1	55 degrees	69 degrees	71 degrees
12:1	51 degrees	59 degrees	65 degrees

Table 3.1. The average MBT spark advance at the rough limit.

Figures 3.6 and 3.7 show the fuel mix at the rough limit. They contain the same data, but Figure 3.6 groups the data by compression ratio, whereas Figure 3.7 groups it by speed. The data in each compression ratio group are uniformly distributed among the three speeds, and the data in each speed group are uniformly distributed among the three compression ratios.

The gasoline input was shut off completely whenever the rough limit could not be found. The points, for which the rough limit could not be found, are a special case, and these points depart discontinuously from the overall rough limit fuel mix trends. The gasoline could not be shut off for any points at 1600 RPM. The points for which the gasoline was shut off were not used to calculate the trend curves for the fuel mix at the rough limit.
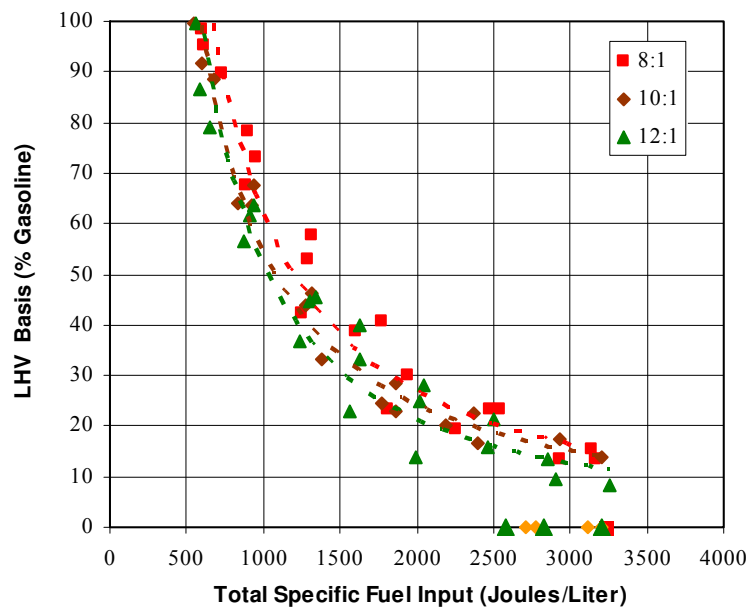
Figure 3.6. Fuel mix at the rough limit, grouped by compression ratio.

49

The fuel mix at the rough limit has a surprisingly weak dependence on compression ratio, given its strong dependence on load. It was anticipated that combinations of load and compression ratio, for which the compressed charge energy density near TC is the same, would have the same fuel mix at the rough limit. For that reason it was expected that the rough limit fuel mix would respond to compression ratio as strongly as it did to load, but it did not. Figure 3.7 shows that the gasoline requirement increases as the engine speed is increased.
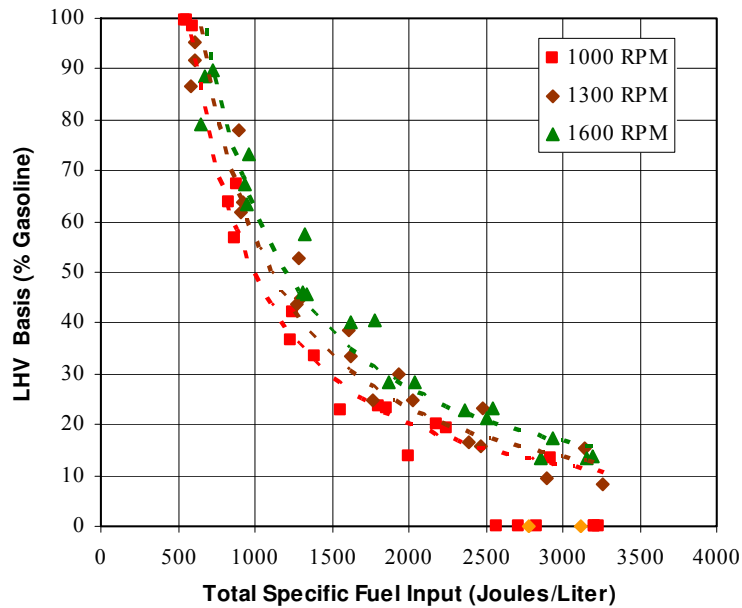
Figure 3.7. Fuel mix at the rough limit, grouped by speed.

Both the load and the compression ratio contribute multiplicatively to the compressed charge energy density near TC, where much of the combustion occurred. Strong compression ratio trends should be expected for events that occur within ±20 degrees. The burn interval obtained for all of the operating points at the rough limit was between about -10 and +40 degrees crank angle, so much of the burn interval was within that ±20 degree window. Caris and Nelson (1959) obtained a similar burn interval for the same compression ratio range.

The fuel mix trends suggest that the fuel mix at the rough limit is determined by the compressed charge energy density at the spark, and not the charge density near TC, and

not the residual fraction either. Equation 3.3 describes the instantaneous compressed charge energy density as a function of crank angle. The units for the instantaneous compressed charge energy density are Joules per liter.

$$\text{Compressed Charge Energy Density} = \frac{\dot{m}_g Q_{LHVg} + \dot{m}_a Q_{LHVa}}{V\{\theta\}} \times \frac{2}{f_{rpm}} \qquad \text{Eq. 3.3}$$

$$= \text{Total Specific Fuel Input} \times \frac{V_d}{V\{\theta\}}$$

The instantaneous compressed charge energy density is equal to a quantity associated with load (Total Specific Fuel Input), times the ratio of displaced volume to instantaneous volume. Figure 3.8 shows the ratio of displaced volume to instantaneous volume, as a function of crank angle. Note that at 0 degrees the ratio is the compression ratio minus 1.
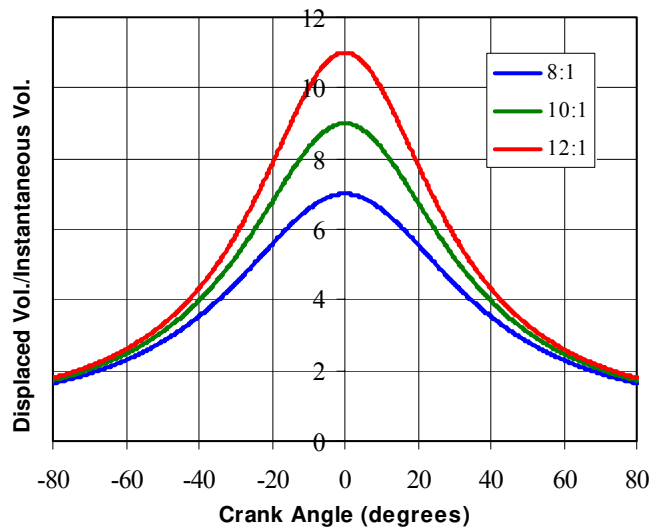
Figure 3.8. The ratio of displaced volume to instantaneous volume.

Ammonia's long ignition delay places the MBT spark in a crank angle region where the compression ratio has little effect on the instantaneous compressed charge energy density. The MBT spark advance was 50 degrees or more BTC ($\theta < $ -50 degrees) for all points at the rough limit. In this crank angle region, the instantaneous compressed charge energy density is still proportional to load, and crank angle has some effect, but the explicit dependence on compression ratio is very weak.

The observed trends for the rough limit fuel mix can be explained by the effect of compression ratio and engine speed on the compressed charge energy density at the spark. Equations 3.4 and 3.5 describe the compressed gasoline and ammonia energy densities at the spark. The units are kilojoules per liter.

$$\text{Gasoline Energy Density at Spark} = \frac{\dot{m}_g Q_{LHVg}}{V\{\theta_{spark}\}} \times \frac{2}{f_{rpm}} \times 0.001 \qquad \text{Eq. 3.4}$$

$$\text{Ammonia Energy Density at Spark} = \frac{\dot{m}_a Q_{LHVa}}{V\{\theta_{spark}\}} \times \frac{2}{f_{rpm}} \times 0.001 \qquad \text{Eq. 3.5}$$

Longer ignition delay and burn duration occur with increasing speed, or decreasing compression ratio, which increases the MBT spark advance (see Table 3.1). The increased MBT spark advance at higher speeds, or lower compression ratios, reduces the compressed fuel energy densities at the spark. Figure 3.9 show the compressed gasoline energy density at the spark at the rough limit, grouped by compression ratio. The effect of ammonia is also shown. The points for which either the gasoline or ammonia input was zero, depart discontinuously from the trends for dual fueled operation, and are not shown.
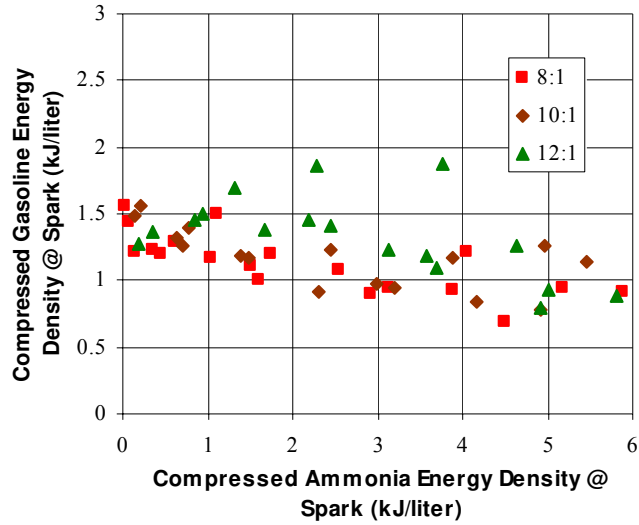
**Figure 3.9. The compressed gasoline energy density
at the spark at the rough limit.**

The presence of more ammonia at the spark appears to have a very weakly positive effect on ignitability, because a slightly lower gasoline density is permitted as the ammonia input is increased.   The 8:1 and 10:1 groups coincide, but the 12:1 group required a greater gasoline energy density at the spark, which suggests that as the compression ratio is raised to 12:1 and beyond, something other than ignitability at the spark is beginning to affect the rough limit.

Equation 3.6 describes the instantaneous expansion ratio from TC. Figure 3.10 shows a graph of Equation 3.6. As the compression ratio is raised, the crank angle duration for maximum confinement gets shorter. The compressed charge reaches an expansion ratio of 2 about 10 degrees earlier at 12:1 than it does at 8:1. The shorter confinement duration and increasing effect of heat loss are probably responsible for the lost return on reducing the required gasoline input per cycle as the compression ratio is raised above 10:1.

$$\text{Instantaneous Expansion Ratio from TC} = \frac{V\{\theta\}}{V\{0°\}} \qquad \text{Eq. 3.6}$$
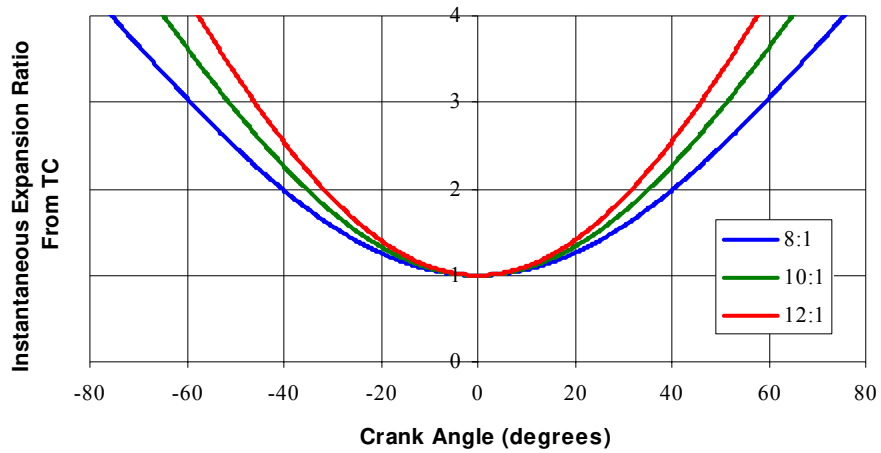
Figure 3.10. The instantaneous expansion ratio from top center.

Figure 3.11 shows the combined 8:1 and 10:1 points from Figure 3.9, grouped by speed. The speed trend disappears when the rough limit fuel mix is plotted in these coordinates.
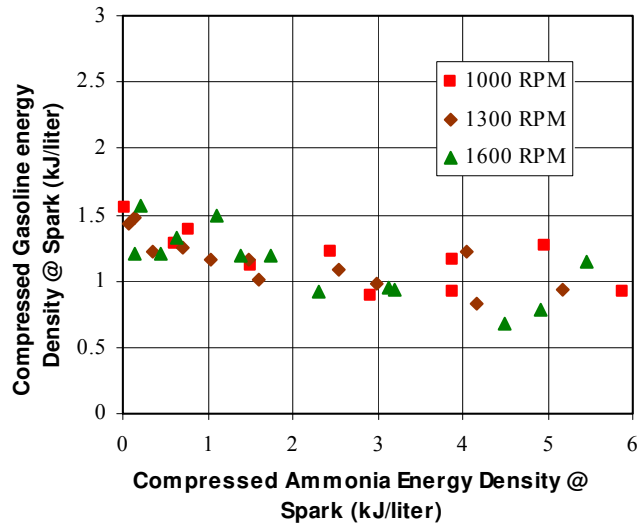
**Figure 3.11. The 8:1 and 10:1 points from
Figure 3.9, grouped by speed.**

A rough limit constant for gasoline and ammonia emerges from the data in Figure 3.11. In the limit that the ammonia input goes to zero, the compressed gasoline energy density

at the spark approaches 1.5 kilojoules per liter. This value would also be sufficient for operation near the rough limit when the ammonia input is not zero. This constant will most likely be different for another combustion promoter, such as hydrogen.

Rough Limit Constant for Gasoline and Ammonia:

Compressed Gasoline LHV Energy Density at the Spark = 1.5 kJ/L.

A similar rough limit map for ammonia promoted with E85 (mostly ethanol) was studied by Rakesh Leeladhar. Figure 3.12 shows the compressed E85 energy density at the spark for rough limit operation. For 8:1, 10:1 and 12:1 the target $COV(IMEP_n)$ was 3%. At 14:1 the target $COV(IMEP_n)$ was 4% because knock disallowed operation at the 3% target. The compressed E85 densities for 14:1 would have been even higher if the 3% target could have been maintained at 14:1.
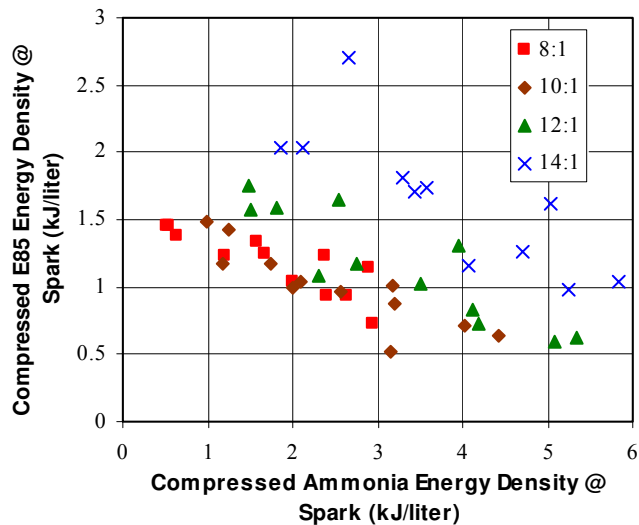
Figure 3.12. The compressed E85 energy density at the spark at the rough limit. (From a study done by Rakesh Leeladhar)

For E85 the points at 8:1 and 10:1 coincide, and the rough limit constant for E85 and ammonia is also about 1.5 kJ/L. It is also clear that effects, other than compressed fuel energy densities at the spark, are affecting the rough limit at 12:1, and even more so at 14:1.

Gasoline probably could be replaced with ammonia to a greater extent if the ignition delay and burn duration were shortened, thereby increasing the charge compression at the ignition event. Plasma jet ignition reduces the ignition delay by about 10 degrees, relative to that obtained with standard spark ignition [Dale and Oppenheim, 1981]. Cornelius et al. (1965) and Graves and Hodgeson (1975) found that dual ignition improves the high-speed power, efficiency, and pressure trace consistency for operation on ammonia without combustion promoter.

3.1.4 Fuel Substitution at the MBT Knock Limit

Operation at the MBT knock limit uses the minimum ammonia input required to enable knock-free combustion with MBT spark timing. Operation at the MBT knock limit is preferred when the available ammonia production capacity is limited, or when the LHV energy equivalent as ammonia costs as much or more than gasoline, either in units of currency per unit of fuel energy or in units of carbon dioxide released from well to wheels per unit of fuel energy. The ratio of Joules of gasoline saved per Joule of ammonia consumed will be maximized when most of the gasoline savings comes from an overall brake thermal efficiency improvement, achieved by shifting the operating envelope to higher mean effective pressures, at which the engine still burns mostly gasoline most of the time.

The MBT knock limit is a soft limit, which means that satisfactory engine operation above the MBT knock limit can be achieved by changing the spark timing, as required to avoid knock. If the gasoline input per cycle is greater than the maximum permitted for using MBT spark timing, then the spark can be retarded from MBT to avoid knock. Retarded combustion allows the use of more gasoline, but it also reduces the efficiency,

similar to reducing the compression ratio. The post-combustion expansion ratio no longer tracks the compression ratio closely when the spark is retarded from MBT.

Satisfactory engine operation can be achieved with retarded combustion, with some efficiency penalty, as long as the combustion phasing is not delayed from the optimum placement by more than about 20 or 30 degrees. This criterion ultimately limits how far above the MBT knock limit the engine can be run. It also limits the maximum load that can be reached when running the engine on gasoline.

Figure 3.13 shows the fuel mix at the MBT knock limit for different loads and compression ratios. The CFR engine was run at the MBT knock limit at compression ratios of 8:1, 10:1, 14:1 and 16:1, and speeds of 1000, 1300 and 1600 RPM. It was already observed that the 12:1 points from Figure 3.6 had very little or no margin for error between the MBT knock and rough limits, and so they were used again in Figure 3.13. There was insufficient speed dependence in the knock properties of ammonia, gasoline, and air mixtures for a significant speed trend to be shown, so all speeds are lumped together.
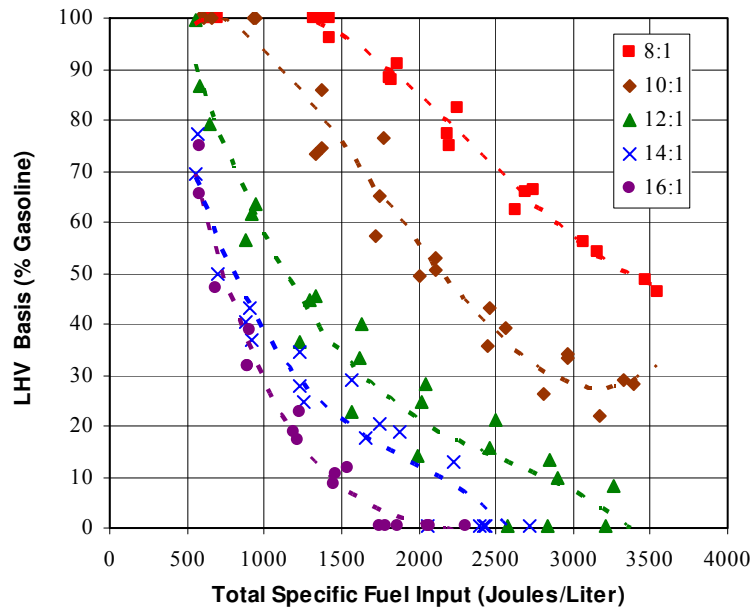
Figure 3.13. Fuel mix at the MBT knock limit.

57

For a given compression ratio, the octane requirement goes up as the load is increased. For a given load, the octane requirement goes up as the compression ratio is increased. The knock resistance of the intake mixture increases with increasing replacement of gasoline with ammonia. The fuel mix at the MBT knock limit meets the octane requirement at each combination of load and compression ratio. The fuel mix at the MBT knock limit is strongly dependent on both compression ratio and load because incipient knock generally occurs near peak pressure, and the peak pressure was always within the ± 20 degree window where both the compression ratio and the load have a strong effect on the compressed charge density.

3.1.5 MBT Knock Limit and Rough Limit Crossover

Smooth, knock-free combustion with MBT spark timing and the best thermal efficiencies occur when the gasoline content is greater than or equal to the minimum required at the rough limit, and less than the maximum permitted at the MBT knock limit. Figure 3.14 shows the placement of the rough limit points for 8:1 and 10:1 (hollow triangles) among the MBT knock limit points for all compression ratios.

A crossover, with respect to compression ratio, occurs where the permitted gasoline content at the MBT knock limit becomes less than the required gasoline content at the rough limit. For 8:1 and 10:1, the desired operating window exists below the solid data points for each compression ratio and within or above the region occupied by the hollow triangle points. At 10:1 this window width is about half of that at 8:1. At 12:1 the margin for error between the rough and MBT knock limits is very small or zero, for all loads and speeds.

At 14:1 and 16:1 the desired operating window has a negative width. It was not possible to add enough gasoline to provide adequate ignitability at the spark, without causing knock near TC at 14:1 and 16:1, and most of these points had a COV(IMEP$_n$) between 4% and 7%, although a few went up to 15%. For that reason 12:1 is considered the upper compression ratio limit for an engine that runs on ammonia promoted with gasoline. However, it is undesirable for an engine to have a vanishingly small margin of

error between the MBT knock limit and rough limit. The fuel mix trends indicate a desired compression ratio of less than 12:1 for an ammonia and gasoline dual fueled spark ignition engine.
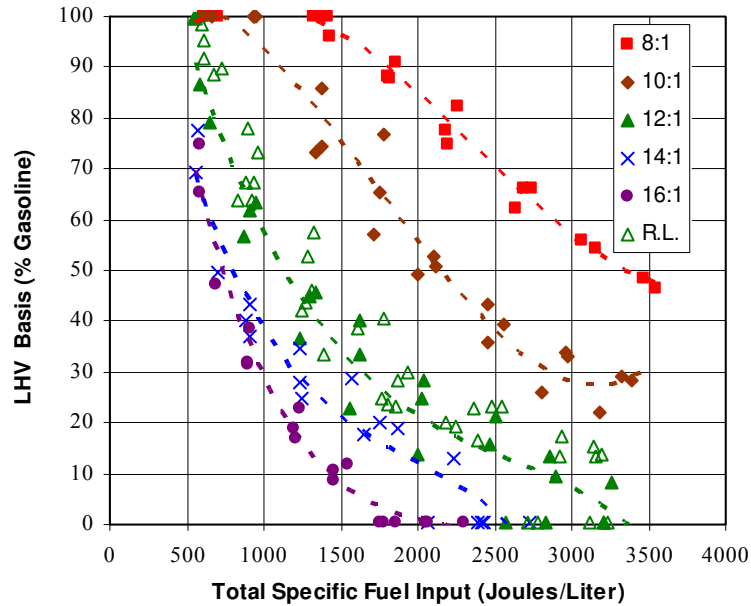
Figure 3.14. Fuel mix at the MBT knock limit (solid shapes) and the combined 8:1 and 10:1 rough limit points from Figure 3.6 (hollow triangles).

3.1.6 Rough Limit and MBT Knock Limit Plotted by Specific Gasoline Input

Equations 3.7 and 3.8 describe the specific gasoline input and specific ammonia input, respectively. The specific gasoline input is the partial LHV energy input from gasoline per cycle, divided by the displaced volume, and the specific ammonia input is the partial LHV energy input from ammonia per cycle, divided by the displaced volume. For each the units are Joules per liter.

$$\text{Specific Gasoline Input} = \frac{\dot{m}_g Q_{LHVg}}{V_d} \times \frac{2}{f_{rpm}} \qquad \text{Eq. 3.7}$$

$$\text{Specific Ammonia Input} = \frac{\dot{m}_a Q_{LHVa}}{V_d} \times \frac{2}{f_{rpm}} \qquad \text{Eq. 3.8}$$

The specific gasoline input was plotted in Figures 3.15, 3.16, and 3.17 to show the MBT knock and rough limits another way. The heavy, dashed line in each figure represents operation on 100% gasoline. The specific gasoline input equals the total specific fuel input on this line. The specific ammonia input equals a point's horizontal distance to the right of the 100% gasoline line.
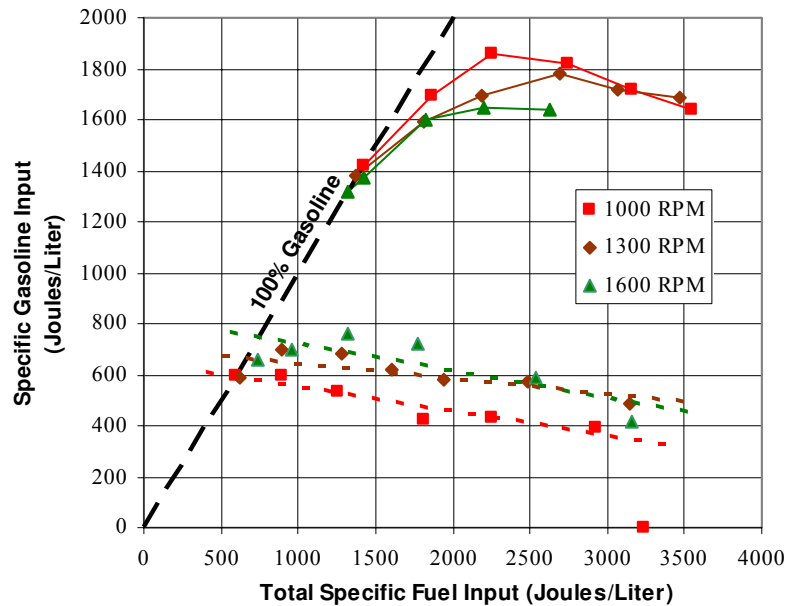
Figure 3.15. Specific gasoline input at the 8:1 rough limit (dashed trend lines) and MBT knock limit (solid curves).

Adequate flammability was achieved for operation on 100% gasoline, at a given speed, where the rough limit trend line for that speed intersects with the 100% gasoline line. This intersection is the ammonia cut-in point at the rough limit. For 8:1 and 10:1 the load could have been increased from the ammonia cut-in point by increasing the specific ammonia input while holding the specific gasoline input constant, and that would have been sufficient for operation near the rough limit, because the actual rough limit lines

point downward from the ammonia cut-in points. Operation at 12:1 is not recommended because of the rough limit/MBT knock limit crossover at 12:1.
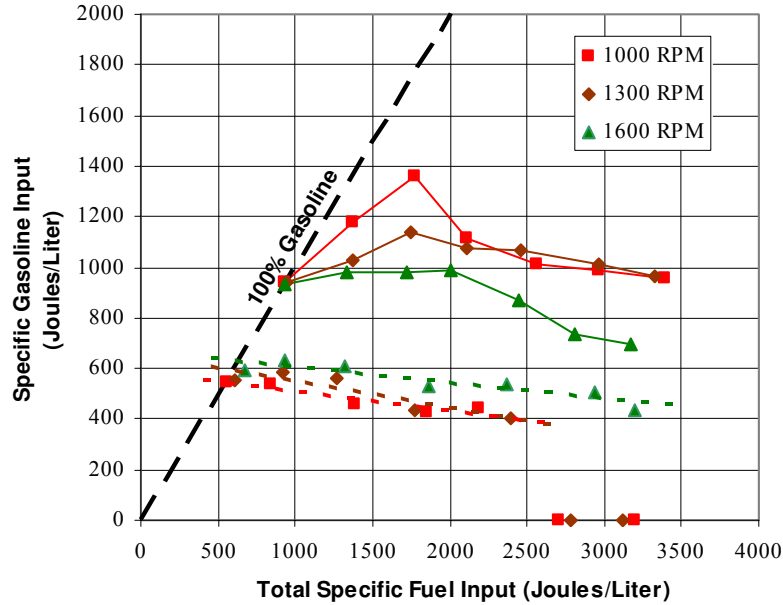
Figure 3.16. Specific gasoline input at the 10:1 rough limit (dashed trend lines) and MBT knock limit (solid curves).

Similarly, operation near the MBT knock limit can be achieved by running the engine on 100% gasoline for points to the left of the MBT knock limit departures from the 100% gasoline line near 1430 and 940 Joules per liter for 8:1 and 10:1, respectively. The load can be increased from the MBT knock limit's departure from the 100% gasoline line by adding more ammonia while holding the gasoline input substantially constant.

The maximum load for which MBT spark advance can be used while running on 100% gasoline occurs where the MBT knock limit curves intersect the 100% gasoline line. KLSA must be used for operation in the region above the MBT knock limit curves. Smooth firing with MBT spark timing can be obtained at 8:1 and 10:1 for operation within the region between the MBT knock limit curves and the rough limit trend lines. The engine fires with an excessive COV(IMEP$_n$) for operation within the region below the rough limit trend lines, except for those points shown at which the gasoline input is zero. The region between the rough limits and MBT knock limits is about half as wide at

10:1 as it is at 8:1. At 12:1 the rough limits and MBT knock limits are very nearly the same.
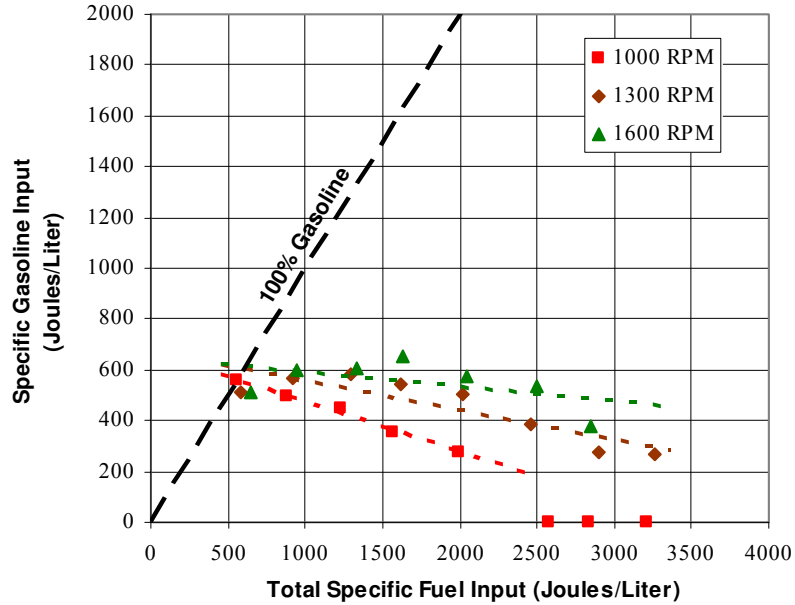
**Figure 3.17. Specific gasoline input
at the 12:1 rough limit.**

The specific gasoline input at the rough limit ammonia cut-in points is shown in Figure 3.18. The rough limit ammonia cut-in points are the intersections between the rough limit trend lines and the 100% gasoline line in Figures 3.15, 3.16 and 3.17. The required gasoline input goes up with increasing speed. Raising the compression ratio from 8:1 to 10:1 reduces the gasoline requirement, but no significant reduction occurs as the compression ratio is raised from 10:1 to 12:1. The specific gasoline input at the rough limit ammonia cut-in point is nearly the same as that required for operation on 100% gasoline at idle.
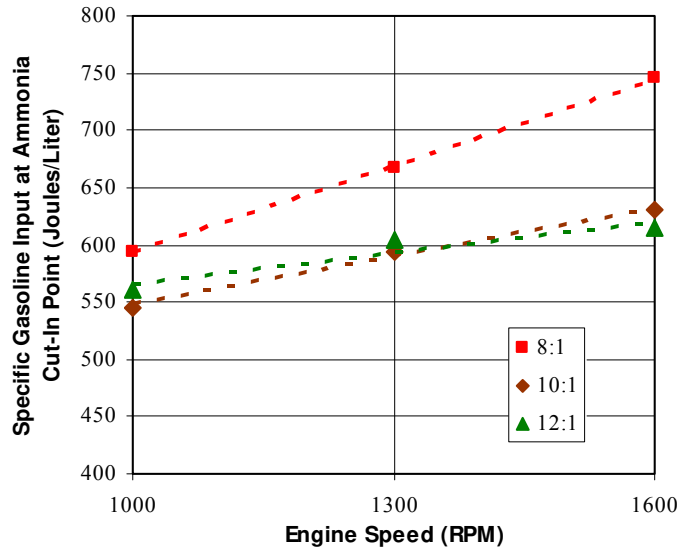
**Figure 3.18. Specific gasoline input at the
rough limit ammonia cut-in points.**

Figure 3.19 shows the specific E85 input for the ammonia cut-in points at the rough limit for E85/ammonia operation, studied by Rakesh Leeladhar. For 8:1, 10:1 and 12:1 the COV(IMEP$_n$) ≈ 3%.   At 14:1 the COV(IMEP$_n$) ≈ 4% because knock disallowed operation at the 3% target. If the actual 3% target could have been reached, then the E85 input at 14:1 would have been higher than that shown.   Once again, the required combustion promoter input went up with increasing speed. Raising the compression ratio from 8:1 to 10:1 reduced the E85 requirement, but there was a diminished return for reducing the E85 requirement as the compression ratio was raised above 10:1.

The specific combustion promoter input at the rough limit ammonia cut-in points is very nearly the same for E85 as it is for gasoline. Therefore, the potency of E85 as a combustion promoter for ammonia is very nearly the same as the potency of gasoline as a combustion promoter for ammonia.
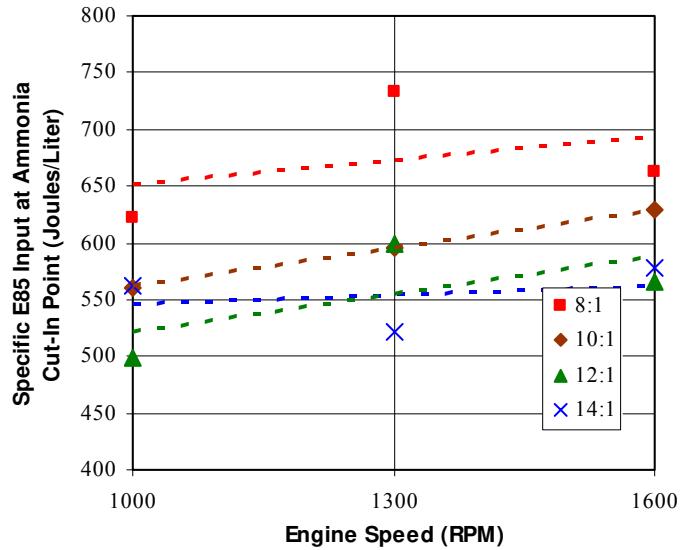
**Figure 3.19. Specific E85 input at the
rough limit ammonia cut-in points.
(From a study done by Rakesh Leeladhar)**

3.2 Efficiency

3.2.1 Gross Indicated Thermal Efficiency

The gross indicated thermal efficiency is the closest experimental analog to the theoretical Otto cycle efficiency. The Otto cycle consists of adiabatic compression of a fuel/air charge through a fixed compression ratio r_c, constant-volume combustion, and adiabatic expansion back to the original volume. Equation 3.9 describes the ideal Otto cycle thermal efficiency in %. The efficiency of the ideal Otto cycle increases monotonically as the compression ratio is raised.

$$\text{Theoretical Otto Cycle Efficiency} = (1 - \frac{1}{r_c^{\gamma-1}}) \times 100\% \qquad \text{Eq 3.9}$$

The features in the gross indicated thermal efficiency trends are explored, and the experimental results are compared to theory. In all cases, the gross indicated thermal efficiency does not significantly depend on the engine speed, so all speeds (1000, 1300 and 1600 RPM) are lumped together. All gross indicated thermal efficiency data are uniformly distributed among the three speeds.

The gross indicated mean effective pressure (IMEP$_g$) is the effective driving pressure for the compression and expansion portions of the work cycle. Equation 3.10 describes the IMEP$_g$, and the units are kilopascals. The bounds on the integral are degrees crank angle. Equation 3.11 describes how the experimental gross indicated thermal efficiency is calculated, in %.

$$\text{IMEP}_\text{g} = \frac{1}{V_d} \int_{-180°}^{180°} P dV \qquad \text{Eq. 3.10}$$

$$\eta_{ig} = \frac{IMEP_g \times V_d}{(\dot{m}_g Q_{LHVg} + \dot{m}_a Q_{LHVa})} \times \frac{f_{rpm}}{2} \times 100\% \qquad \text{Eq. 3.11}$$

For operation on gasoline, increasing spark retard from MBT with increasing load is required to avoid knock. When the combustion is significantly retarded from MBT, then the corresponding modified Otto cycle consists of adiabatic compression through the ratio r_c, then slight adiabatic re-expansion without combustion, then constant volume combustion at reduced compression, and finally adiabatic expansion back to the original volume. The theoretical efficiency of the Otto cycle with retarded combustion is the same as it would be if the actual post-combustion expansion ratio were to be used in the formula in place of r_c. Figure 3.20 shows how the experimental gross indicated thermal efficiency for gasoline varies with increasing spark retard from MBT. Increasing spark

retard away from MBT corresponds also to increasing load. The spark retard from MBT was calculated from Equation 2.5.
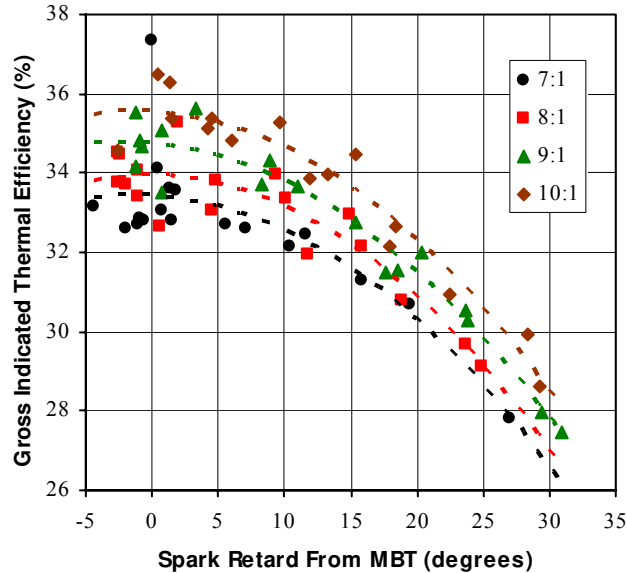
Figure 3.20. The gross indicated thermal efficiency for gasoline, plotted as a function of spark retard away from MBT.

The effect of retarded combustion on efficiency is similar to the effect obtained by reducing the compression ratio, because the post-combustion expansion ratio is reduced similarly by both. A combustion phase delay of 15 degrees away from optimum has the same effect as a reduction of two compression ratio numbers, according to Figure 3.20.

Figure 3.21 shows the spark retard from MBT as a function of $IMEP_g$ for gasoline. MBT spark timing was used for points near zero on the vertical axis. The transition from MBT spark timing to KLSA occurs at a lower load with increasing compression ratio. The maximum attainable load is also reduced as the compression ratio is raised. Rapidly declining efficiencies with increasing load, and a diminished return on additional power, with further attempts to increase the load, occur when the combustion is delayed by about 20-30 degrees. This range of delay occurs at mean effective pressures that are about 200 kPa lower at 10:1 than they are at 7:1. The post-combustion expansion ratio decreases with increasing load as a consequence of spark timing settings required to avoid knock at a given compression ratio. Lowering the compression ratio, also reduces the post-

66

combustion expansion ratio, but permits operation at higher loads at a given combustion phasing. The knock constraint thus places an inherent limitation on the thermal efficiencies and the power density attainable for operation on gasoline.
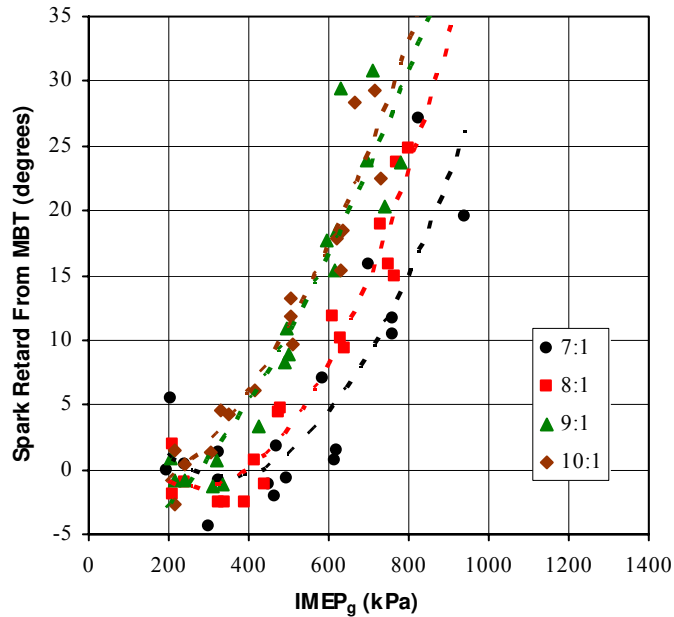
Figure 3.21. The spark retard away from MBT, plotted as a function of IMEP$_g$ for gasoline.

Figure 3.22 shows the gross indicated thermal efficiency as a function of IMEP$_g$ for operation on gasoline. For IMEP$_g$ < 300 kPa, MBT spark timing can be used for all compression ratios up to 10:1, and the gross indicated thermal efficiency goes up with increasing compression ratio because the post-combustion expansion ratio tracks the compression ratio. For IMEP$_g$ > 600 kPa the spark must be retarded further from MBT with increasing compression ratio at a given IMEP$_g$. The compression ratio trend reverses there because the combination of effects reduces the post-combustion expansion ratio as the compression ratio is raised in this load range.
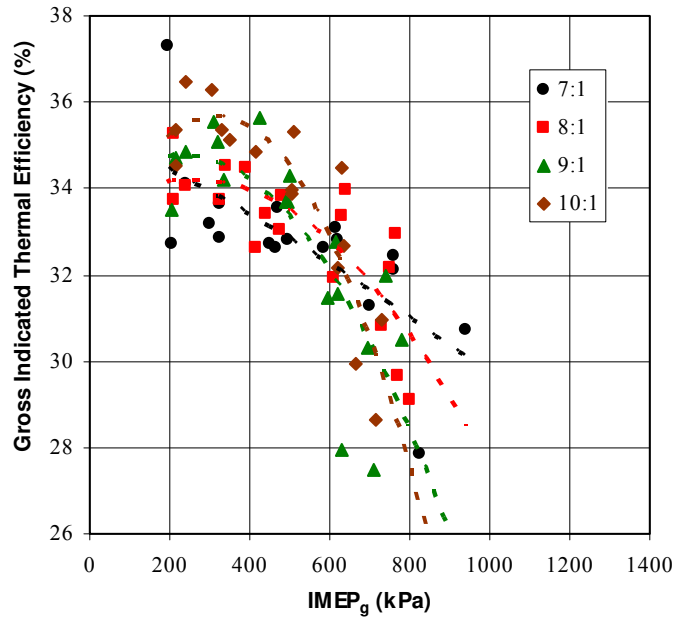
**Figure 3.22. The gross indicated thermal efficiency,
plotted as a function of IMEP$_g$ for gasoline.**

Figures 3.23 and 3.24 show the gross indicated thermal efficiency for dual fueled operation at the rough limit and MBT knock limit, respectively. These are the same operating points for which the fuel mix was characterized at the rough limit and MBT knock limit. The gross indicated thermal efficiency goes up slightly with increasing load, probably because the heat loss becomes a smaller fraction of the total charge energy, with increasing load. For 8:1 and 10:1, the gross indicated thermal efficiency was slightly, but not significantly better for operation at the rough limit than for operation at the MBT knock limit.

For 8:1 and IMEP$_g$ = 800 kPa, the gross indicated thermal efficiency for gasoline is about 29-31%, and for dual fuel the gross indicated thermal efficiency is about 33-35%. For 8:1 and IMEP$_g$ = 200 kPa, the gross indicated thermal efficiencies for gasoline and dual fuel are about the same, near 33-35% For 10:1 and IMEP$_g$ = 700 kPa, the gross indicated thermal efficiency for gasoline is about 29-31%, and for dual fuel the gross indicated thermal efficiency is about 35-36%. For 10:1 and IMEP$_g$ = 200 kPa, the gross indicated thermal efficiencies for gasoline and dual fuel are about the same, near 34-36% The high load efficiencies clearly show that ammonia makes a significant difference.
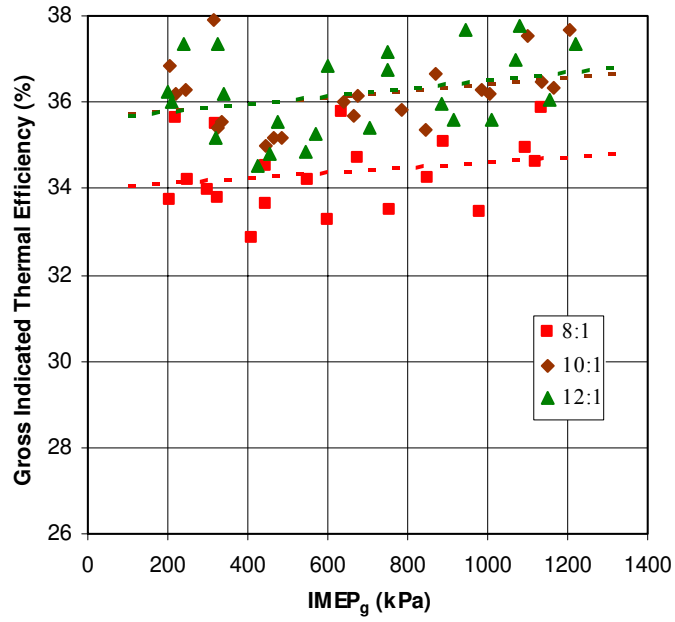
Figure 3.23. The gross indicated thermal efficiency for dual fueled operation at the rough limit.
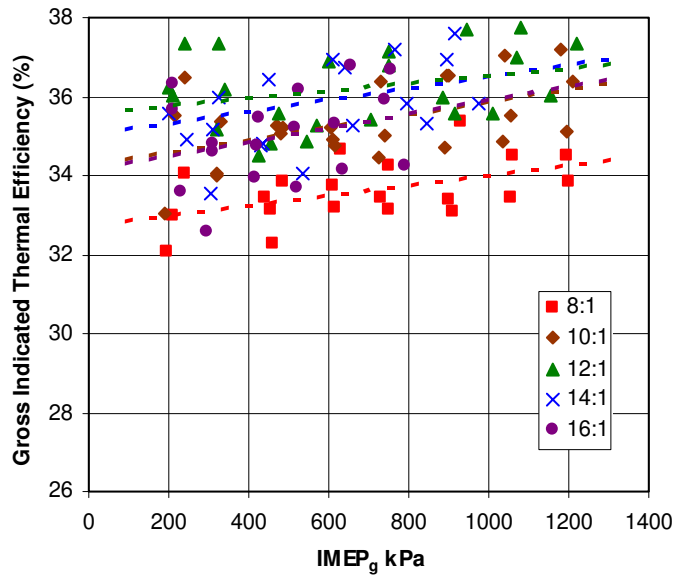
Figure 3.24. The gross indicated thermal efficiency for dual fueled operation at the MBT knock limit.

69

The best fit lines from Figures 3.23 and 3.24 were evaluated at $IMEP_g = 700$ kPa, which is near WOT. These values at $IMEP_g = 700$ kPa were used to generate the efficiency trend curve in Figure 3.25. The 12:1 line is the same in Figures 3.23 and 3.24. The average of the rough limit and MBT knock limit efficiencies was used for 8:1 and 10:1.
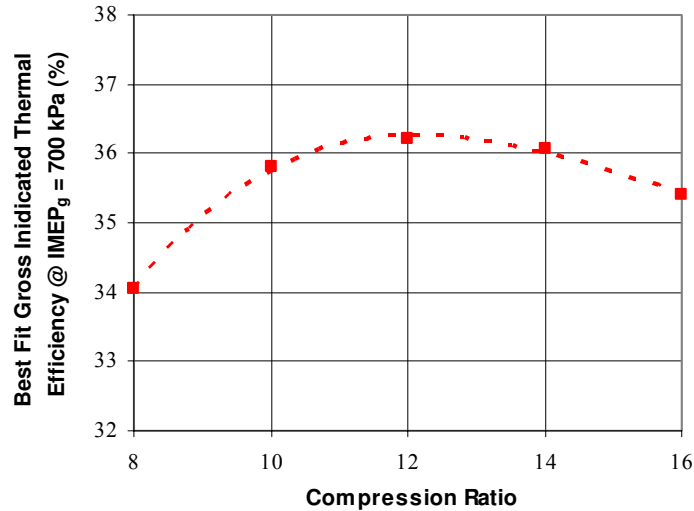
**Figure 3.25. The gross indicated thermal efficiency
at $IMEP_g = 700$ kPa, dual fuel.**

The best gross indicated thermal efficiency at WOT is 36.2% at 12:1 compression ratio, and there is little gained by raising the compression ratio above 10:1. Caris and Nelson (1959) achieved a maximum gross indicated thermal efficiency of about 45% at 17:1, WOT, for lean operation on gasoline, and there was little gained by raising the compression ratio above 14:1 in their results. The CFR engine's pancake combustion chamber geometry is probably responsible for an exaggerated heat loss effect. An increased percentage of heat loss lowers the efficiency for the entire compression ratio range. It also shifts the optimum compression ratio for efficiency to a lower value.

The points for 14:1 and 16:1 had a $COV(IMEP_n)$ between 4% and 15%. However, the $COV(IMEP_n)$ was between 4% and 7% for most of the points. The inability to run with enough gasoline for rough limit operation without knock at 14:1 and 16:1 probably did

not affect the gross indicated thermal efficiency significantly, so the results are still indicative of the overall compression ratio vs. efficiency trends.

The experimental curve in Figure 3.26 is the same curve used for Figure 3.25, and a theoretical Otto cycle efficiency curve is also included, for comparison. The theoretical curve was generated from Equation 3.9. The ratio of specific heats $\gamma = 1.3$ was used because that was the typical value derived from pressure-volume data near the end of the compression stroke. Caris and Nelson (1959) also obtained a ratio of specific heats that was very near 1.3.
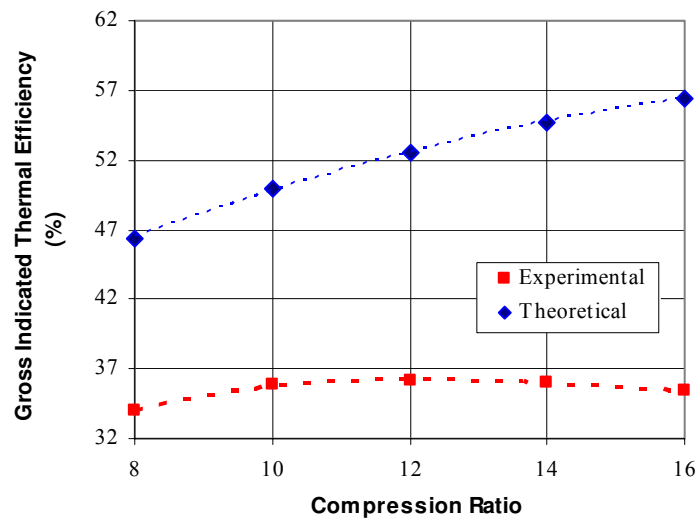
Figure 3.26. Experimental and theoretical gross indicated thermal efficiencies as a function of compression ratio.

The difference between the theoretical and experimental gross indicated thermal efficiencies is large, and the difference becomes larger as the compression ratio is raised. The effect of heat loss explains the difference. Heat loss becomes a larger fraction of the total energy input as the compression ratio is raised. The quenching length and skin depth for conduction become larger fractions of the minimum piston and cylinder head separation at higher compression ratios.

Figure 3.27 shows a comparison of the gross indicated thermal efficiencies for gasoline and dual fuel (rough limit and MBT knock limit) at 8:1. These are the same 8:1 curves from Figures 3.22, 3.23, and 3.24. The gross indicated thermal efficiencies for gasoline

and for dual fueled operation agree closely at low load, where MBT spark timing can be used for gasoline. Dual fueled operation is significantly more efficient than operation on gasoline at 8:1 for $IMEP_g > 650$ kPa because MBT spark timing can be used for dual fueled operation, but for gasoline the spark must be retarded far from MBT to avoid knock in this region. For dual fueled operation the use of MBT spark timing continues for $IMEP_g > 800$ kPa. This load region is inaccessible for operation on gasoline at 8:1.
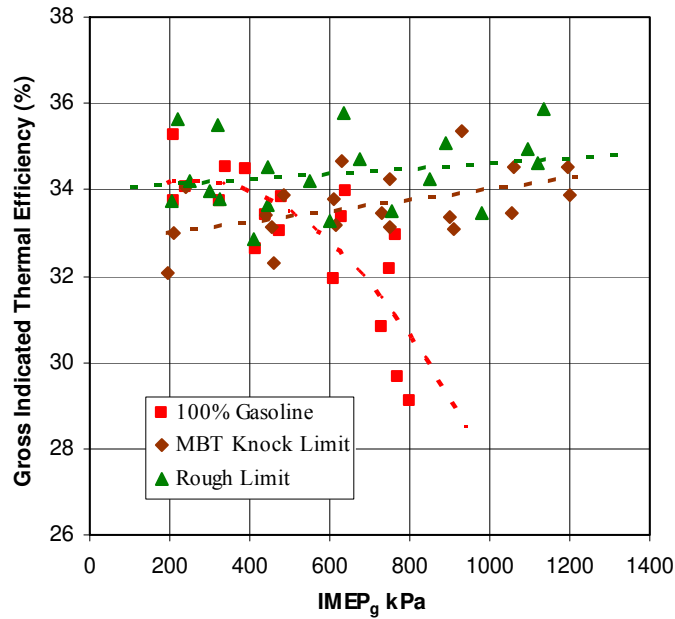
Figure 3.27. A comparison of the gross indicated thermal efficiencies for gasoline and dual fuel at 8:1.

Figure 3.28 shows the gross indicated thermal efficiencies for gasoline and for dual fueled operation at 10:1. These are the same 10:1 curves from Figures 3.22, 3.23 and 3.24. Dual fueled operation is significantly more efficient than operation on gasoline at 10:1 for $IMEP_g > 550$ kPa.
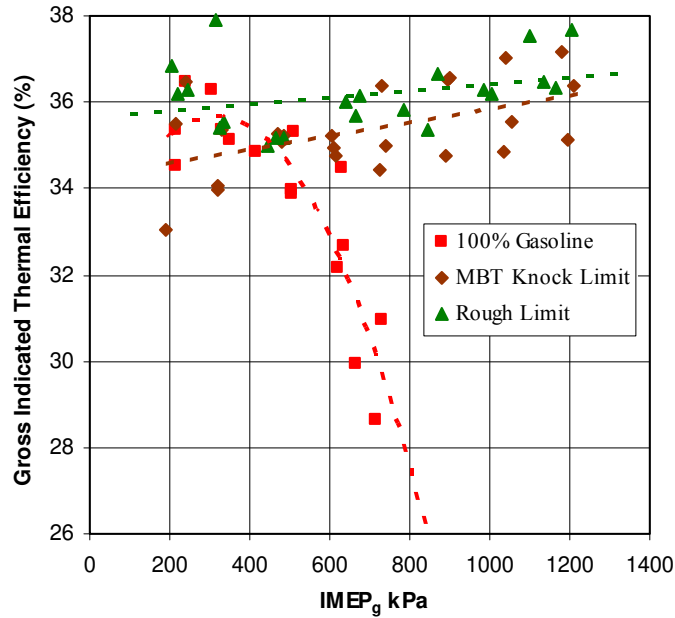
Figure 3.28. A comparison of the gross indicated thermal efficiencies for gasoline and dual fuel at 10:1.

3.2.2 Net Indicated Thermal Efficiency, Brake Thermal Efficiency, and Firing Pressure

Figure 3.29 shows how the $IMEP_g$ is partitioned into pumping losses, friction, and useful work obtained at the crankshaft. All operating points are included. The spread of points for the work series and the friction series is due to the variation of friction with speed. For operation on gasoline, the maximum $IMEP_g$ is limited, because of the knock constraint. However, for dual fueled operation the load can be increased by using more and more ammonia while still using MBT spark timing. The partitioning of gross indicated work improves as the load is increased to arbitrarily high mean effective pressures.

73
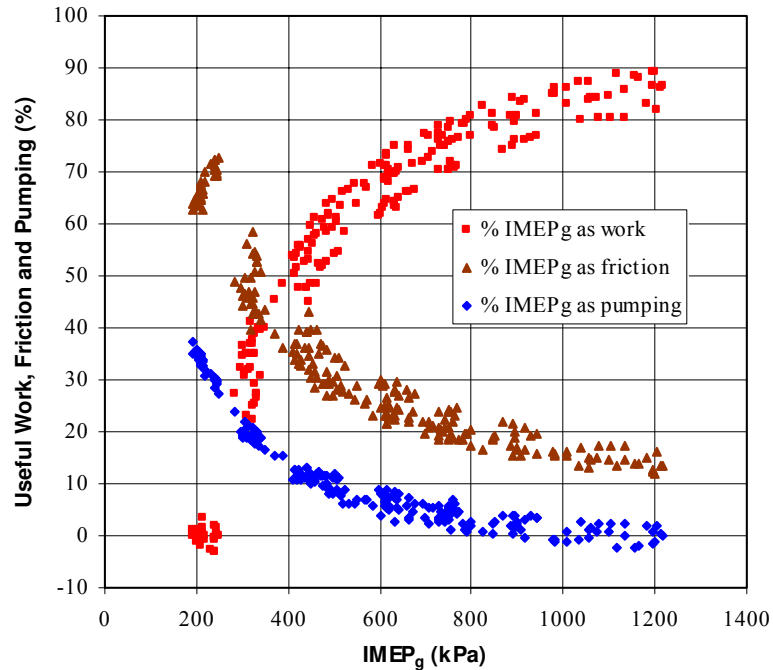
Figure 3.29. The partitioning of IMEP$_g$ into pumping losses, friction, and crankshaft work.

The compression ratio and fuel trends for the net indicated and brake thermal efficiencies have the same basic features as those for gross indicated thermal efficiency. However, the net indicated thermal efficiency is affected by the PMEP, and the brake thermal efficiency is affected by both PEMP and FMEP. For that reason, the net indicated and brake thermal efficiencies depend most strongly on load.

The net indicated mean effective pressure (IMEP$_n$) is the effective driving pressure for the entire the work cycle. Equation 3.12 describes the IMEP$_n$, and the units are kilopascals. The bounds on the integral are degrees crank angle. Equation 3.13 describes how the net indicated thermal efficiency is calculated, in %.

$$\text{IMEP}_n = \frac{1}{V_d} \int_{-360°}^{360°} P \, dV \qquad \text{Eq. 3.12}$$

74

$$\eta_{in} = \frac{IMEP_n \times V_d}{(\dot{m}_g Q_{LHVg} + \dot{m}_a Q_{LHVa})} \times \frac{f_{rpm}}{2} \times 100\% \qquad \text{Eq. 3.13}$$

Figure 3.30 shows the net indicated thermal efficiency for gasoline. All speeds are lumped together and the data are uniformly distributed among 1000, 1300 and 1600 RPM. No matter what fuel is used, the pumping losses due to throttling reduce the net indicated thermal efficiency for low $IMEP_n$. However, for gasoline the net indicated thermal efficiency also goes down for high $IMEP_n$ because the gross indicated thermal efficiency also goes down with increasing load. The compression ratio trend for the net indicated thermal efficiency reverses near $IMEP_n = 600$ kPa, in the same manner and for the same reasons as it also does for the gross indicated thermal efficiency.

Figure 3.30. The net indicated thermal efficiency for gasoline, graphed as a function of $IMEP_n$.

Figure 3.31 shows the net indicated thermal efficiency for dual fueled operation. All speeds and the rough limit and MBT knock limit are lumped together, because the net

indicated thermal efficiency did not depend significantly on speed or which fuel mix limit was used. The net indicated thermal efficiency is significantly better for dual fueled operation than for gasoline when $IMEP_n > 600$ and 500 kPa at 8:1 and 10:1, respectively. The net indicated thermal efficiency curves for 10:1 and 16:1 coincide, as do also the 12:1 and 14:1 curves. The difference between the 10:1 and 12:1 curves is marginally significant.
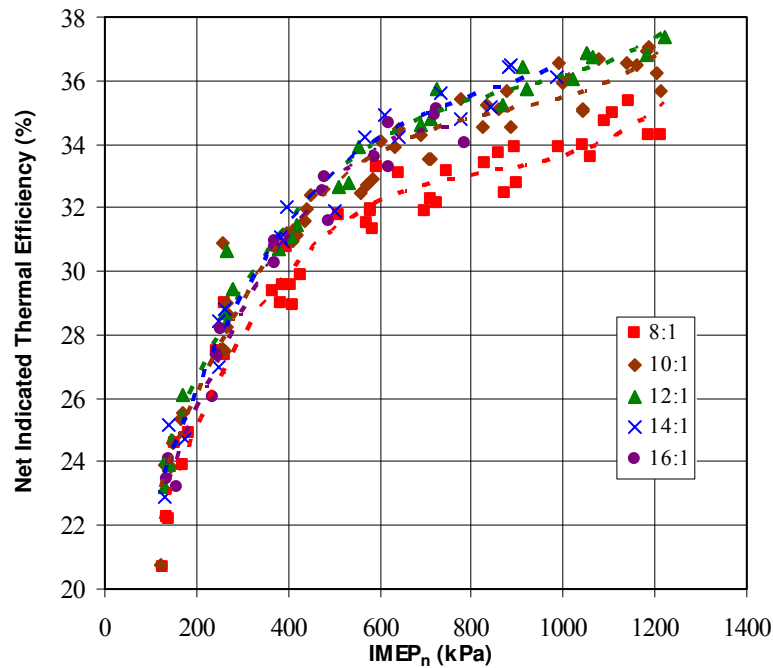
Figure 3.31. The net indicated thermal efficiency for dual fuel, graphed as a function of $IMEP_n$.

It is not realistic to design engines that operate with arbitrarily high mean effective pressures at arbitrarily high compression ratios. The average peak firing pressure must be held at or below a particular maximum value which is chosen by an engine designer. There may be an advantage in reducing the compression ratio slightly from the optimum for best efficiencies at a given load, such that a higher load can be used for the same average peak firing pressure. Figure 3.32 shows how the $IMEP_n$ varies as a function of the average peak firing pressure at different compression ratios. All dual fuel results are included in this graph.

**Figure 3.32. The IMEP$_n$ graphed as a function of firing pressure
at different compression ratios for all dual fuel results.**

For a given average peak firing pressure, the IMEP$_n$ increases as the compression ratio is reduced, and this contributes to raising the net indicated thermal efficiency at a given firing pressure, because the net indicated thermal efficiency increases with increasing IMEP$_n$ at a given compression ratio. However, for low compression ratios the net indicated thermal efficiency goes down with decreasing compression ratio, at a given IMEP$_n$. Figure 3.33 shows the net indicated thermal efficiency as a function of the average peak firing pressure, which is the result of these two competing effects.

The optimum compression ratio for best efficiencies, for efficiencies graphed as a function of average peak firing pressure, is slightly lower than the optimum compression ratio for best efficiencies, for efficiencies graphed as a function of load. The optimum compression ratio for best efficiency also depends on what maximum average peak firing pressure is chosen.

The graph of the net indicated thermal efficiency, as a function of average peak firing pressure, can be used to optimize the net indicated thermal efficiency for a chosen

maximum average peak firing pressure.   The net indicated thermal efficiency at 10:1 is clearly better than that for 8:1 when the average peak firing pressure is greater than 4000 kPa. At 7000 kPa the net indicated thermal efficiency at 10:1 is still slightly better than it is at 12:1, even though the net indicated thermal efficiencies for 12:1 are marginally better than those for 10:1 when graphed as a function of $IMEP_n$.
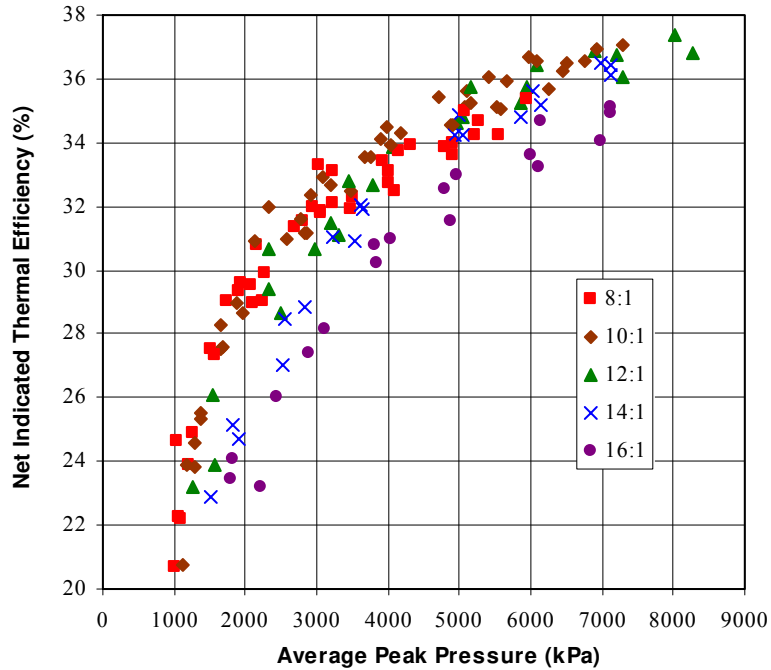
Figure 3.33. The net indicated thermal efficiency for dual fuel, graphed as a function of average peak firing pressure.

The brake mean effective pressure (BMEP) is the effective driving pressure for work obtained per cycle at the crankshaft. Equation 3.14 describes the BMEP, and the units are kilopascals. Equation 3.15 describes how the brake thermal efficiency is calculated, in %.

$$BMEP = \frac{1}{V_d} \times 4\pi\tau \qquad Eq.\ 3.14$$

$$\eta_b = \frac{BMEP \times V_d}{(\dot{m}_g Q_{LHVg} + \dot{m}_a Q_{LHVa})} \times \frac{f_{rpm}}{2} \times 100\% \qquad \text{Eq. 3.15}$$

Figure 3.34 shows the brake thermal efficiency for gasoline. All speeds are lumped together and the data are uniformly distributed among 1000, 1300 and 1600 RPM. The effect of load on brake thermal efficiency is much stronger than it was for the net indicated and gross indicated thermal efficiencies. The maximum BMEP attainable at each compression ratio is limited by the knock constraint. A higher maximum BMEP is attainable as the compression ratio is lowered. The effect of compression ratio on brake thermal efficiency is very weak for gasoline, because the compression ratio and spark timing effects largely cancel each other out. The brake thermal efficiency is 0% at BMEP = 0 kPa by definition, and the indicated thermal efficiency curves, for different compression ratios, cross near loads corresponding to BMEP = 400 kPa.
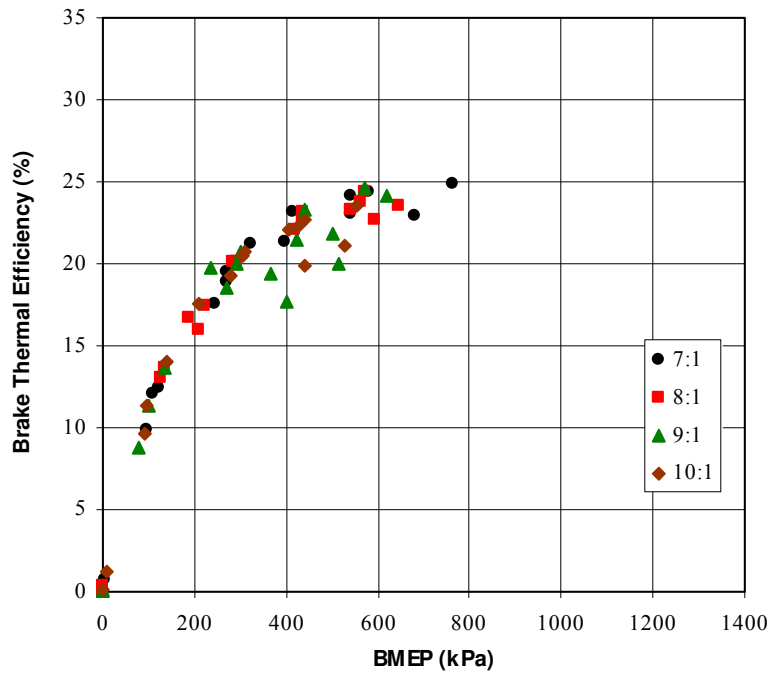
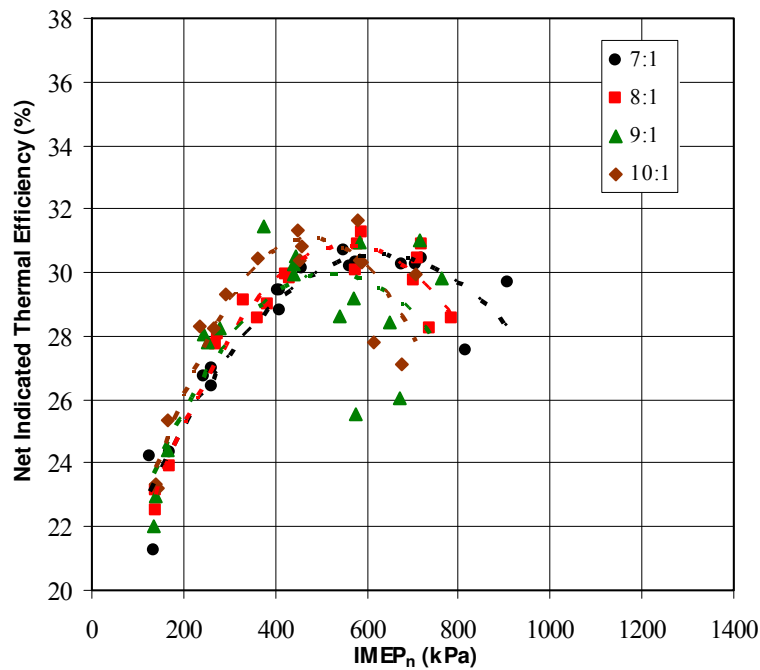**Figure 3.34. The brake thermal efficiency for gasoline, graphed as a function of BMEP.**

Figure 3.35 shows the brake thermal efficiency for dual fueled operation. All speeds for the rough limit and MBT knock limit are lumped together, and the data are uniformly distributed among 1000, 1300, and 1600 RPM. The brake thermal efficiency is significantly better for dual fueled operation than for gasoline when BMEP > 400 and 300 kPa at 8:1 and 10:1, respectively. The dual fuel brake thermal efficiency for 10:1 through 16:1 is nearly the same at a given BMEP. The brake thermal efficiency for 8:1 is slightly lower than for 10:1 through 16:1.
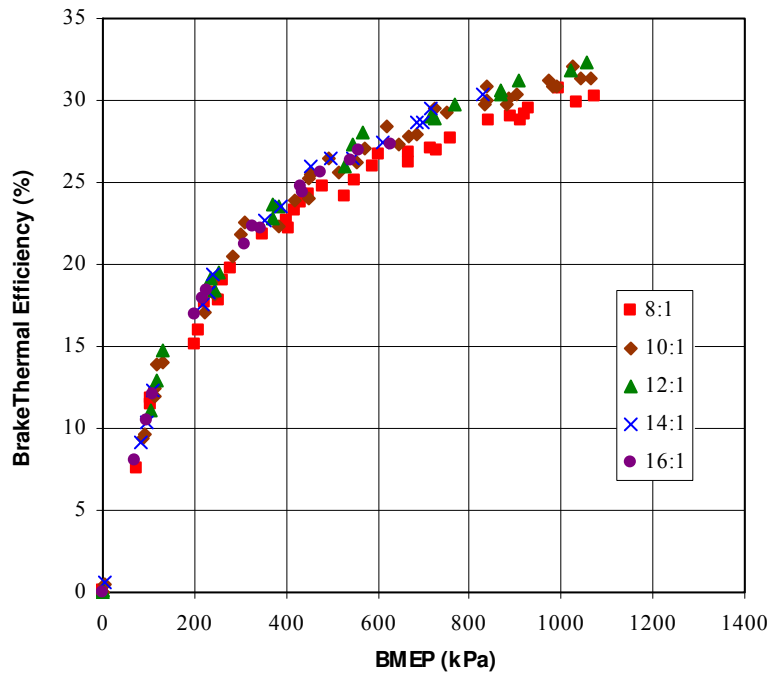
**Figure 3.35. The brake thermal efficiency for
dual fuel, graphed as a function of BMEP.**

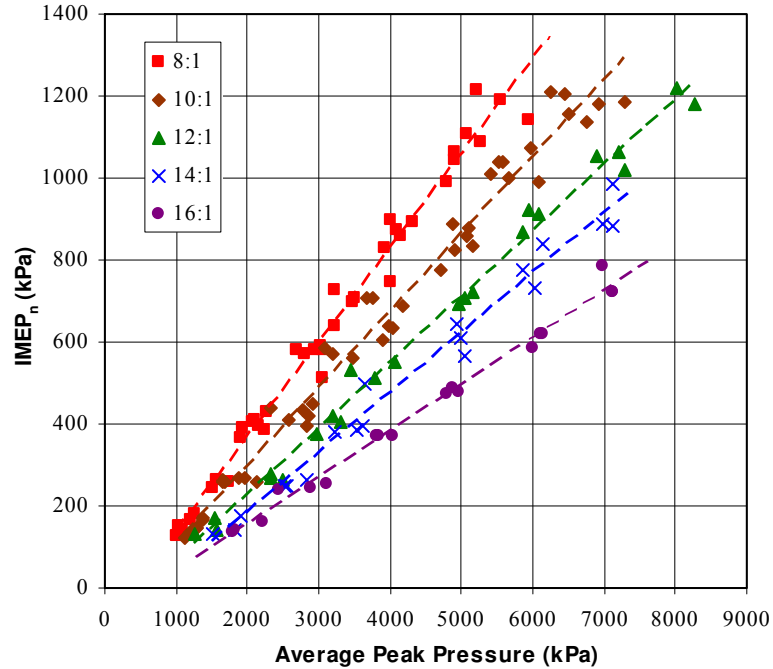Figure 3.36 shows how the BMEP varies as a function of the average peak firing pressure at different compression ratios. All dual fuel results are included in this graph. For a given average peak firing pressure, the BMEP increases as the compression ratio is reduced, in much the same way as does also the $IMEP_n$.

The effect of the firing pressure constraint on the compression ratio ranking for efficiency is stronger for brake thermal efficiency than it is for net indicated thermal

efficiency because the brake thermal efficiency depends more strongly on load. Figure 3.37 shows the brake thermal efficiency, as a function of the average peak firing pressure.
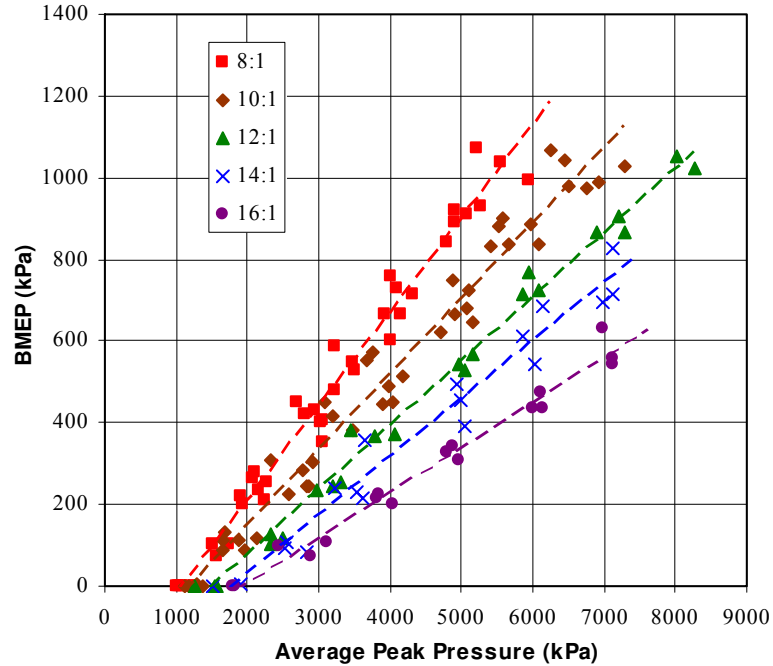
Figure 3.36. The BMEP graphed as a function of firing pressure at different compression ratios for all dual fuel results.

The graph of the brake thermal efficiency as a function of firing pressure can be used to optimize the brake thermal efficiency for a chosen maximum average peak firing pressure. The brake thermal efficiency at 10:1 does not become better than that for 8:1 unless the engine designer chooses a maximum average peak firing pressure greater than about 5000-6000 kPa. At 7000 kPa the brake thermal efficiency at 10:1 is still clearly better than it is at 12:1, even though the brake thermal efficiencies at 12:1 and 10:1 are very nearly the same when graphed as a function of BMEP.
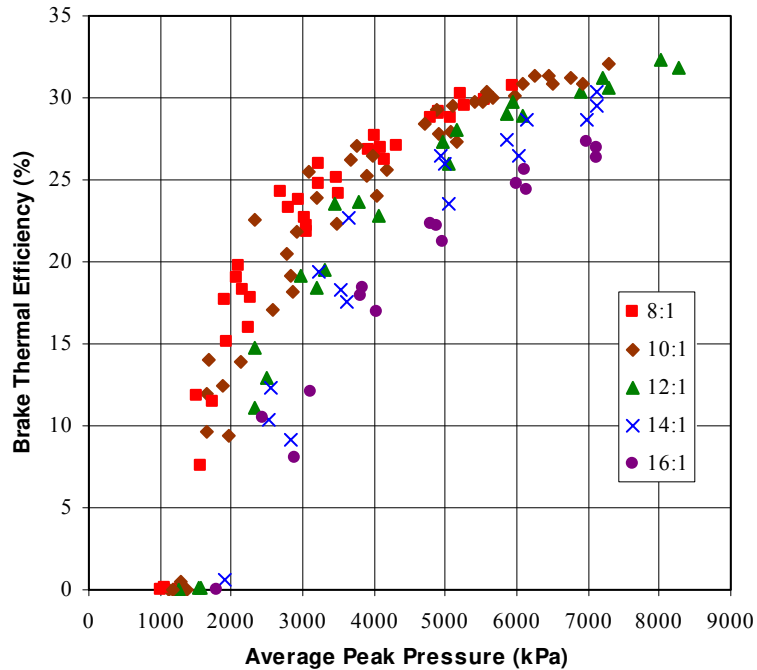
**Figure 3.37. The brake thermal efficiency for dual fuel,
graphed as a function of average peak firing pressure.**

3.3 The Effect of Fuel Mix on Power at WOT

The reduced energy densities of ammonia/air and ammonia/gasoline/air mixtures can be overcome with the use of supercharged intake pressures. Ammonia's knock resistance permits operation on ammonia with gasoline at much higher mean effective pressures, and higher efficiencies, than are possible when only gasoline is used. However, the partial replacement of gasoline with ammonia might result in a different effect on the maximum attainable mean effective pressures for engines not equipped with supercharge capability. For that reason, it is of interest to briefly cover what happens to the mean effective pressures when the fuel mix is varied at WOT.

The energy density of the intake mixture goes down as more gasoline is replaced with ammonia. It was predicted that for a given temperature and pressure, a stoichiometric mixture of ammonia and air should have 83% of the energy density of a stoichiometric mixture of vaporized gasoline and air. Figure 3.38 shows the $IMEP_g$ obtained while the

fuel mix was varied, the intake pressure was maintained at WOT, and the throttle temperature was regulated between 55 and 60º C. The supercharge hose was removed for this test to ensure that the intake pressure would be exactly the same for all points in this test.
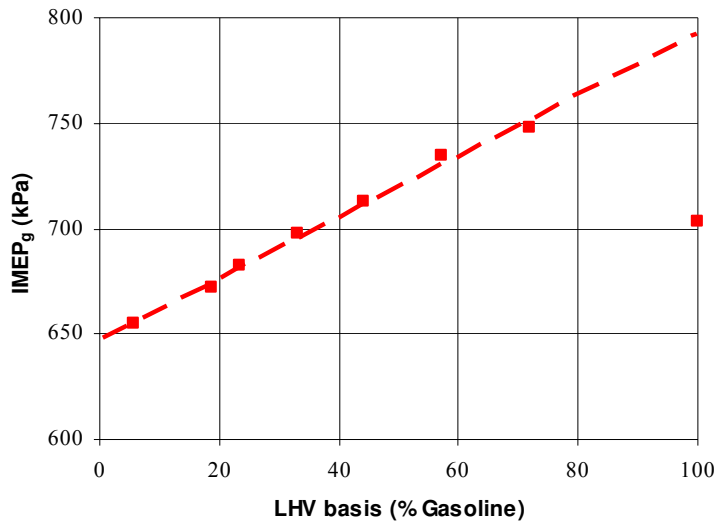
Figure 3.38. Gross indicated mean effective pressure, graphed as a function of fuel mix for 9:1, WOT, 1000 RPM.

The 73% gasoline point required KLSA which was only slightly retarded of MBT. The 100% gasoline point featured KLSA, significantly retarded of MBT, and it was not used in the calculation of the trend line. The $IMEP_g$ for the trend line crossing at 100% ammonia is 82% of the $IMEP_g$ for the crossing at 100% gasoline, which agrees closely with the predicted energy yield ratio of 83%. The actual power difference between operation at 100% gasoline and operation with some ammonia is different from the theoretical prediction because the efficiencies at 100% gasoline are reduced by the inability to use MBT spark timing for gasoline at 9:1, WOT.

Figure 3.39 shows the corresponding BMEP for the same points featured in Figure 3.38. Figures 3.38 and 3.39 show that the mean effective pressures at WOT are actually highest at 73% gasoline, where the KLSA was only slightly retarded of MBT. The BMEP at 73% gasoline was 6.6% greater than the BMEP at 100% gasoline. The BMEP for operation at the rough limit at 18% gasoline was 5.1% lower than the BMEP at 100%

83

gasoline. Ammonia can be used without a substantial power loss, and in fact the maximum attainable mean effective pressures of even a normally aspirated engine can be significantly greater when ammonia is used for operation near the MBT knock limit.
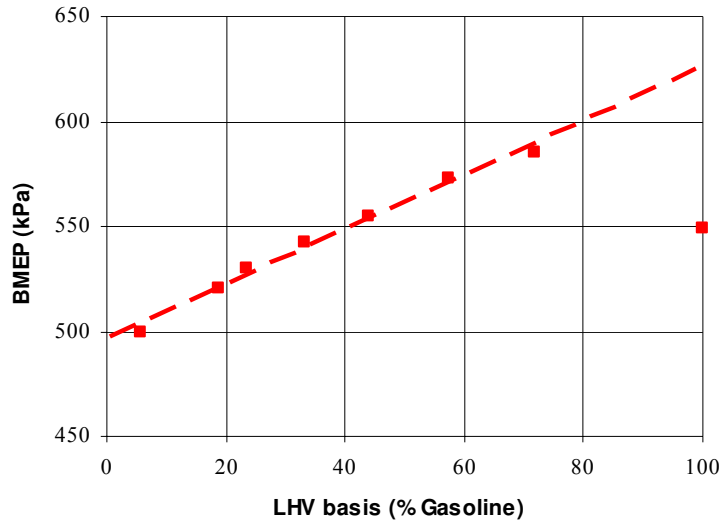
**Figure 3.39. Brake mean effective pressure, graphed
as a function of fuel mix for 9:1, WOT, 1000 RPM.**

3.4 Spark Advance Map

3.4.1 Spark Timing for Gasoline

For operation on gasoline, the separation of curves related to spark timing for 1000 RPM and 1600 RPM was 4 degrees or less, so there was not enough difference between the highest and lowest speed for a significant speed trend. All speeds are lumped together for the results related to spark timing for gasoline.

Figure 3.40 shows the spark advance used for gasoline, graphed as a function of load, grouped by compression ratio. The solid points in Figures 3.40, 3.41, and 3.42 use MBT spark timing, and the hollow points use KLSA.
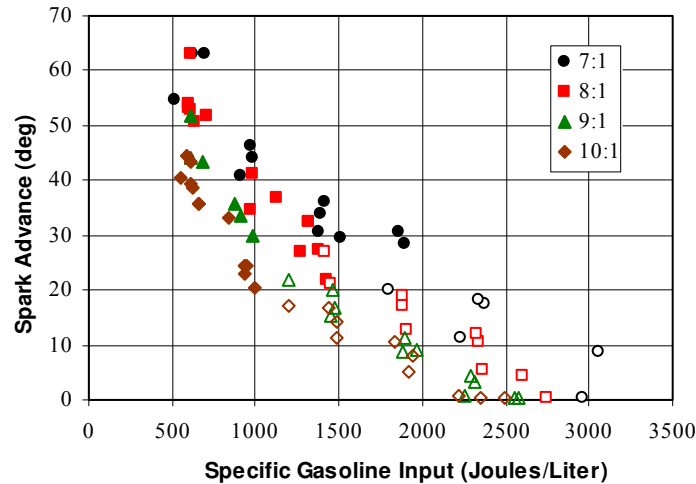
Figure 3.40. The spark advance for gasoline.

The specific gasoline input goes up with increasing load, when gasoline is the only fuel. The charge flammability goes up and the spark advance goes down with increasing specific gasoline input, until the charge actually becomes too flammable and the spark must be retarded from MBT to avoid knock. Raising the compression ratio also increases the flammability, which decreases the required or permitted spark advance, for MBT spark timing or KLSA, respectively. The transition from MBT spark timing to KLSA occurs at a lower load as the compression ratio is raised.

The ignition delay for MBT spark timing is similar to the MBT spark advance, and most of the MBT spark advance requirement appears to be due to the ignition delay. The ignition delay for gasoline, shown in Figure 3.41, changes little as the specific gasoline input is raised beyond the transition from MBT timing to KLSA, despite the higher gasoline density during the ignition interval.

The burn duration for gasoline, shown in Figure 3.42, is mostly affected by load for the MBT region. The burn duration gets longer when the spark is retarded far from MBT because of the reduced charge densities during the burn interval. When the spark is fired near TC, the burn duration for 9:1 and 10:1 is 10 degrees longer than the burn duration for 7:1, probably because of a combination of greater heat loss and faster expansion from TC at higher compression ratios.
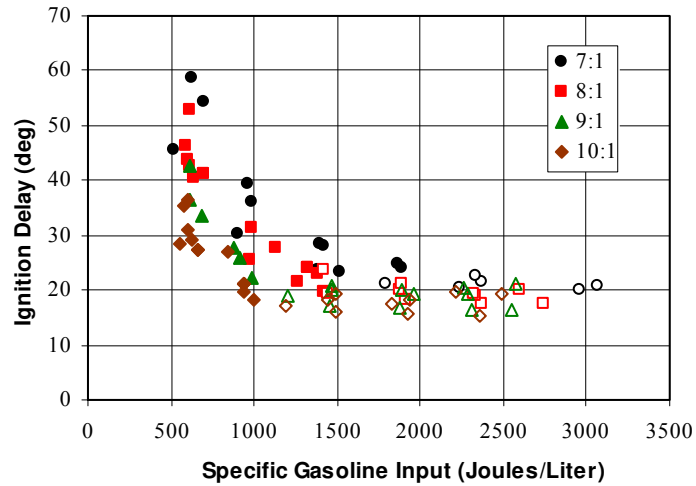
Figure 3.41. The ignition delay for gasoline.
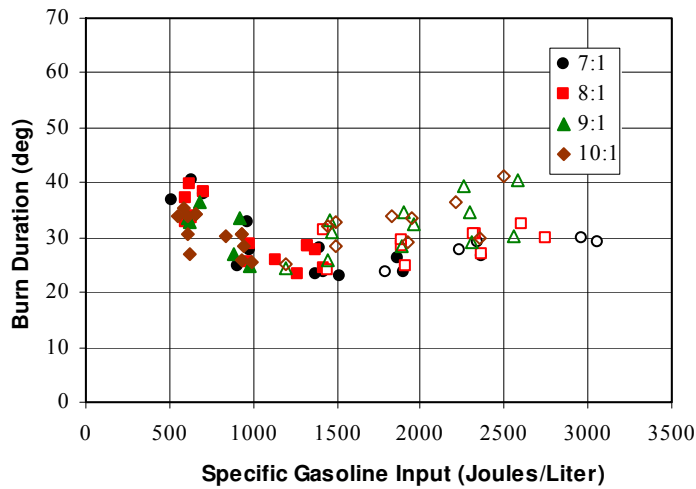
Figure 3.42. The burn duration for gasoline.

Figures 3.41 and 3.42 suggest that the MBT spark advance for gasoline would have been nearly constant with respect to load in the KLSA region if MBT spark timing could have been maintained there. The flame speed and ignitability do not change much when the specific gasoline input is increased beyond the transition between MBT spark timing and KLSA.

3.4.2 The Effect of Ammonia Addition on MBT Spark Timing

For dual fueled operation the load can be changed by changing either the specific gasoline input or the specific ammonia input. The addition of ammonia instead of gasoline, with increasing load, has a different effect on the charge flammability. Figure 3.43 shows the effect of ammonia addition on the MBT spark advance. The curve was extracted from the 8:1, 1600 RPM operating points for which the specific gasoline input was between 656 and 722 Joules per liter. The leftmost point had no ammonia, and the points to the right of that had more and more ammonia and nearly the same gasoline input.
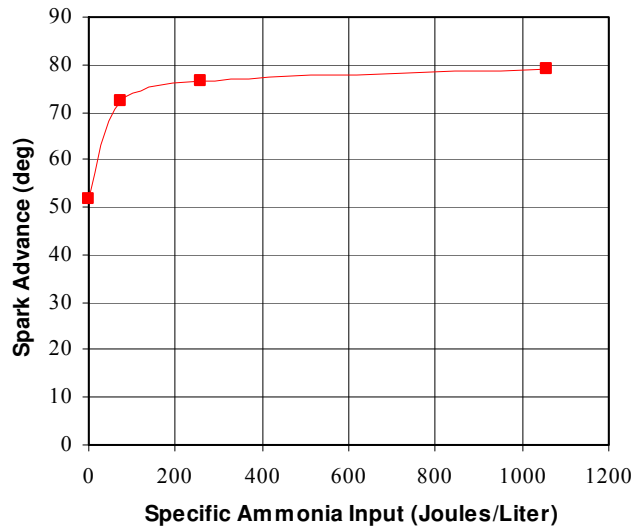
Figure 3.43. The effect of ammonia addition on the MBT spark advance.

The spark advance increases abruptly when a little ammonia is introduced. Most of the spark advance change with ammonia addition occurs when the ammonia is about 10% of the total fuel energy input. Additional increases to the specific ammonia input at constant specific gasoline input appear to have a neutral effect on the flame speed. The neutral effect of ammonia addition on combustion is also demonstrated by the near-flatness of the specific gasoline input curves in Figures 3.15, 3.16, and 3.17, and the near-flatness of the compressed gasoline and E85 density curves in Figures 3.9, 3.11, and 3.12.

Theoretical studies also agree that a nearly neutral effect on flame speed is achieved by increasing the density of an ammonia/air mixture beyond a certain point [Liu et al., 2003].

For operation on gasoline, there is a spark map which is a function of specific gasoline input (load for gasoline), speed, and compression ratio. When ammonia is used, the spark map transitions to another function of specific gasoline input, speed, and compression ratio, which is independent of the specific ammonia input (or very nearly so) once the transition is complete.

3.4.3 Dual Fuel Spark Timing

The spark advance map for dual fueled operation is presented for 8:1 and 10:1 because these are the useful compression ratios for dual fueled operation. Compression ratios of 12:1 or higher are not desired because of the MBT knock limit and rough limit crossover. Compression ratios of less than 8:1 are probably also not desired because of a large efficiency loss for operation below 8:1.

For dual fueled operation, load is the specific ammonia input plus the specific gasoline input. However, the ignitability and flame speed appear to depend only on the specific gasoline input. The dependence on the specific ammonia input drops out because of ammonia's neutral effect on flame speed and its very weakly positive effect on ignitability. For a given speed and compression ratio, only the effect of gasoline addition needs to be shown. The grouping of the points about the trend lines is tight despite the large variation of the specific ammonia input among the points.

Figure 3.44 shows the MBT spark advance at 8:1 for dual fueled operation as a function of specific gasoline input and speed, and also the spark advance for gasoline at 8:1 for comparison. For the dual fuel points the specific ammonia input varies from several times less than the specific gasoline input, to several times more than the specific gasoline input. The gasoline points in Figure 3.44 are the 8:1, MBT points from Figure 3.40, and for these the specific ammonia input was zero. The dual fuel MBT knock limit

points are grouped near 1700 Joules per liter, and 35 degrees. The dual fuel rough limit
points are grouped near 600 Joules per liter, and 60-80 degrees.
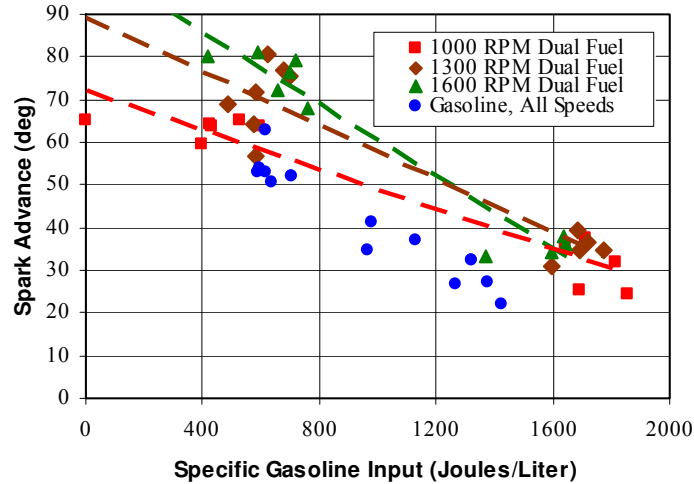
Figure 3.44. The MBT spark advance for 8:1.

The dual fuel spark advance data are tightly grouped along the trend lines despite the
large variation of the ammonia input within each group. There is very little speed
dependence at the MBT knock limit for dual fuel, and the trend lines cross there. The
spark advance depends strongly on the speed at the rough limit. For operation at the
rough limit, increasing speed requires more spark advance and a greater specific gasoline
input.

The spark advance jump for the transition from 100% gasoline to dual fuel is larger at
higher speed near the rough limit. The required spark advance for dual fueled operation
at 8:1 and 10:1 was 10-30 degrees greater than the required spark advance for 100%
gasoline for the same speed, compression ratio and specific gasoline input.

The ignition delay for 8:1 dual fuel is shown in Figure 3.45. Most of the MBT spark
advance requirement is due to the ignition delay. The gasoline points in Figure 3.45 are
the 8:1 MBT points from Figure 3.41.
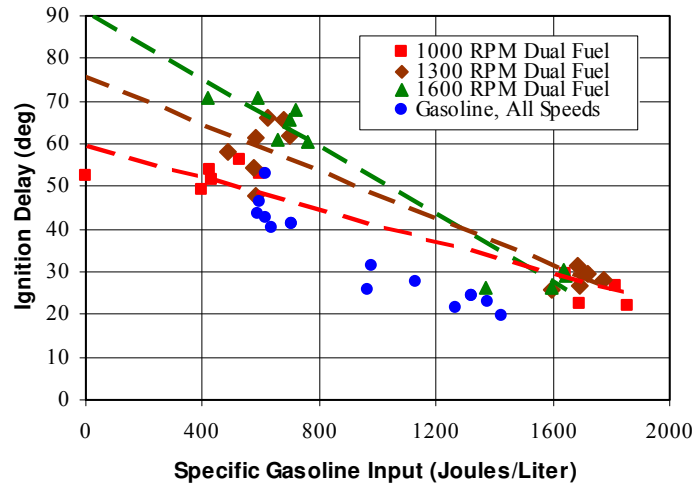
Figure 3.45. The ignition delay for 8:1.

The burn duration for 8:1 dual fuel is shown in Figure 3.46. The gasoline points in Figure 3.46 are the 8:1 MBT points from Figure 3.42. Like for the spark advance, the trend lines at different speeds for ignition delay and burn duration cross at the MBT knock limit.
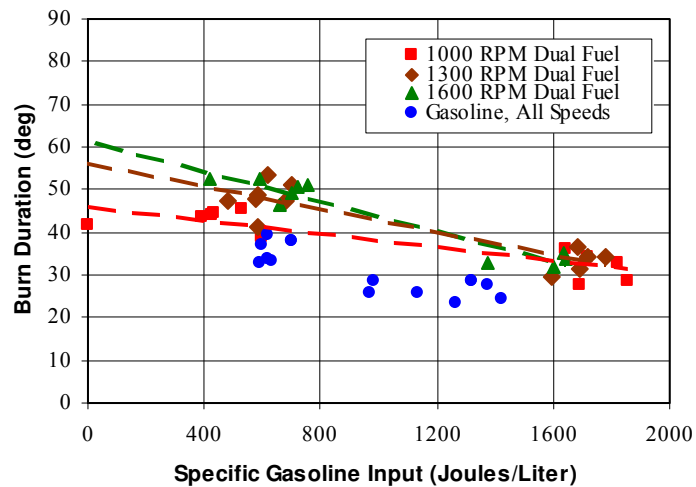
Figure 3.46. The burn duration for 8:1.

Figures 3.47, 3.48 and 3.49 show the spark advance, ignition delay and burn duration for dual fueled operation at 10:1. The gasoline points are the 10:1, MBT points from Figures 3.40, 3.41 and 3.42.
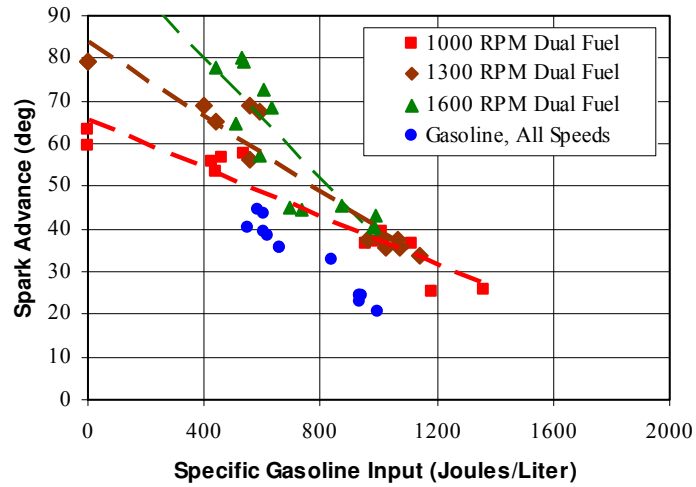
Figure 3.47. The MBT spark advance for 10:1.
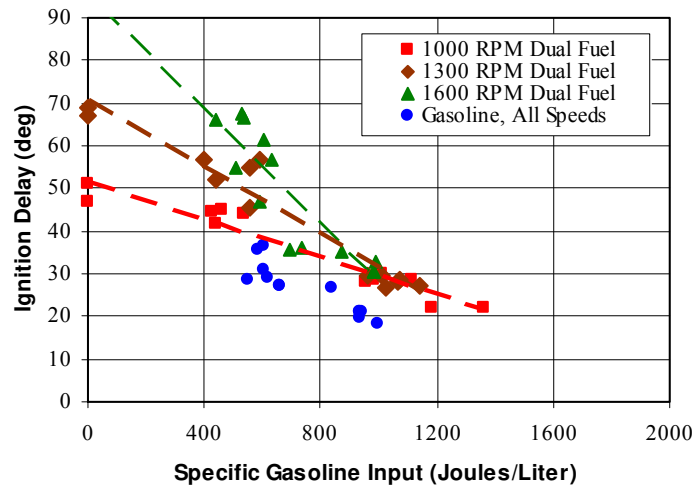
Figure 3.48. The ignition delay for 10:1.
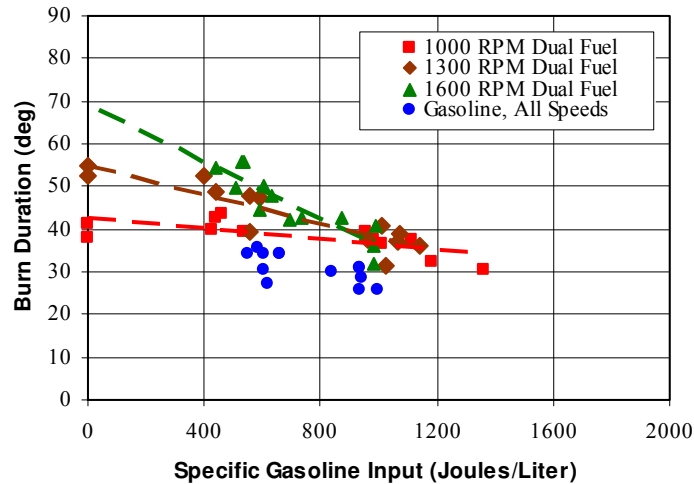
Figure 3.49. The burn duration for 10:1.

The ignition delay and spark advance are slightly less at 10:1 than at 8:1, which reduces the gasoline requirement at the dual fuel rough limit. The specific gasoline input at the dual fuel MBT knock limit occurs near 1000 Joules per liter at 10:1, and the trend lines for different speeds cross there.

3.5 Exhaust Gas Temperature

Figure 3.50 shows the engine-out exhaust gas temperature for operation at 8:1, 1600 RPM. The exhaust gas temperature for dual fueled operation increases gradually with load because of increased mass flow, but in the limit of very high load the exhaust gas temperature appears to asymptote to modest values. The exhaust gas temperature for gasoline continues to rise sharply at high load because the spark must be retarded further from MBT with increasing load to avoid knock.
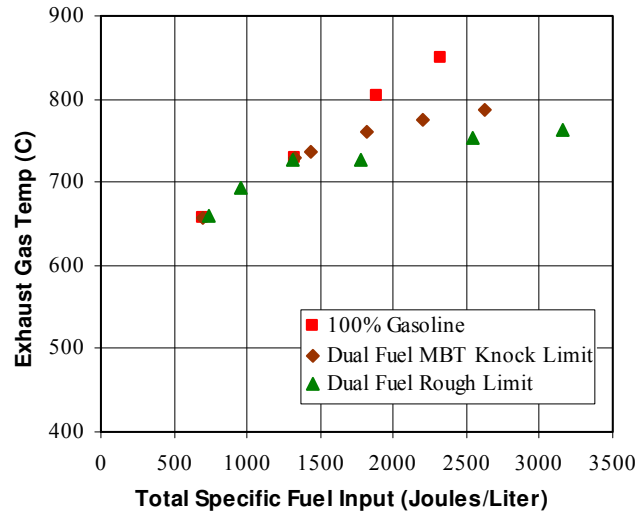
Figure 3.50. Engine-out exhaust gas temperature for 8:1, 1600 RPM.

The exhaust gas temperature is lower for the rough limit than it is for the MBT knock limit because more ammonia and less gasoline are used at the rough limit, which lowers the adiabatic flame temperature slightly. However, most of the difference between the exhaust gas temperatures for gasoline vs. dual fuel appears to be due to the use of MBT spark timing for dual fueled operation, as opposed to gasoline, which uses spark timing progressively retarded away from MBT with increasing load.

Figure 3.51 shows the engine-out exhaust gas temperature for operation at 10:1, 1600 RPM. The temperature difference between the rough limit and MBT knock limit is less at 10:1 than at 8:1 because the fuel mix window between the rough limit and MBT knock limit is narrower at 10:1 than it is at 8:1. The exhaust gas temperatures are generally lower at 10:1 than at 8:1 because of greater heat loss in the cylinder, and also because of the higher thermal efficiencies achieved at 10:1.

93
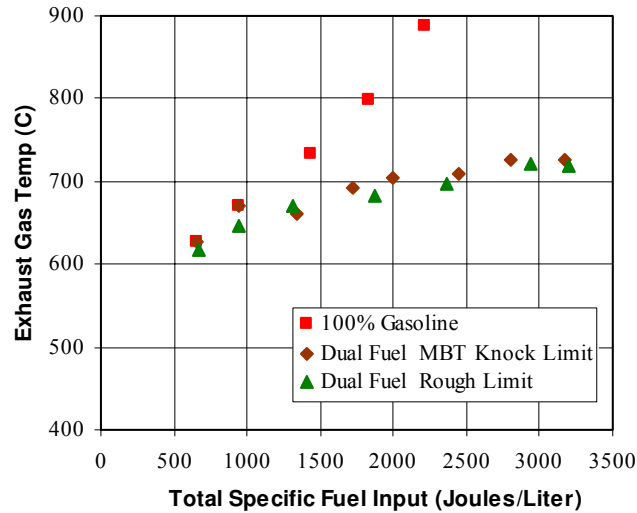
Figure 3.51. Engine-out exhaust gas temperature for 10:1, 1600 RPM.

The reduced exhaust gas temperatures, and the absence of large temperature swings with varying load for operation on ammonia with gasoline, should substantially lengthen the service life of turbochargers and exhaust components, especially the exhaust manifolds and pipes, and catalytic converter. The use of ammonia with gasoline should also enable the use of a close-coupled catalyst built into the exhaust manifold, and permit operation at a wider range of loads without degradation of the catalyst, than is possible with gasoline alone.

3.6 Engine Design Considerations

3.6.1 Operating Cost Analysis

The maximum load for normally aspirated operation is WOT. The best brake thermal efficiency for gasoline at WOT occurs at 9:1. For CFR engine operation on gasoline at 9:1, the BMEP is 550 kPa at WOT, according to Figure 3.39. A fair compromise between fuel economy and performance is reached by placing the road load at halfway between idle and maximum load. The brake thermal efficiency is 20% for gasoline at 9:1 and BMEP = 275 kPa, which is halfway between idle and WOT. All other operating

94

points are compared to this baseline condition for the purpose of calculating a relative operating cost.

An engine's operating cost is inversely proportional to the brake thermal efficiency at each point. Figure 3.52 shows the relative operating cost for operation on gasoline, as a function of load. All speeds are lumped together. The relative operating cost is set equal to 1 for operation on gasoline at $\eta_b = 20\%$.
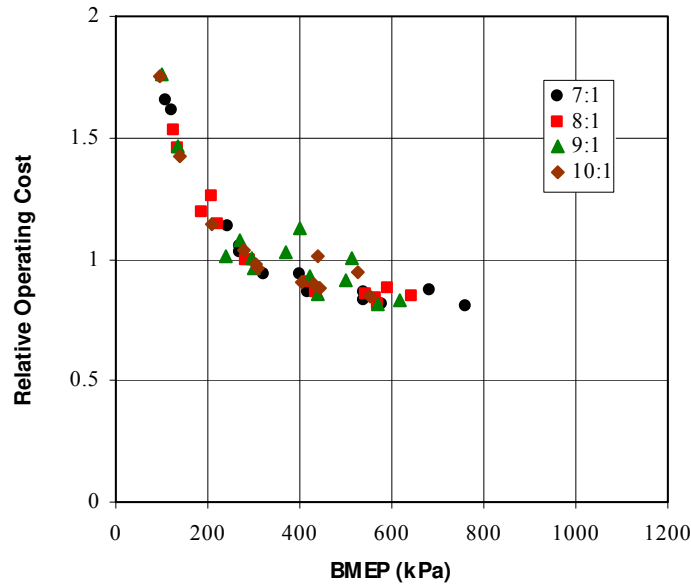
Figure 3.52. The relative operating cost for gasoline.

For gasoline there is a diminished return on cost reduction for operation at loads above BMEP = 275 kPa. When some ammonia is used, the brake thermal efficiency climbs faster with increasing load than it does for gasoline, and the maximum load is not limited by knock. Equation 3.16 describes the relative operating cost. Note that the relative operating cost = 1 at $b_e = 100\%$ and $\eta_b = 20\%$.

$$\text{Relative Operating Cost} = \frac{b_e + (100\% - b_e)N}{100\%} \times \frac{20\%}{\eta_b} \qquad \text{Eq. 3.16}$$

Recall that b_e is the gasoline fraction on a LHV energy basis, expressed as a percent. N is the ratio of ammonia's cost to gasoline's cost, per unit of LHV energy. The cost of a fuel could be currency paid per unit of fuel energy, or mass of carbon dioxide released from well to wheels per unit of fuel energy, or any other cost basis one may wish to use.

Figures 3.53, 3.54 and 3.55 show the relative operating cost for dual fueled operation at the rough limit and MBT knock limit at 8:1 and 10:1. Each figure uses a different ammonia/gasoline cost ratio. The 12:1 curves (not shown) are not significantly different from the 10:1 rough limit curves. All speeds 1000 RPM, 1300 RPM, and 1600 RPM are lumped together.

Figure 3.53 shows the relative operating cost for dual fueled operation when $N = 0$. Such is the case when the cost basis is the mass of carbon dioxide released per unit of fuel energy, and ammonia is made with nuclear power or some other energy source that does not involve carbon.
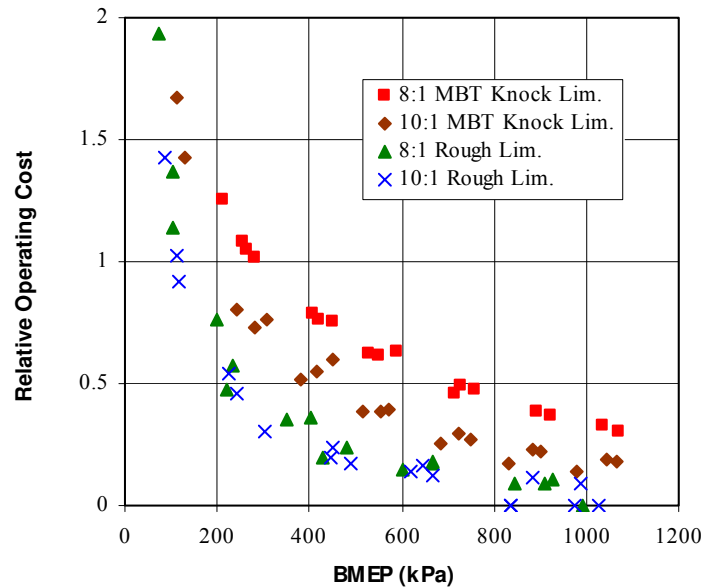
Figure 3.53. The relative operating cost for dual fueled operation when the ammonia cost is zero.

Operation at the 10:1 rough limit is favored when the cost of ammonia is less than the cost of gasoline. The brake thermal efficiency is higher at 10:1 than it is at 8:1 at a given BMEP, and the gasoline requirement at the rough limit is lower for 10:1 than for 8:1.

96

The permitted fuel mix favors ammonia more with increasing load, and the brake thermal efficiency improves with increasing load, so it will make sense to design engines to operate at the dual fuel rough limit, at high BMEP most of the time, when ammonia's cost is low.

Figure 3.54 shows the relative operating cost for dual fueled operation when $N = 1$. Such is the case when the retail price per unit of fuel energy is the same for ammonia as it is for gasoline, or when ammonia is made by means which emit the same mass of carbon dioxide per unit of fuel energy from well to wheels as does gasoline.
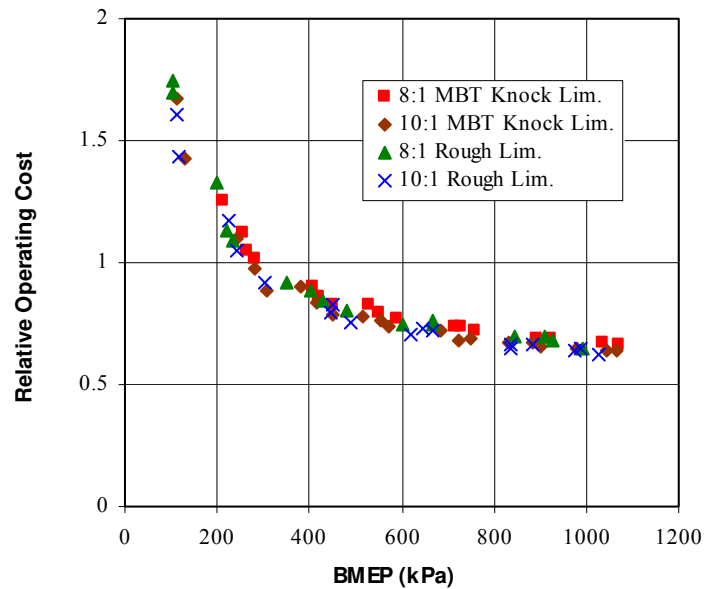
Figure 3.54. The relative operating cost for dual fuel when the ammonia/gasoline cost ratio $N = 1$.

The relative operating cost is determined only by the brake thermal efficiency when the cost of ammonia is the same as the cost of gasoline. Operation at 10:1 is favored over 8:1, because the brake thermal efficiency is higher at 10:1 than at 8:1. The rough limit and MBT knock limit are equally favored. Design for operation at high average load is preferred to design for operation at light average load as was also the case in Figure 3.53.

Figure 3.55 shows the relative operating cost for dual fueled operation when $N = 2.3$. Such could be the case when ammonia's retail price per unit of fuel energy is more than twice as much as it is for gasoline. The MBT knock limit is favored over the rough limit

97

when ammonia is more expensive than gasoline. The 8:1 MBT knock limit is favored over the 10:1 MBT knock limit, despite the higher thermal efficiencies at 10:1, when ammonia is substantially more expensive than gasoline.
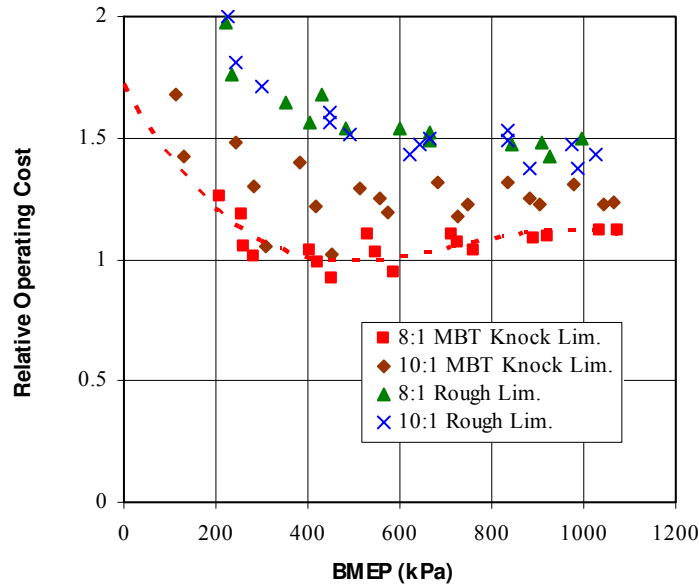
Figure 3.55. The relative operating cost for dual fuel when the ammonia/gasoline cost ratio $N = 2.3$.

$N = 2.3$ is the highest ammonia/gasoline cost ratio, for which there is a breakeven point somewhere at the 8:1 MBT knock limit. That last breakeven point occurs at BMEP = 500 kPa, at which the engine is only slightly throttled. This particular load is special because its operating cost remains competitive with the baseline gasoline condition over the widest range of ammonia/gasoline cost ratios. At lower loads, the operating cost goes up because of thermal efficiency loss. At higher loads, the increasing ammonia requirement drives the operating cost up. Even when ammonia costs more than twice as much as gasoline for the same quantity of energy, the brake thermal efficiency gains, obtained by redesigning engines to operate at BMEP = 500 kPa most of the time rather than at BMEP = 275 kPa, can still offset the cost of ammonia.

Operation at 8:1 and BMEP = 500 kPa gives the greatest economic flexibility, and is favored when the ammonia/gasoline cost ratio is uncertain. Operation at the MBT knock limit can be chosen when $N > 1$, and the rough limit can be chosen when $N < 1$, if the

engine is equipped to allow its user to make this choice. Dual fueled operation at the 8:1 MBT knock limit at BMEP = 500 kPa loses favor to operation on gasoline at BMEP = 275 kPa only when $N > 2.3$.

3.6.2 Engine Designs Derived from Experimental Data

Table 3.2 summarizes possible engine designs, which are based on experimental data. The data for operation on gasoline show that the knock constraint places a limitation on how much the power density and efficiency can be improved for a gasoline fueled engine. The use of ammonia with gasoline allows much better efficiencies at much higher power densities than possible for operation on gasoline alone. The use of ammonia should also permit higher engine power/weight and engine power/cost ratios than are possible when only gasoline is used.

For all designs it is assumed that the engines are to be exchanged, and that the application parameters, such as speed and road load torque, are left unchanged. Engine size is traded for load, relative to those for the baseline condition, and ammonia is used in some of the designs. The maximum torque and power, which are sensed by the operator, are kept the same unless otherwise specified.

For each design, the brake thermal efficiency at road load was derived using the BMEP at road load and either Figure 3.34 (for the gasoline designs) or Figure 3.35 (for the dual fueled designs). The total specific fuel input at road load (not shown) was derived using the BMEP at road load and brake thermal efficiency at road load. The specific gasoline input at the rough limit (not shown) was derived using the 1600 RPM ammonia cut-in points from Figure 3.18 (the average of 8:1 and 10:1 was used for 9:1). The gasoline percentage at road load for the rough limit designs was derived from the specific gasoline input at the rough limit and the total specific fuel input at road load. The gasoline percentage at road load for the MBT knock limit design was derived using the total specific fuel input at road load and Figure 3.13. The method for choosing the road load BMEP and maximum BMEP is explained for each design.

Compression Ratio and Fuel	Fuel/Air Induction Method	Max BMEP	BMEP @ Road Load	Percent Gasoline @ Road Load	Brake Thermal Eff. @ Road Load	Engine Size Reduction Factor
9:1 Gasoline	Normally Aspirated	550 kPa	275 kPa	100%	20%	1.00
7:1 Gasoline	Supercharged	760 kPa	380 kPa	100%	22%	1.38
9:1 NH$_3$/Gasoline @ Rough Limit	Normally Aspirated	580 kPa	275 kPa	50%	20%	1.00
8:1 NH$_3$/Gasoline @ MBT knock limit	Supercharged	≥1000 kPa	500 kPa	85%	25%	1.82
8:1 NH$_3$/Gasoline @ Rough Limit	Supercharged	≥1000 kPa	500 kPa	37%	25%	1.82
10:1 NH$_3$/Gasoline @ Rough Limit	Supercharged	≥2000 kPa	1000 kPa	20%	31%	3.64

**Table 3.2. A summary of different engine
designs, based on experimental data.**

The 9:1, 100% gasoline fueled design is the baseline design, and it is intended to represent normally aspirated operation on gasoline, with throttled load control. The maximum load at WOT occurs at BMEP = 550 kPa, from Figure 3.39. The road load point is chosen at BMEP = 275 kPa, halfway between idle and maximum load for the best compromise between fuel economy and performance. The throttling loss (PMEP) consumes 10% of the gross indicated work at road load. The friction (FMEP) consumes about 1/3 of the net indicated work at road load.

For gasoline, the compression ratio can be reduced to allow a higher maximum accessible BMEP. The 7:1 gasoline design has a maximum BMEP = 760 kPa when the KLSA reaches TC. The road load BMEP at 380 kPa was chosen because it is ½ of the maximum BMEP. The engine displacement for the 7:1 gasoline design would have to be

made 380/275 = 1.38 times smaller than the displacement for the 9:1 gasoline design to produce the same road load torque and to possess identical performance characteristics from the operator's point of view. The brake thermal efficiency at road load is significantly better for the 7:1 design because of improved conversion of $IMEP_g$ into BMEP at higher mean effective pressures (see Figure 3.29).

The 9:1 rough limit design is intended to represent the conversion of existing, normally aspirated, gasoline fueled engines to run on ammonia with gasoline at the rough limit. It is the same engine as is the 9:1 gasoline fueled engine, except that an ammonia input is added. The 9:1 rough limit engine can be run near the MBT knock limit for maximum power at WOT, and the rough limit can be used at all other loads. The maximum load at WOT occurs at BMEP = 580 kPa (from Figure 3.39), which results in a slight, but significant performance improvement. The road load efficiencies and BMEP are the same for the 9:1 gasoline and 9:1 rough limit designs. The road load fuel mix for the 9:1 rough limit design agrees closely with the average road trip result of 50% gasoline/50% ammonia, which is also described at the front.

Operation at 8:1 is characterized by a wide fuel mix window between the MBT knock limit and rough limit, and the brake thermal efficiency is still reasonably good. The two 8:1 designs are for the same engine, except for the fuel mix limit which can be chosen by the operator. The road load BMEP = 500 kPa is chosen for both because this is the load at which the operating cost remains competitive with that of the 9:1 gasoline design over the widest range of ammonia/gasoline cost ratios. The combination of the 8:1 rough limit and MBT knock limit designs into a single engine gives the operator the greatest economic flexibility. The MBT knock limit can be chosen when $N > 1$, and the rough limit can be chosen when $N < 1$. The 8:1 engine's displacement is 500/275 = 1.82 times smaller than that for the 9:1 gasoline design to keep the road load torques equal. The performance of the much smaller 8:1 engine would be as good as or better than that of the 9:1 gasoline engine when the 8:1 engine has a maximum BMEP $\geq$ 1000 kPa.

The 10:1 design maximizes the brake thermal efficiency while minimizing the use of gasoline. It also minimizes the operating cost when $N \leq 1$ (see Figures 3.53 and 3.54). The road load BMEP = 1000 kPa was chosen because it is nearly the highest load included in this study, though a higher road load and even smaller engine could have

been chosen. The 10:1 engine's displacement is 1000/275 = 3.64 times smaller than that for the 9:1 gasoline design to keep the road load torques equal. The performance of the 10:1 engine would be as good as or better than that of the 9:1 gasoline engine when the 10:1 engine has a maximum BMEP $\geq$ 2000 kPa, which is outside the limits of this study.

3.7 Repeatability Analysis for Performance Results

Repeated measurements of the fuel mix at the rough limit show that the uncertainty in b_e is 3% for all nonzero results. For example, if the fuel mix is 40% gasoline, it is 40% ± 3%. The main source of uncertainty was the determination of the COV(IMEP$_n$). During continuous monitoring, the COV(IMEP$_n$) would fluctuate typically between 2-4% when the average value was 3%. This uncertainty accounts for most of the fuel mix uncertainty, because the inverse slopes db_e/dCOV(IMEP$_n$) of the COV(IMEP$_n$) curves in Figures 3.1 and 3.2 are about 2 near the rough limit. Similarly, the specific gasoline input uncertainty of the rough limit cut-in point is 13 Joules per liter, or about 2% of the measurement. The uncertainty in the specific gasoline input at the rough limit is 50 Joules per liter, and the uncertainty in the compressed gasoline energy density at the spark at the rough limit is 0.15 kilojoules per liter.

Repeated measurements of the fuel mix at the MBT knock limit show that the uncertainty in b_e is 10%. For example, if the fuel mix is 60% gasoline, it is 60% ± 10%. The main source of uncertainty was the determination of the MBT spark timing, which had an uncertainty of ± 3 degrees. The location of the MBT spark also changed as the fuel mix was varied, and there was a judgment call at each point about whether the knock occurred on the advanced or retarded side of MBT as the spark timing was varied. Similarly, the uncertainties in the specific gasoline input at the MBT knock limit and also the MBT knock limit's departure from the 100% gasoline line are both 200 Joules per liter. Any apparent speed trends for the fuel mix and specific gasoline input at the MBT knock limit should not be interpreted as meaningful, given the uncertainties and given that the range of speeds investigated was narrow.

Repeated measurements of the gross and net indicated thermal efficiencies and brake thermal efficiency reveal an uncertainty of 1% for all thermal efficiencies, using ammonia with gasoline for all loads, and also for gasoline when $IMEP_g$, $IMEP_n < 600$ kPa or BMEP < 400 kPa. For example, when the net indicated thermal efficiency is 30%, it is 30% ± 1%. The uncertainty is about evenly split between the fuel flow measurement uncertainty and the set-to-set fluctuation of the average mean effective pressures.

For gasoline, when $IMEP_g$, $IMEP_n > 600$ kPa or BMEP > 400 kPa, the uncertainty is 3% for all efficiencies. When the spark is retarded substantially to avoid knock, the variation of the knock limited spark timing is responsible for most of the variation in the thermal efficiencies. Repeated measurements of the engine-out exhaust gas temperature reveal an uncertainty of 40º C.

Error bars are left out of the data figures because the Excel program, with which the figure were made, does not permit placement of error bars on individual points, or allow the height of error bars to be varied for different points in a series. However, if the error bars were to be included, then the error bar height for the various fuel-mix-related quantities and thermal efficiencies would have been nearly the same as the vertical spread of the data points around a trend line or curve, or within a small horizontal section. Therefore, unless otherwise noted, the spread of the data points can be interpreted in the same way that error bars would be interpreted, especially for figures containing a large number of data points in each series.

CHAPTER 4
EXHAUST EMISSIONS

4.1 Introduction and Background

An ammonia and gasoline dual fueled engine is expected to emit some ammonia (NH_3), hydrocarbons, and carbon monoxide (CO) in the exhaust. Nitric oxide (NO) and nitrous oxide (N_2O) are also known to be significant exhaust constituents. However, for near stoichiometric operation, nitrogen dioxide (NO_2) is expected to be present in only about 1% or less of the typical total NO_x concentration. Near stoichiometric, ammonia fueled spark ignition engines are known to emit about 30-50 PPM N_2O and less than 30 PPM NO_2 whenever there is enough time and spark advance for adequate combustion [Gray et al., 1966]. The FTIR did not indicate significant quantities of NO_2 for either the engine-out or post-catalyst measurements in this study, so NO_2 is not reported. Only the NO portion of NO_x is measured and reported.

Ammonia is an irritant. Nitric oxide and hydrocarbons are precursors for ground level ozone. Carbon monoxide is toxic. N_2O is a greenhouse gas that is about 300 times more potent than carbon dioxide [US EPA, 2006]. A stoichiometric, ammonia fueled engine that emits 40 PPM N_2O, without any CO_2 has about 1/10 of the brake specific global warming potential as does one fueled by gasoline that emits 15% carbon dioxide without any N_2O, if the engines have the same efficiency.

The engine-out exhaust emissions measurements represent the worst case scenario for how much of the various pollutants are produced when the engine is simply left to bark. The combustion inefficiency is calculated from the engine-out emissions. The post-catalyst exhaust emissions show how the emissions clean up for near-stoichiometric operation.

104

4.2 Engine-Out Exhaust Emissions

The engine-out exhaust emissions of NH_3, NO, N_2O, and CO were measured on a wet basis, using the FTIR. Hydrocarbons were measured on a dry hexane basis, using the NDIR. The hydrocarbon emissions are stated in the C_1 (methane) basis. The overall combustion inefficiency is also characterized.

The FTIR's reading for NH_3 saturated whenever the NH_3 concentration within the analyzer exceeded about 1500 PPM. NH_3 was the only component for which saturation was a significant concern for the engine-out exhaust emissions. The saturation problem was solved by metering mostly dry air into the FTIR unit along with a comparatively small exhaust gas input, thereby diluting the exhaust gas to the extent required to avoid saturating the NH_3 reading. Dilution ratios typically between 5 and 40 were used. For each reading, the dilution ratio was found by comparing the FTIR's H_2O and CO_2 readings for diluted and undiluted exhaust.

Each engine-out exhaust emissions measurement taken with the FTIR consists of an average of at least 4 unsaturated readings of 30 seconds duration each, and these readings were split between at least two different dilution ratios. The NDIR hydrocarbon readings were run continuously, and each measurement consists of an average of 2 readings. The typical spread between the highest and lowest FTIR readings at each point was 10-20%, and for the NDIR hydrocarbon readings it was 5%.

Most of the engine-out exhaust emissions data were taken for combinations of load and fuel mix within the region bounded by the rough limit and MBT knock limit at 10:1, as shown in Figure 4.1. These previously established MBT knock limit data (solid lines) and rough limit trend lines (dashed lines) are from Figure 3.16. 10:1 appears to be the best compression ratio for an ammonia and gasoline dual fueled engine, although a different combustion chamber shape, etc. may change this slightly.
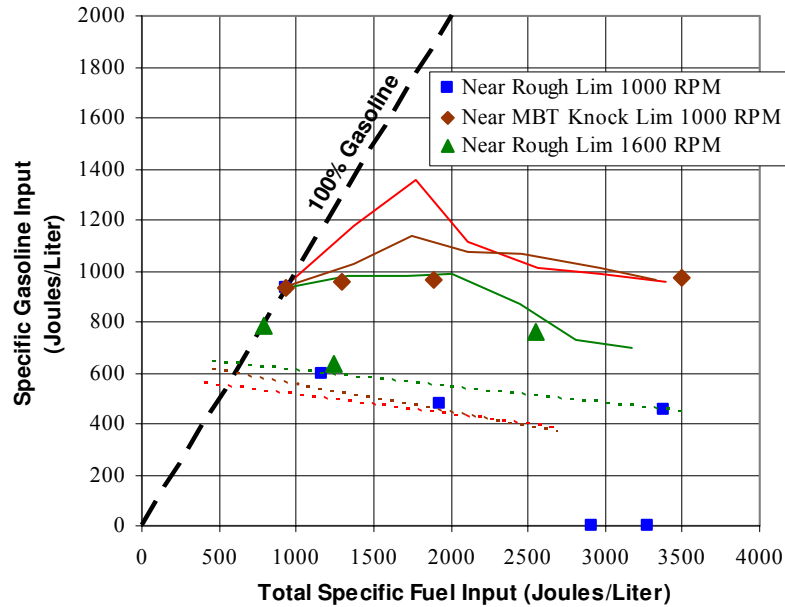
Figure 4.1. The 10:1 points, for which engine-out emissions were measured, shown among the previously established knock and rough limits.

MBT spark advance and gasoline were used for the points on the 100% gasoline line. Two other points that use KLSA and gasoline at 10:1 are included in the engine-out exhaust emissions study, but these are not shown in Figure 4.1.

Engine-out emissions were also characterized at 9:1, WOT, 1000 RPM for varying fuel mixtures. For the 9:1 sweep the rough limit occurred near 20% gasoline, and the MBT knock limit occurred near 60% gasoline. The 100% gasoline point for 9:1, WOT and the two KLSA points at 10:1 are lumped together in the assorted gasoline, KLSA group. For the 9:1, WOT point at 73% gasoline, the spark was only slightly retarded of MBT to avoid knock. The engine-out oxygen sensor was used for the closed loop fuel control, and the threshold voltage was set at 0.45 volts for all engine-out emissions results.

The engine-out NH_3 exhaust emissions, shown in Figure 4.2, are proportional to the concentration of ammonia in the intake mixture as long as the gasoline input is adequate. There is little difference between operation at the rough limit and MBT knock limit, and the speed does not make a significant difference. There is no significant engine-out emission of NH_3 during operation on 100% gasoline. The engine-out emission of NH_3 in the exhaust increases markedly when the gasoline input is shut off.

106
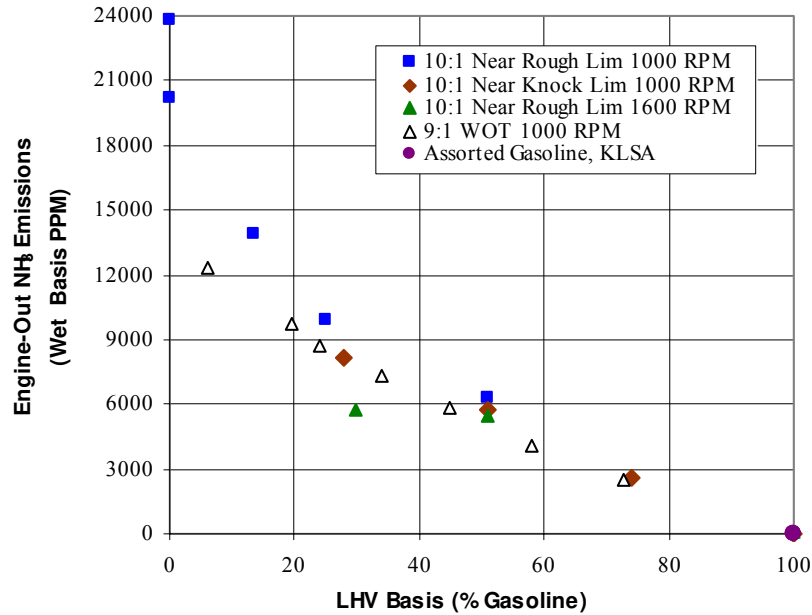
Figure 4.2. The engine-out NH$_3$ exhaust emissions, graphed as a function of fuel mix.

The NH$_3$ emissions data show that it is not desirable to turn off the combustion promoter input even when a low COV(IMEP$_n$) is observed when the combustion promoter is turned off at high loads and low speeds. For a given load, the gasoline input must be set at or above the rough limit trend lines pictured in Figure 4.1. About 4-5% of the ammonia input and 1-2% of the total hydrocarbon input escaped into the exhaust pipe for most operating points. The engine-out NH$_3$ measurements at or near 0% gasoline agree substantially with the 15000 PPM value reported by Graves et al. (1974) and 12000 PPM reported by Shand et al. (1985), for operation on ammonia without combustion promoter.

Figure 4.3 shows the engine-out NO emissions, which did not depend strongly on the fuel mix. Figure 4.3 agrees closely with Sawyer's engine-out NO measurements of 1900 PPM for stoichiometric operation on ammonia, and 2500 PPM for stoichiometric operation on isooctane.
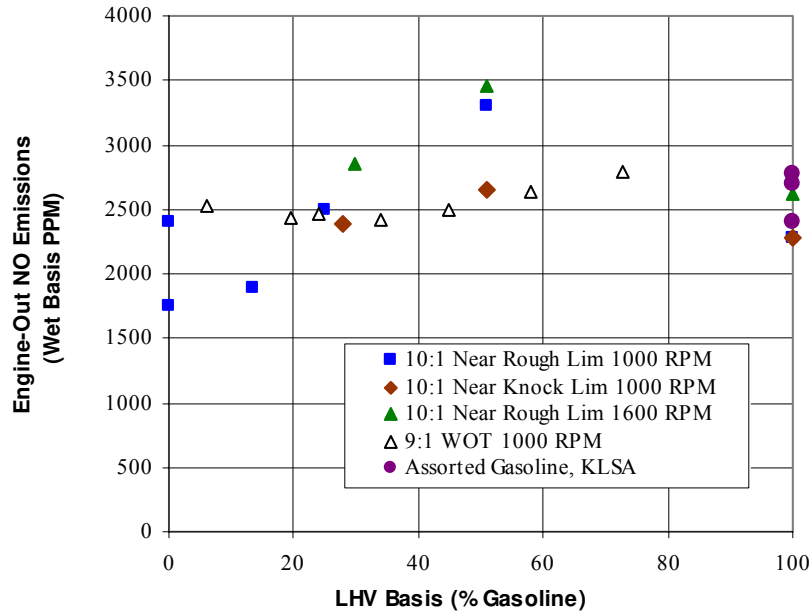
Figure 4.3. The engine-out NO emissions graphed as a function of fuel mix.

The adiabatic flame temperature is expected to be lower when more ammonia is used, but there are also nitrogen-hydrogen bonds being broken which may facilitate the formation of NO as part of the ammonia combustion process. The in-cylinder NO concentration during combustion of ammonia can be up to 10 times greater than the engine-out NO concentration [Sawyer et al., 1968].

Figure 4.4 shows that insignificant quantities of N_2O were produced for operation on 100% gasoline, but that usually 10-40 PPM of N_2O is present whenever some ammonia is used. This result agrees closely with Gray et al. (1966) who observed typically 30-50 PPM N_2O for near stoichiometric operation on ammonia at or below 1600 RPM with adequate spark advance and no combustion promoter.

The most important factor that determines CO emissions is the fuel mix. Figure 4.5 shows that the engine-out CO emissions are proportional to the concentration of gasoline in the intake mixture. The CO emissions for 100% gasoline do not depend significantly on whether KLSA or MBT spark timing is used.
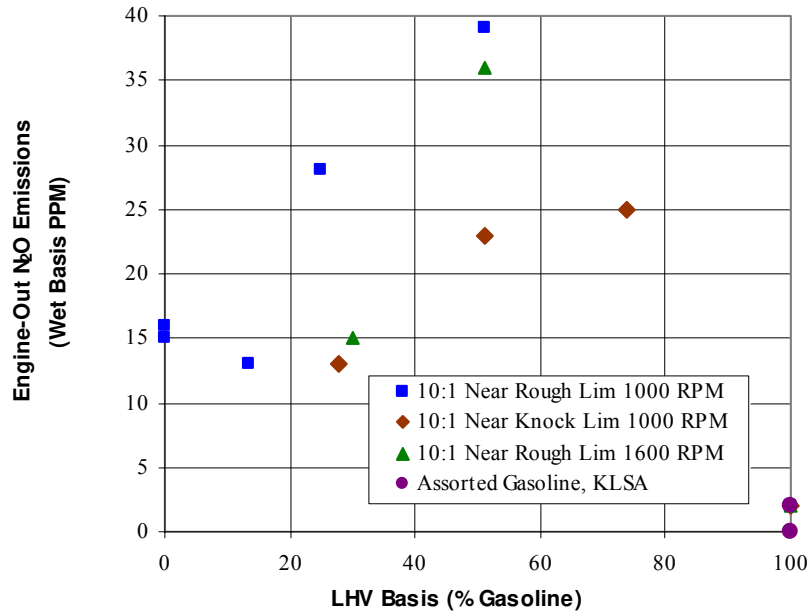
Figure 4.4. The engine-out N₂O emissions graphed as a function of fuel mix.
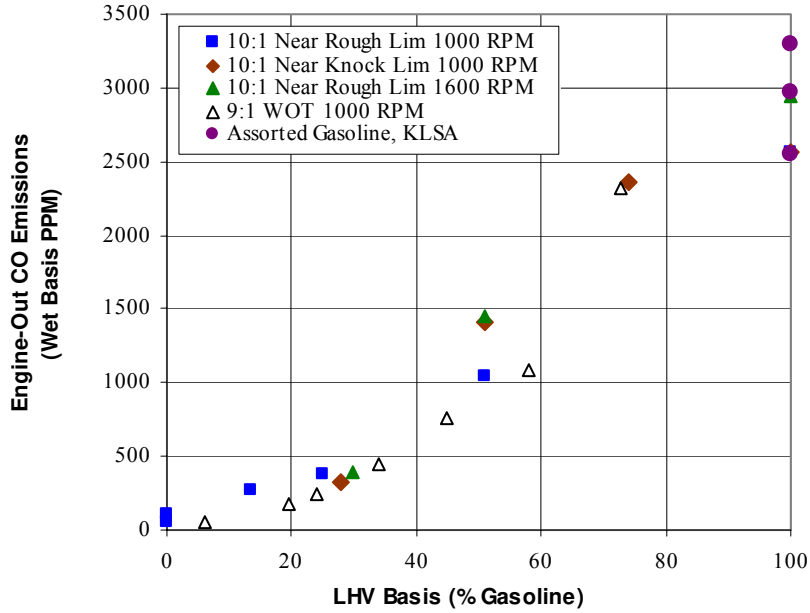
Figure 4.5. The engine-out CO emissions graphed as a function of fuel mix.

The engine-out hydrocarbon emissions shown in Figure 4.6 change little as the gasoline content in the fuel mix is reduced from 100% to 70%. The hydrocarbon emissions go down as the gasoline content is reduced below 70%. The most important factors that determine hydrocarbon emissions are the fuel mix, and whether MBT spark timing is used. The hydrocarbon emissions are reduced significantly when KLSA is required, probably because the burning gases are not pushed into crevice volumes as much when the flame reaches those regions. The 9:1 point at 73% gasoline also required the use of KLSA. The 10:1, 1600 RPM point at 100% gasoline occurred near idle, and it registered a low hydrocarbon reading probably because of a delayed end of burn similar to that obtained when KLSA is required.

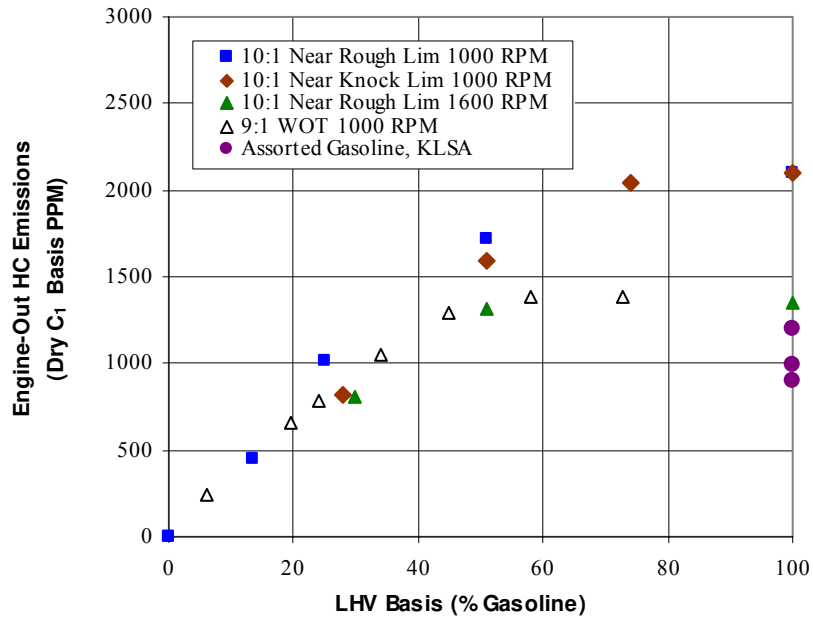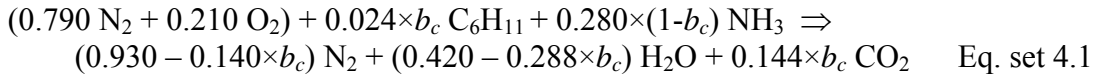**Figure 4.6. The engine-out hydrocarbon emissions, graphed as a function of fuel mix.**

4.3 Combustion Inefficiency

The engine-out emissions data were used to calculate the hydrocarbon and ammonia unburned fractions, and also the total combustion inefficiency. The hydrocarbon

unburned fraction was calculated from the dry C_6 basis engine-out exhaust hydrocarbon emission measurement and is expressed as a percentage of the total hydrocarbon input. The ammonia unburned fraction was calculated from the wet basis engine-out exhaust NH_3 emission measurement and is expressed as a percentage of the total ammonia input. The total combustion inefficiency takes into account the enthalpy of combustion of hydrocarbons, NH_3, NO, and CO, and is expressed as a percentage of the total fuel input. Whenever measured, the N_2O contribution was also included, but it was insignificantly small. The hydrocarbons found in the exhaust are assumed to have the same heating value and H/C ratio as does the gasoline, such that one C_6 unit is expressed as C_6H_{11} for performing various calculations. One C_6 unit contains six C_1 units. The products of incomplete combustion are treated as a perturbation on the combustion equation, and ideal combustion is assumed in all calculations. Equation set 4.1 describes the relationship between intake composition and exhaust composition for the stoichiometric combustion of gasoline and ammonia in one mole of air.

$$(0.790 \ N_2 + 0.210 \ O_2) + 0.024 \times b_c \ C_6H_{11} + 0.280 \times (1\text{-}b_c) \ NH_3 \ \Rightarrow$$
$$(0.930 - 0.140 \times b_c) \ N_2 + (0.420 - 0.288 \times b_c) \ H_2O + 0.144 \times b_c \ CO_2 \qquad \text{Eq. set 4.1}$$

LHV energy yield per mole of air: $(88.7 - 4.0 \times b_c)$ kJ

Moles of dry exhaust product per mole of air: $(0.930 + 0.004 \times b_c)$ moles.

Moles of wet exhaust product per mole of air: $(1.350 - 0.284 \times b_c)$ moles.

For example, when $b_c = 1$ (100% gasoline) the hydrocarbon unburned fraction is 1% when there are $0.01 \times 0.024 \times 1 = 0.00024$ moles of C_6H_{11} per $(0.930 + 0.004 \times 1) = 0.934$ moles of dry exhaust product, which is 257 PPM dry C_6 basis, or 1542 PPM dry C_1 basis. For $b_c = 0.3$, the ammonia unburned fraction is 5% when there are $0.05 \times 0.28 \times (1 - 0.3) = 0.0098$ moles of NH_3 per $(1.35 - 0.284 \times 0.3) = 1.2648$ moles of wet exhaust product, which is 7748 PPM NH_3, wet basis. Similar calculations were done to find the total combustion inefficiency, for which all of the pollutants register a LHV combustion energy per mole of air, and this is expressed as a percentage of the total fuel LHV energy

input. At $b_c = 1$, the hydrocarbons and CO are the principal carriers of unused chemical energy, and at $b_c = 0$ most of the combustion inefficiency is due to the NH_3 in the exhaust.

Figure 4.7 shows that the total combustion inefficiency goes from about 2% for 100% gasoline, up to 4-5% for operation on 50-80% ammonia. The combustion inefficiency deviates upward from this smooth variation when the gasoline is turned off. It appears that the combustion promoter should not be turned off at low speed and high load even if the COV(IMEP$_n$) remains low when that is done. A combustion inefficiency increase of 4% (from 2% to 6%) should have produced a net indicated thermal efficiency loss of about 1%, but a substantial efficiency loss is not observed unless the engine is run with COV(IMEP$_n$) in excess of 5-10%.
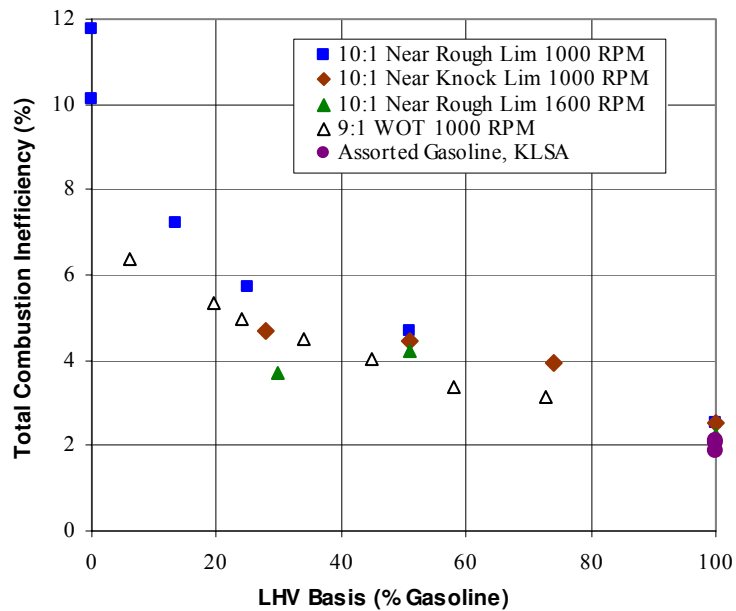
Figure 4.7. The total combustion inefficiency.

Figure 4.8 shows an example in which the net indicated thermal efficiency did not respond to a loss of combustion efficiency. The net indicated thermal efficiency went up when the operation was moved away from 100% gasoline because KLSA was required at 100% gasoline. The net indicated thermal efficiency remained essentially unchanged in

response to further substitution of gasoline with ammonia, despite the apparent combustion efficiency loss.
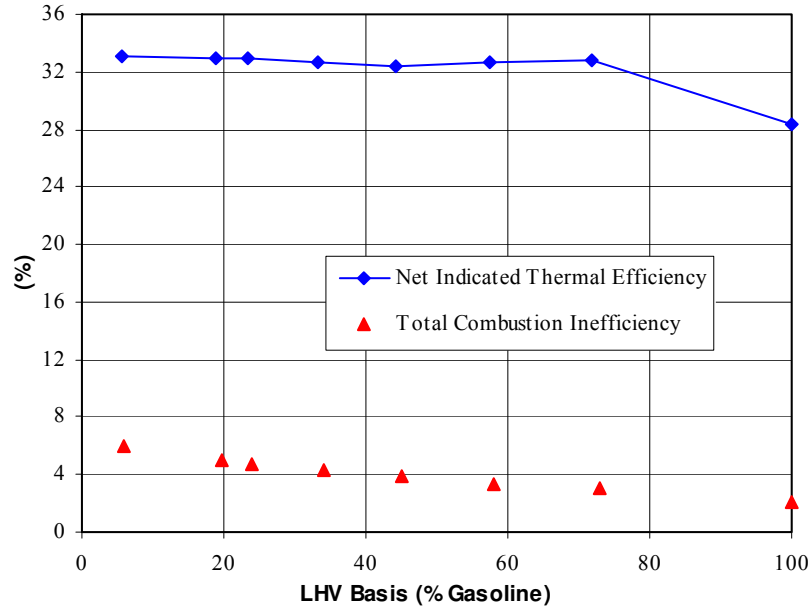
Figure 4.8. The net indicated thermal efficiency and combustion inefficiency, graphed as a function of fuel mix at 9:1, WOT, 1000 RPM.

Figure 4.9 shows that there is a discrepancy between the unburned fractions of ammonia and hydrocarbons. One should expect that any combustion chamber quench zones, such as crevice volumes, would produce the same unburned fraction for both fuels, but the observed hydrocarbon unburned fraction was only about $^2/_5$ of the observed ammonia unburned fraction when both fuels were used.

It is likely that, although both fuels are present in the same unburned fractions after the initial combustion, the hydrocarbons continue to oxidize in the post flame condition, but the ammonia does not. For that reason, the engine-out pollutant concentrations are not fully indicative of the in-cylinder combustion efficiency before post-flame burn-up. The in-cylinder combustion efficiency before post-flame burn-up is probably not much worse for ammonia promoted with gasoline than it is for gasoline alone. Some strategies for improving the combustion efficiency, such as minimizing the occurrence of quench zones, would be equally applicable in the use of both fuels.
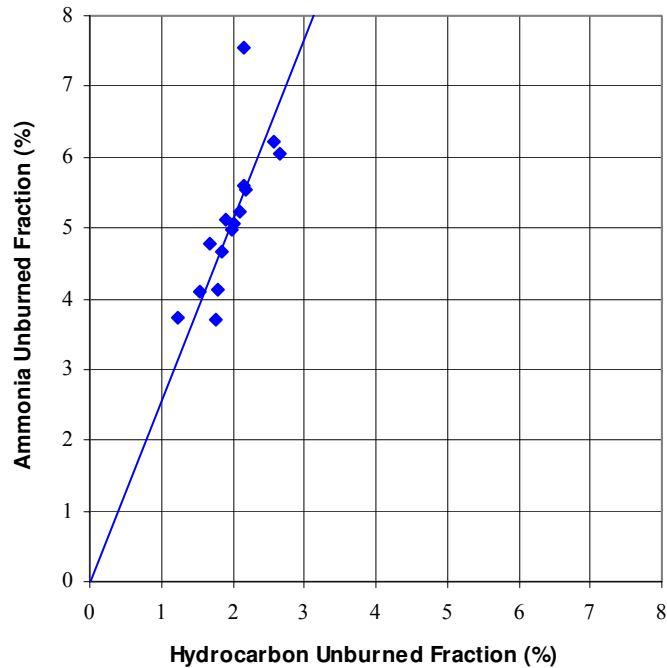
Figure 4.9. The hydrocarbon and ammonia unburned fractions.

4.4 Post-Catalyst Exhaust Emissions and Oxygen Sensor Characteristics

The post-catalyst emissions of NH_3, NO, N_2O, CO and hydrocarbons were measured at 10:1, 1000 RPM, and combinations of load and fuel mix for which the gasoline input was slightly above the rough limit (except 100% ammonia). Fuel mixtures consisting of 100% gasoline, ½ gasoline and ½ ammonia, ¼ gasoline and ¾ ammonia, $^1/_8$ gasoline and $^7/_8$ ammonia, and 100% ammonia (LHV energy basis) were used. The goal is to characterize an emission clean-up point and show how the engine-out and post-catalyst oxygen sensors respond to the use of ammonia.

No exhaust dilution was used for any post-catalyst emissions measurements, because post-catalyst pollutant concentrations were much lower than the engine-out concentrations for near-stoichiometric operation. The FTIR's NH_3 reading saturated sometimes when the average equivalence ratio was more than 0.5% rich, so the NH_3 reading for those points is sometimes too low. Nevertheless the results below 0.5% rich are adequate to demonstrate post-catalyst emissions clean-up.

Each post catalyst emissions measurement taken with the FTIR consists of an average of 2 readings of 30 seconds duration each. The NDIR hydrocarbon readings were run continuously, and each measurement consists of an average of 2 readings. The typical spread between the highest and lowest FTIR readings at each point was 20-30%, and for the NDIR hydrocarbon readings it was 10-20%. The spread was larger for post-catalyst emissions than for engine-out emissions because of the variation in the clean-up efficiency during the measurement.

For each post-catalyst emissions measurement, the state of the fuel control loop was frozen at various average equivalence ratios that were very close to stoichiometric. Both the engine-out and post-catalyst oxygen sensor voltages were noted, and the center of the range of fluctuation was reported. If, during an emissions measurement, an oxygen sensor voltage was found to fluctuate between 0.3 and 0.5 volts, then 0.4 volts was reported for that sensor. Fluctuations ranging between 0.58 and 0.62 volts, 0.3 and 0.5 volts, and 0.1 and 0.15 volts, were typical for either sensor.

Figure 4.10 shows that the post-catalyst emissions correlate poorly with the engine-out oxygen sensor voltage when the results for all fuel mixtures ranging from 100% gasoline to 100% NH_3 are lumped together. In all post-catalyst emissions plots, the hydrocarbon emissions are stated in the dry C_1 basis, and the N_2O measurements are rescaled by a factor of 10 so that the same axes can be used to plot all pollutants.

Figure 4.11 shows that the post-catalyst emissions correlate very strongly with the post-catalyst oxygen sensor voltage. Figure 4.11 includes results for all fuel mixtures ranging from 100% gasoline to 100% ammonia. The combustion products were more fully reacted upon leaving the catalytic converter, so the post-catalyst oxygen sensor readings correlate better with the stoichiometric point. The best clean up occurred for post-catalyst oxygen sensor readings between 0.25 and 0.55 volts. The post-catalyst exhaust gas temperature remained between 340 and 570 Celsius during the post-catalyst emissions tests.
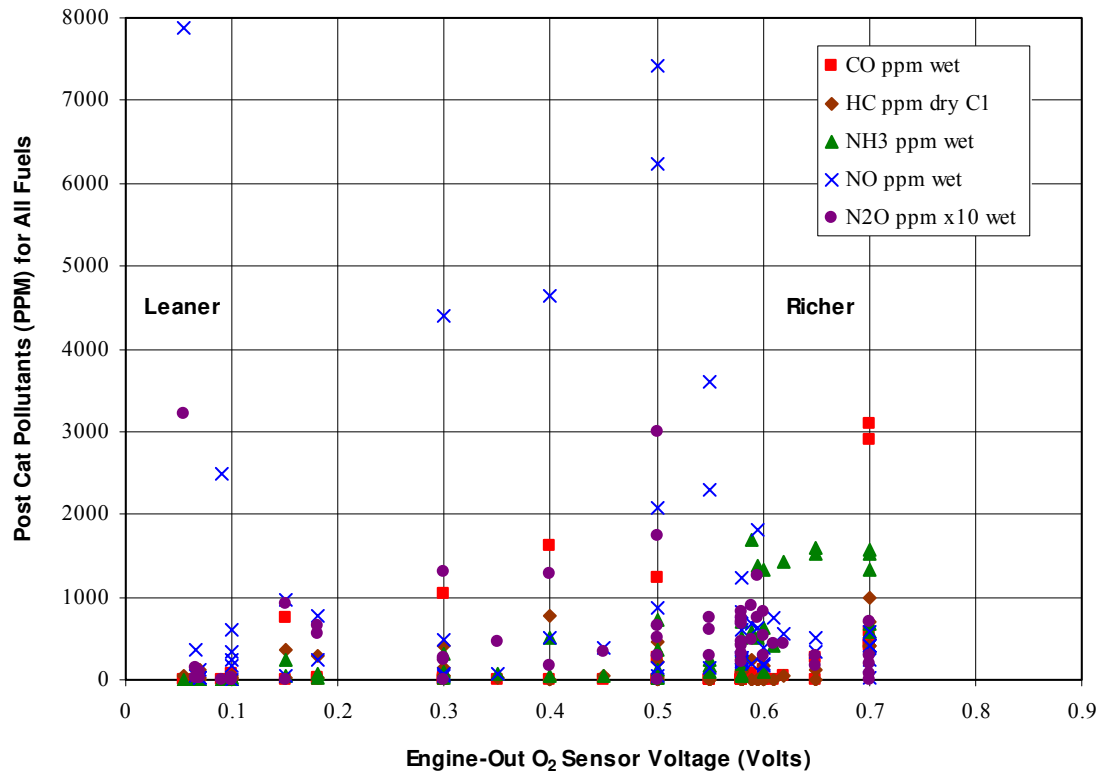
Figure 4.10. The post-catalyst emissions graphed as a function of engine-out oxygen sensor voltage for all fuels.
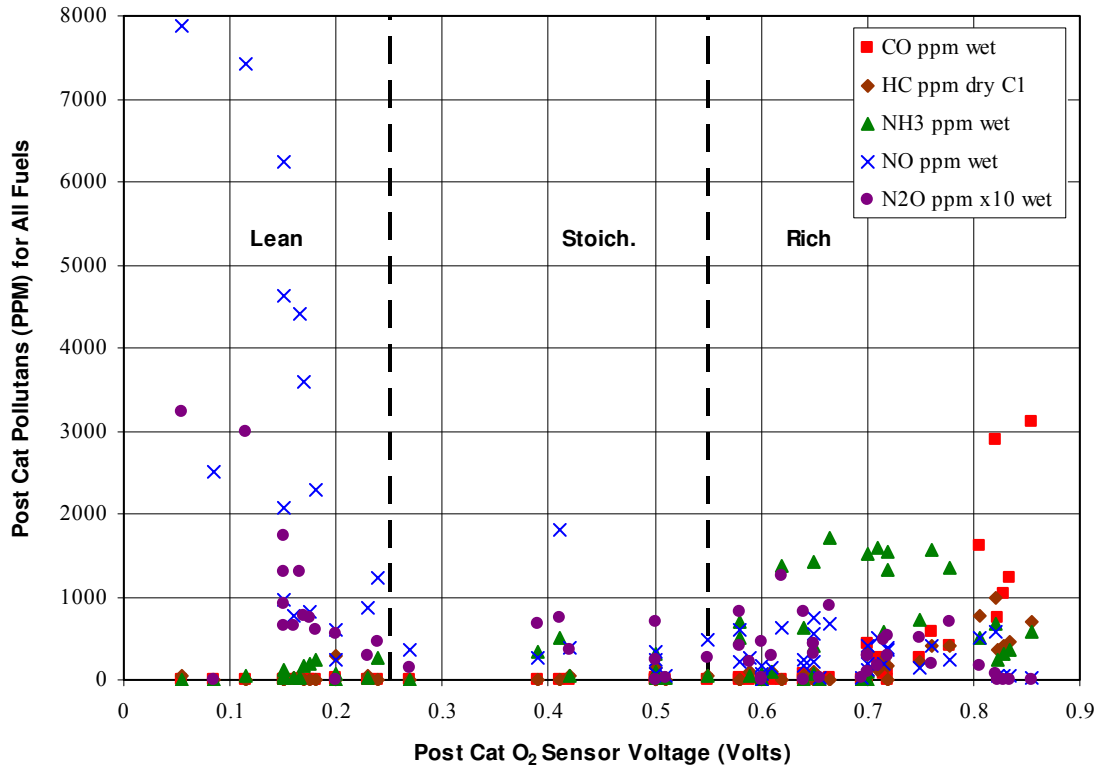
Figure 4.11. The post-catalyst emissions graphed as a function of post-catalyst oxygen sensor voltage for all fuels.

Ideally, the engine-out and post-catalyst oxygen sensor readings should have been the same. Figure 4.12 shows the deviation from the ideal oxygen sensor agreement. For 100% gasoline the engine-out oxygen sensor reading was biased low, most likely because of an incomplete reaction of residual exhaust products on the sensor's catalyst surface. For 100% ammonia the engine-out oxygen sensor reading was biased high, most likely because the over oxidation of NH_3 into NO, at the sensor surface, consumed the available oxygen even to the extent that there was very little molecular oxygen present when the overall exhaust chemistry was still slightly lean.
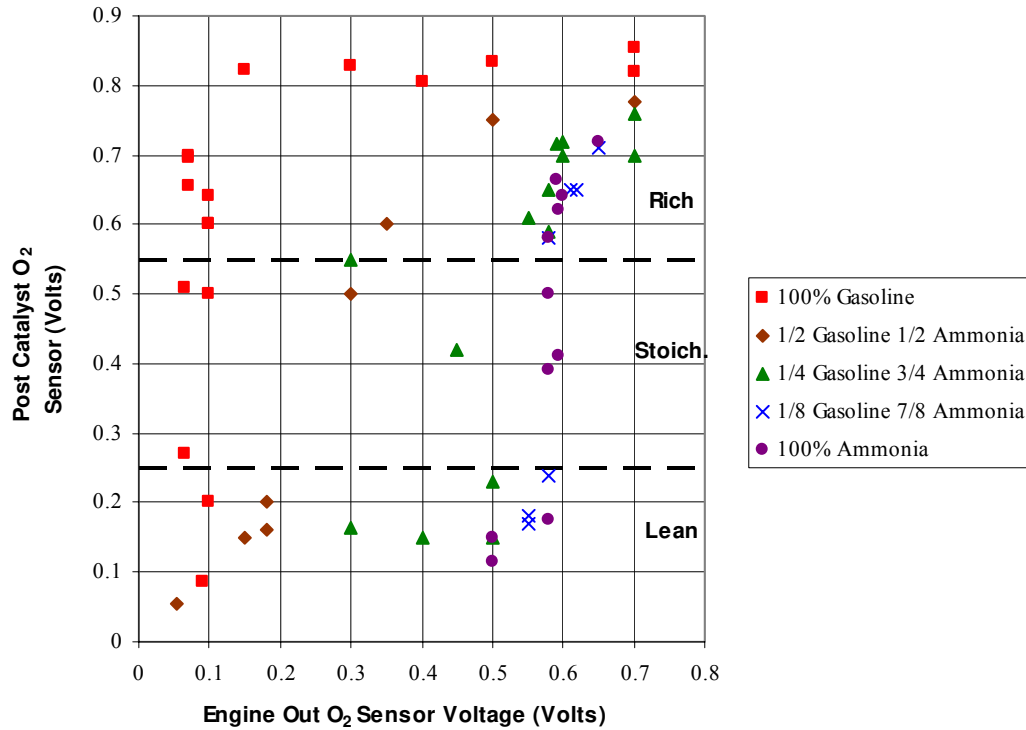
**Figure 4.12. The correlation between the engine-out
and post-catalyst oxygen sensor readings.**

Figure 4.13 shows that there was an imperfect relation between the engine-out oxygen sensor readings and equivalence ratio. The equivalence ratio deviation from stoichiometric was calculated from the post-catalyst exhaust emissions. A negative equivalence ratio deviation from stoichiometric corresponds to slightly lean operation, for which the principal leftover component was NO. A positive value corresponds to slightly rich operation, for which the principal leftover components were NH_3, CO, and hydrocarbons. The post-catalyst oxygen sensor reading provided a much more reliable indication of the stoichiometric point than did the engine-out oxygen sensor reading.
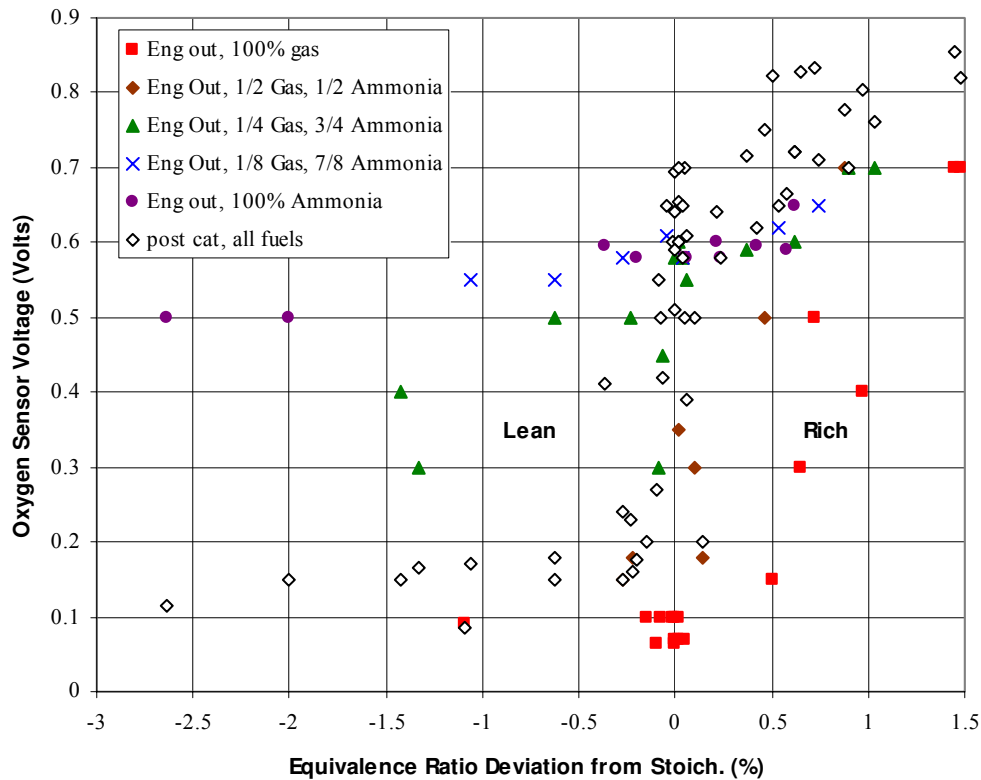
**Figure 4.13. The engine-out and post-catalyst oxygen
sensor readings at different equivalence ratios.**

The points at 1.1%, 2.6%, and 5.8% lean also included corrections for the molecular
oxygen in the post-catalyst exhaust. The molecular oxygen content was estimated from
the post-catalyst oxygen sensor voltage and post-catalyst exhaust gas temperature for
those three points. All other points had very little molecular oxygen in the post-catalyst
exhaust, despite the comparatively large quantities of NO present for slightly lean
operation. Also, no measurements of, or corrections for, molecular hydrogen were made
for slightly rich operation.

The post-catalyst emissions near the clean up point are plotted as a function of the
equivalence ratio deviation from stoichiometric for different fuel mixtures in Figures 4.14
through 4.18. Figure 4.14 shows that for operation on 100% gasoline, NH_3 was produced
on the catalyst during slightly rich operation. The NH_3 was most likely produced by the
over-reduction of NO on the catalyst [Shores et al., 2001]. Hydrocarbons and CO also
passed through the catalyst during rich operation. The post-catalyst NO emissions for

gasoline plateau at the engine-out value near 2000-3000 PPM under slightly lean operation.
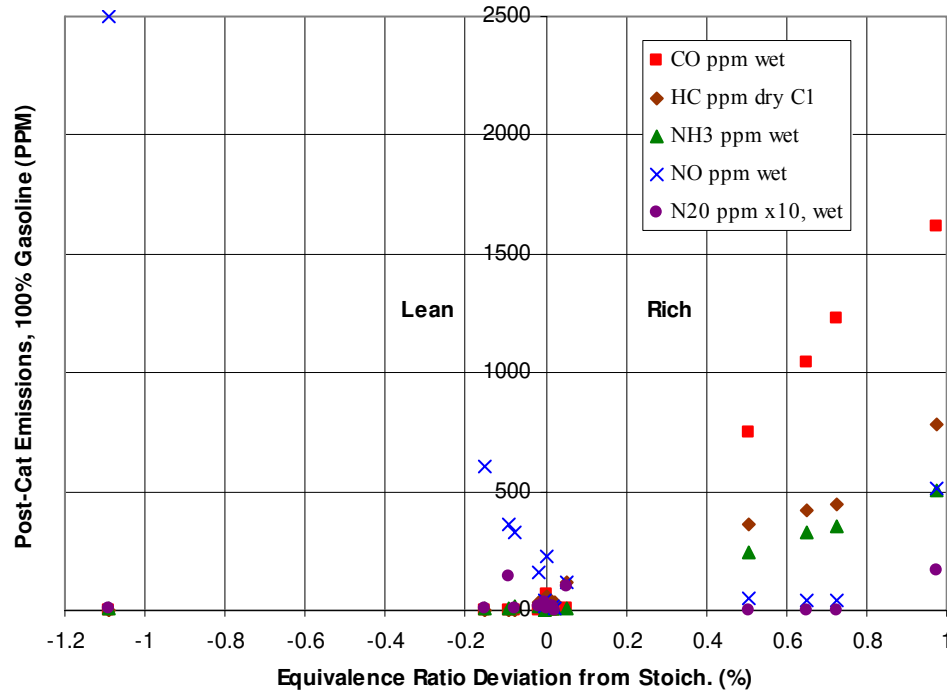
Figure 4.14. The cleanup graph for 100% gasoline.

For part ammonia, part gasoline operation, (Figures 4.15 through 4.17) there are less hydrocarbons and CO going through the catalyst under rich operation, because less are produced by the engine. N_2O is present at a range of 20-50 PPM in the clean up region, which is between stoichiometric and 0.2% rich. For 3% lean operation, the post-catalyst concentration of N_2O reaches 300 PPM, and NO nearly reached 8000 PPM, far in excess of the engine-out values for these pollutants. It appears that N_2O and NO are formed in the catalytic converter from the over oxidation of NH_3 whenever the engine runs lean. For that reason, lean operation on ammonia must be absolutely avoided when a standard three-way catalyst is used.
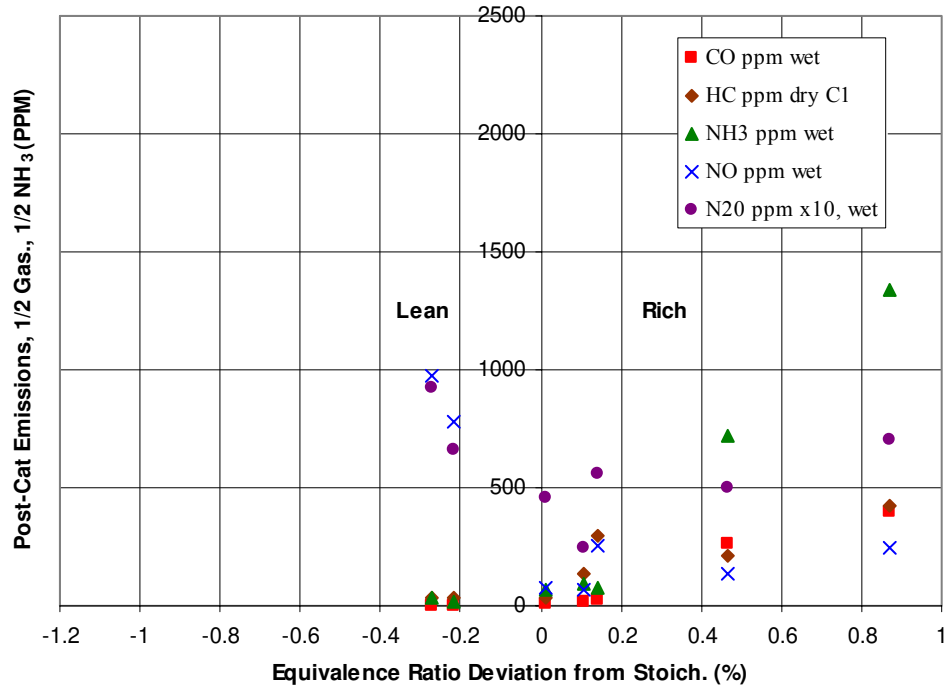
Figure 4.15. The cleanup graph for 1/2 gasoline, 1/2 ammonia.
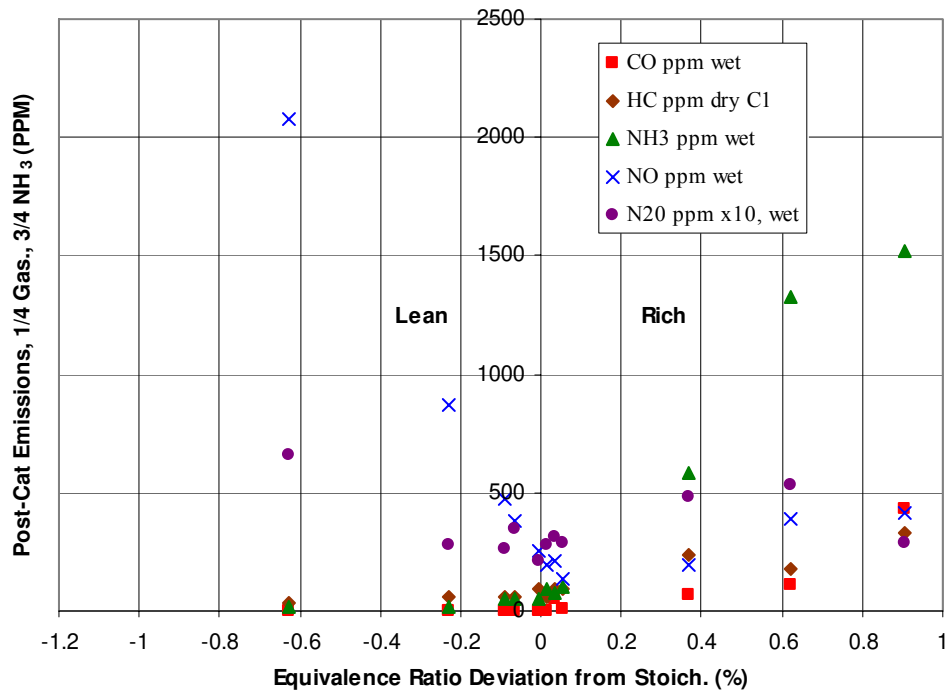
Figure 4.16. The cleanup graph for 1/4 gasoline, 3/4 ammonia.

121
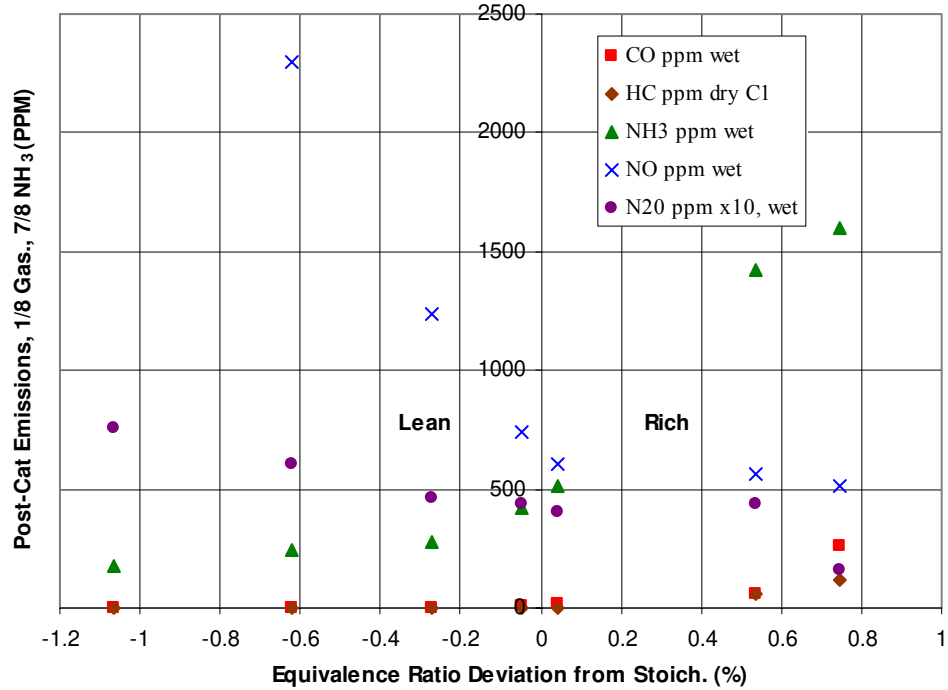
Figure 4.17. The cleanup graph for 1/8 gasoline, 7/8 ammonia.

Figure 4.18 shows the cleanup characteristics for operation on 100% ammonia. There were no detectable post-catalyst hydrocarbon emissions, and the CO concentration remained below 20 PPM, even for rich operation on 100% ammonia. The post-catalyst N_2O emissions in the clean up region were about 70 PPM, roughly 3 times the engine-out value, and significantly higher than the post-catalyst emissions of N_2O for part ammonia, part gasoline operation. The increased post-catalyst emission of N_2O was probably caused by the elevated engine-out emission of NH_3, which is known to occur when the gasoline is completely turned off. The NH_3 and NO still cleaned up to a few hundreds of parts per million when the equivalence ratio was between stoichiometric and 0.2% rich.
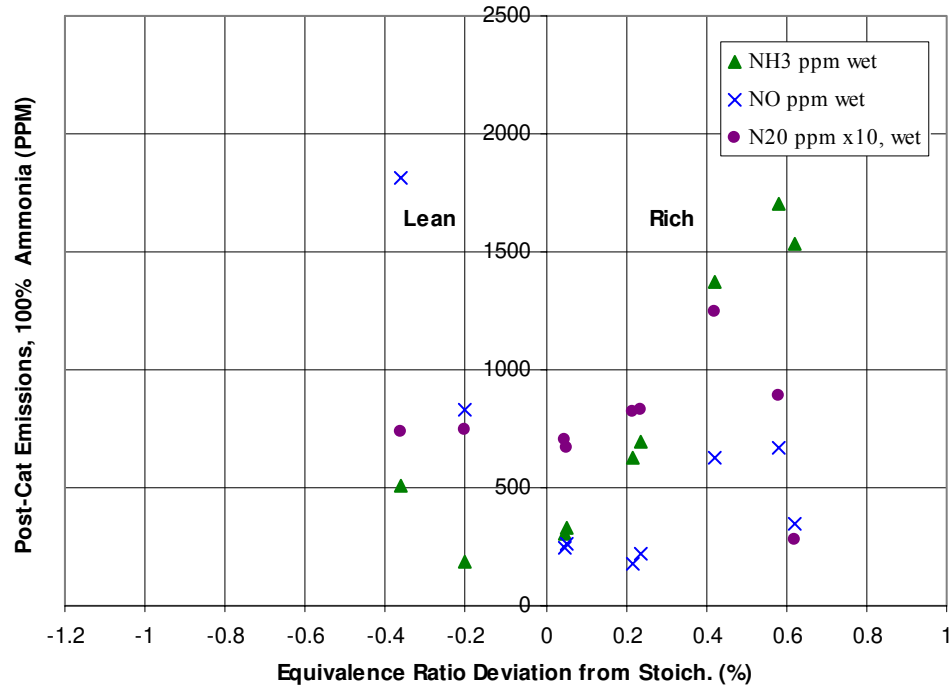
Figure 4.18. The cleanup graph for 100% ammonia.

Figure 4.19 shows the post-catalyst emissions for operation on all fuels. NH_3, CO, and hydrocarbons pass through the catalyst during rich operation. Excessive quantities of N_2O and NO are made on the catalyst during lean operation whenever any ammonia is used. Shand et al. (1985) found excessive post catalyst emissions of NO, which tracked the engine-out NH_3 emissions, and nearly complete removal of NH_3 by the catalyst for both rich and lean operation. The most likely explanation of this difference in their result is that air was introduced somewhere within or before the catalyst, although this was not specified in their work.

The ideal equivalence ratio for clean up is between stoichiometric and 0.2% rich, for all fuels. The catalyst has some effectiveness for reducing most pollutants below the engine-out values when the equivalence ratio deviation from stoichiometric is between 0.6% lean and 1.5% rich, for all fuels. The quantities of N_2O and NO significantly exceed the engine-out values when ammonia is used at an equivalence ratio deviation from stoichiometric which is leaner than about 1% lean.
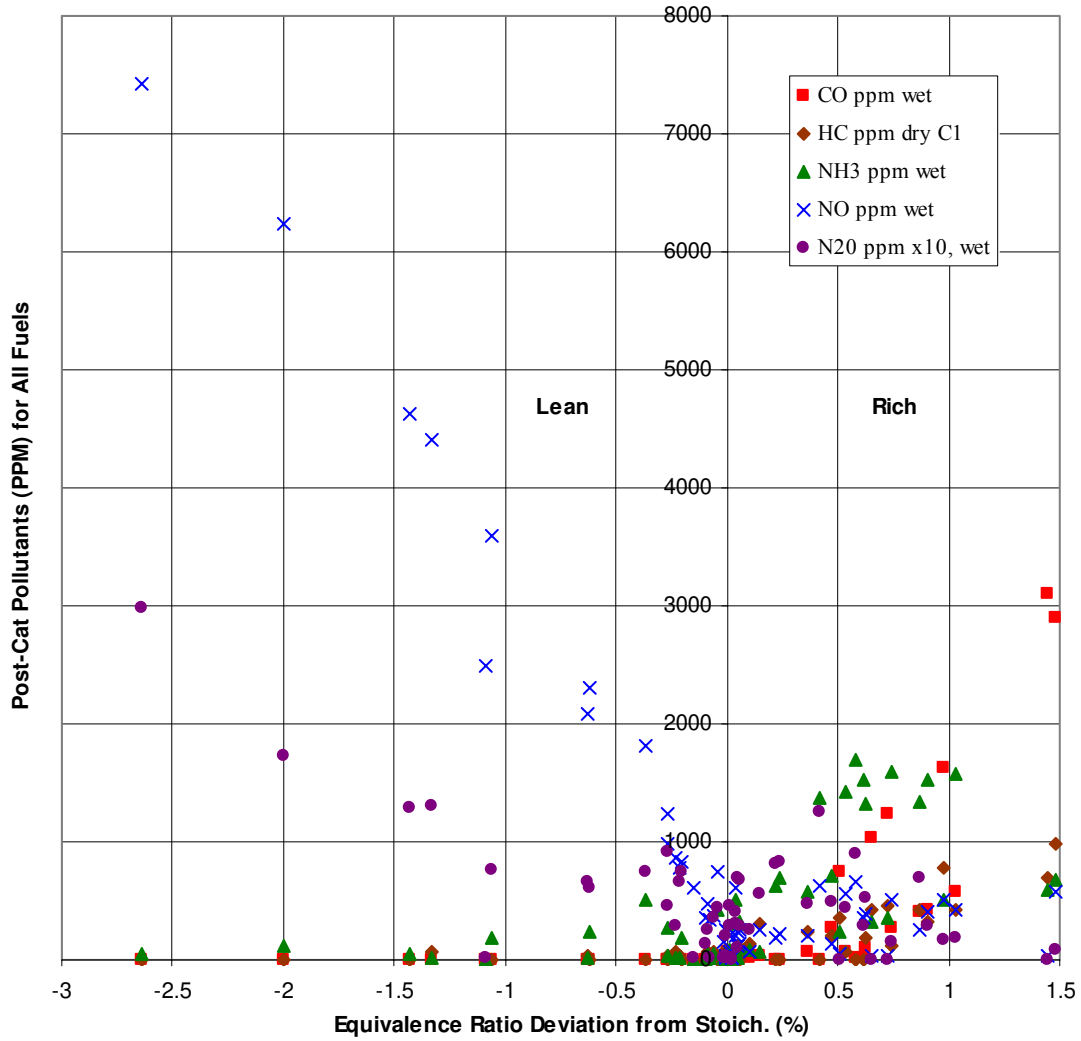
Figure 4.19. The post-catalyst emissions for all fuels.

Figure 4.20 shows post catalyst emissions in the cleanup region for gasoline and dual fueled operation. It contains three points for 100% gasoline, three for ½ gasoline, ½ ammonia, four for ¼ gasoline, ¾ ammonia, and two points for $^1/_8$ gasoline, $^7/_8$ ammonia. Operation on 100% ammonia is excluded from Figure 4.20, because discontinuously excessive engine-out NH_3 emissions and elevated post-catalyst N_2O emissions occur when the gasoline is turned off. The points shown are representative of how the clean-up region should typically behave for dual fueled operation. The emissions results support the suggestion first made in Chapter 3 that the gasoline input per cycle should kept constant with respect to load whenever any ammonia fuel is used.
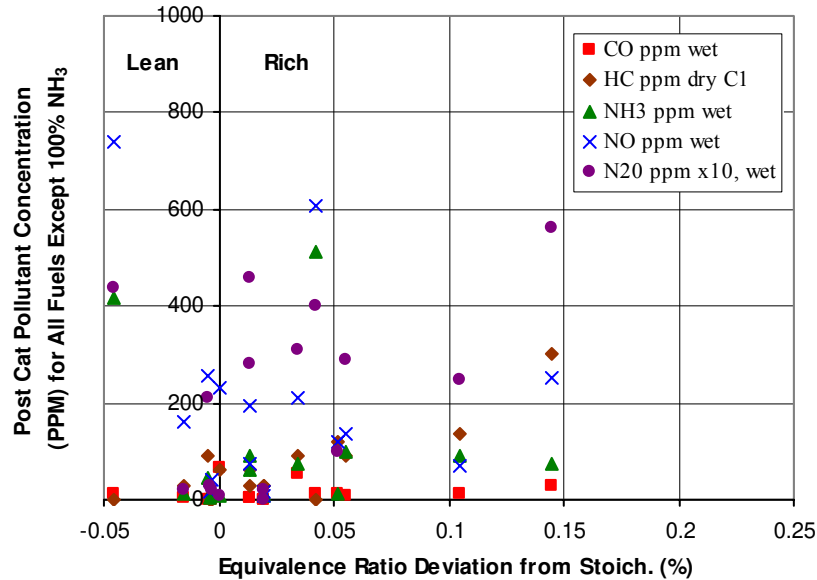
Figure 4.20. The post-catalyst emissions in the cleanup region for gasoline and dual fueled operation.

The typical post-catalyst emissions of NH_3, NO, CO and N_2O (wet basis) in the clean-up region are 100 PPM, 200 PPM, 30 PPM, and 30 PPM, respectively. The typical dry C_1 basis hydrocarbon emissions are 100 PPM. All pollutant emissions are reduced sharply from the engine-out values, except for N_2O, for which the engine-out emissions and post-catalyst emissions in the clean-up region are nearly the same. The partial brake specific global warming potential due to 30 PPM N_2O from an ammonia fueled engine operating at 30% brake thermal efficiency, is about $^1/_{20}$ of the brake specific global warming potential due to CO_2 from a gasoline fueled engine operating at 20% brake thermal efficiency.

Standard oxygen sensors and standard catalytic converters can be used for emissions clean-up when ammonia is used with gasoline, but lean operation must be absolutely avoided. The threshold voltage for the engine-out oxygen sensor must be set at about 0.6 volts to avoid a lean bias while running the engine on mostly ammonia. The engine-out oxygen sensor might also be heated so that the exhaust products react more fully on the surface of the sensor, thereby possibly avoiding a rich bias when running on mostly gasoline when the threshold voltage is set at 0.6 volts.

A post-catalyst oxygen sensor can also be used, so that true stoichiometric operation can be verified by the controller, and so that the state of the catalyst can be included within the control loop. A chemical economy of fixed nitrogen exists within the catalytic converter even when only gasoline is used, but the effect of rich and lean operation on post-catalyst NH_3, N_2O and NO emissions becomes much stronger whenever any ammonia fuel is used. For that reason, the inclusion of a post-catalyst oxygen sensor, while not absolutely necessary, is warranted much more strongly when some ammonia is used, than when only gasoline is used.

CHAPTER 5

CONCLUSION

5.1 Conclusions

Most of the gasoline burned by spark ignition engines can be replaced with ammonia when the $IMEP_n \geq 400$ kPa. A spark ignition engine cannot generally give acceptable performance while fueled by ammonia alone. However, there is a fuel mix map, as a function of load, speed and compression ratio, which specifies the degree to which gasoline can be replaced with ammonia while yielding acceptable operation. The required combustion promoter fraction is not constant, and it goes down with increasing load, and up with increasing speed. The compression ratio has a surprisingly weak effect on the combustion promoter requirement at the rough limit.

A similar, rescaled map of the rough limit should be expected when other fuels are used as combustion promoters for ammonia, or when a different engine design is used, such as the use of dual ignition or a different combustion chamber shape. There is no single, constant ratio of gasoline to ammonia that works appropriately for every combination of load and speed. For that reason, the combustion promoter and the ammonia should be stored in either separate tanks, or possibly separate phases within the same tank, and metered into the engine independently.

A compression ratio of 10:1 is recommended for the ammonia and gasoline dual fueled engine. There is a diminished return on raising the thermal efficiency, and also on reducing the gasoline requirement at the rough limit, for compression ratios above 10:1. The margin of error between the MBT knock limit and rough limit becomes small for ammonia promoted with either gasoline or E85 when the compression ratio is increased to 12:1. Improved combustion chamber geometry should yield a slightly higher optimal compression ratio for efficiency, and also for the knock and rough limit crossover, probably near 12:1 for both.

Ammonia's knock resistance allows engine operation at much higher mean effective pressures than those possible with the use of gasoline alone. The efficiencies at high load are also better, where comparable, when ammonia is used because MBT spark timing can be used with ammonia at high load. The use of ammonia with gasoline enables the continued use of MBT spark timing at combinations of load and compression ratio which are inaccessible to gasoline.

The exhaust emissions of an ammonia and gasoline dual fueled engine are reasonable when the engine is operating acceptably from the standpoint of combustion stability and overall thermal efficiency. The engine-out emissions appropriately reflect the proportioning of fuel content in the intake mixture. The standard three-way catalyst currently in use for gasoline fueled engines also works with ammonia, and the clean-up region occurs between stoichiometric and 0.2% rich, just as it also does for gasoline. Post-catalyst emissions show that standard oxygen sensors are at least nominally usable for closed loop fuel control while using ammonia.

5.2 Recommendations for Future Work

A fuel mix map, similar to the one found for the use of ammonia with gasoline, also needs to be found for the use of ammonia with methane, and also for the use of ammonia with hydrogen. The fuel mix map for the use of ammonia with hydrogen has been only partially established, and without the consideration of $COV(IMEP_n)$.

Hydrogen can either be stored separately from the ammonia, or it can be obtained by decomposing a controlled fraction of the ammonia mass flow into hydrogen and nitrogen. For the latter option it will be necessary to characterize the full interaction between an engine and an ammonia cracker heated by the engine exhaust, and improve the controllability of the device if necessary. One possible solution involves making most of the ammonia bypass the cracker, such that the entire ammonia stream need not be brought up to cracking temperature in order to decompose a small percentage of the ammonia. Instead, the cracker might be designed to nearly fully decompose a much

smaller ammonia stream, and then the decomposition ratio can be controlled by varying the ratio of ammonia directed through the cracker to that bypassing the cracker.

The recovery of blow down energy, as a feature possibly integrated into turbocharged operation, is not covered in this study. The operation of an engine, possibly incorporating a pulse turbo with electric assist, on ammonia and other fuels bears further investigation. Parameters such as compression ratio, turbo design, combustion chamber shape, ignition method, and adiabaticity should be varied to show the effect on efficiency and on the fuel mix map.

The exhaust catalyst could be reformulated to better optimize the clean-up characteristics for ammonia. For example, a catalyst component specialized for decomposing ammonia into hydrogen and nitrogen might be used to remove ammonia under slightly rich conditions, and minimize the transformation of ammonia into additional NO and N_2O under slightly lean conditions.

APPENDIX
OPEN FLAME AMMONIA COMBSTION EXPERIMENTS.

A.1 Introduction and Methods

The required ratio of combustion promoter to ammonia was characterized for an open flame at 1 bar pressure. Ammonia and hydrocarbon mixtures were metered into an open-air burner. The burner was fitted with two fuel nozzles: one for ammonia and another for hydrocarbons similar to propane. The fuel streams draft air into the burner by momentum transfer, and the burner has an air vent for adjusting the overall equivalence ratio. Appropriate nozzle diameters were used, such that the air flow required for stoichiometric combustion occurred somewhere within the air vent's range of adjustment. The ammonia nozzle diameter was made a bit less than 4 times the hydrocarbon nozzle diameter. This ratio of ammonia nozzle diameter to hydrocarbon nozzle diameter allows the ammonia and hydrocarbon mass flows to be varied independently without requiring the air vent to be adjusted.

The hydrocarbon mixtures tested were LPG and MAPP® gas. MAPP® gas is a mixture of 44% propyne and propadiene, 56% LPG. The lower heating value of both hydrocarbon mixtures is 46 MJ/kg. Ammonia has a lower heating value of 18.6 MJ/kg.

The burner was started, and then the hydrocarbon and ammonia inputs were adjusted to give a reasonable flame size and quality. The air vent on the burner was adjusted for best flame quality, which is assumed to occur near stoichiometric. The ratio of hydrocarbon flow to ammonia flow was minimized while still giving acceptable flame quality. The burner was run for 11-12 minutes.

Fuel mixtures consisting of mostly ammonia with a little hydrogen were also used. A balloon was partially filled with hydrogen, and its three principal diameters were measured. The balloon was then filled the rest of the way with ammonia and measured

again. The resulting hydrogen/ammonia mixture was fed into the ammonia nozzle, and the air vent was closed down slightly to compensate for the hydrogen. Different hydrogen concentrations were tried.

A.2 Results for Combustion of Ammonia and Hydrocarbons

At the start and end of the run, the ammonia and hydrocarbon bottles were weighed to determine the mass ratio at which the ammonia and hydrocarbon were consumed. The maximum permitted mass ratio of ammonia to LPG is 2.6, which corresponds to a combustion promoter requirement of 50% on a LHV energy basis. The maximum permitted mass ratio of ammonia to MAPP® gas is 3.6, which corresponds to a combustion promoter requirement of 40%. The total fuel energy per volume of the pre-flame mixture is about 3 kJ per liter for the test conditions. An ammonia and gasoline dual fueled engine has a combustion promoter requirement of 30-50% at the rough limit at 8:1 and 10:1 when the total in-cylinder fuel energy density at the spark is 3 kJ/liter. It appears that the combustion promoter requirement for consistent ignition and combustion of air/ammonia/hydrocarbon mixtures is similar, whether it takes place in an engine or in an open flame burner. Figure A.1 shows what an open flame looks like under different ammonia/hydrocarbon fueling conditions.
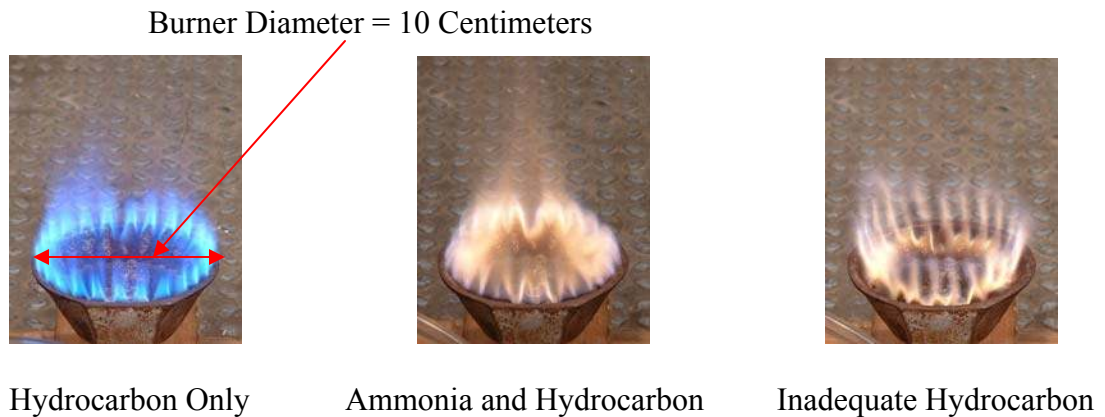
Burner Diameter = 10 Centimeters

Hydrocarbon Only   Ammonia and Hydrocarbon   Inadequate Hydrocarbon

Figure A.1. Open flames fueled by hydrocarbon, or ammonia with hydrocarbon.

The flame in the center photo of Figure A.1 is fueled by ammonia with adequate hydrocarbon input, and produces very little or no odor. The photo on the right shows that if too little combustion promoter is used, then the flame starts to form a finger-like structure. A strong ammonia smell is also observed when too little combustion promoter is used. The flame lifts away from the burner and develops intermittent gaps when the ratio of combustion promoter to ammonia is decreased further. The flame cannot be consistently sustained when fueled by ammonia alone.

A.3 Results for Combustion of Ammonia and Hydrogen

An ammonia/hydrogen flame is yellow. The flame in the right photo of Figure A.2 has an inadequate hydrogen input, and once again the finger-like structure is seen. The flame on the left has enough hydrogen. It was observed that a fuel mixture consisting of 25% hydrogen, 75% ammonia by volume also makes a good flame. The minimum required hydrogen content for an open flame at 1 bar is thus about 25% hydrogen, 75% ammonia by volume, or 20% hydrogen, 80% ammonia on a LHV energy basis. The open flame results suggest that the specific hydrogen input map for the rough limit for an ammonia and hydrogen dual fueled engine should be a rescaled version of the map for ammonia and hydrocarbons, and the rescaling factor should be somewhere around one half.

28% H_2/72% NH_3 by volume.   18% H_2/82% NH_3 by volume.

Figure A.2. Open flames fueled by ammonia with hydrogen.

132

A.4 Possibilities for an Ammonia and Hydrogen Dual Fueled Engine

The ammonia and hydrogen dual fueled engine offers the promise of operation independent of hydrocarbon fuels. Near-stoichiometric operation can be used right at startup, as opposed to running rich, because the engine does not receive any liquid fuels. The use of ammonia with hydrogen also enables tunable flammability to suit each operating point, including startup and stoichiometric operation at very high loads. The hydrogen could be stored separately from the ammonia, or it could be obtained by decomposing some of the ammonia on a catalyst heated by the engine exhaust.

When ammonia is 23-56% decomposed into hydrogen and nitrogen, it has an ignition energy, flame stability and quenching length that are similar to those of hydrocarbons [Verkamp et al., 1967]. The flame stability is characterized by flow velocity at which the flame blows out. Table A.1 summarizes the percent decomposition for which a property of partially decomposed ammonia matches that of a hydrocarbon at 1 bar, room temperature, and stoichiometric air/fuel ratio. The results in Table A.1 are interpolated from Verkamp's graphs.

Percent Decomposition	Matching Property	Hydrocarbon
23%	Ignition Energy	Propane
56%	Flame Stability	Methane
34%	Quenching Length	Propane

Table A.1. Properties of partially decomposed ammonia.

Both an engine and an open flame burner can be made to work well using ammonia and hydrocarbons. The engine works best when the fuel flammability lies somewhere between that of hydrocarbons and that of ammonia. If ammonia of a fixed degree of decomposition could replace gasoline in the rough limit experiments and yield the same result, then the rough limit combustion promoter map for the hydrogen and ammonia fueled engine should be a rescaled version of the map for the gasoline and ammonia fueled engine. For example, if the rescaling factor turned out to be 0.5, then any operating point that required 30% gasoline, 70% ammonia on a LHV energy basis should

require that 30%x0.5 = 15% of the total ammonia flow be decomposed into hydrogen and nitrogen at the rough limit when an ammonia cracker is used. A decomposition rate of 50% would be required at idle. A specific hydrogen input of approximately 300 Joules per liter is expected at the rough limit ammonia cut-in point when hydrogen is used as a combustion promoter.

A detailed evaluation of the rescaling factor, using $COV(IMEP_n)$ to find the rough limit for an ammonia and hydrogen fueled engine, remains to be carried out. According to Verkamp's results, the rescaling factor is somewhere between 0.23 and 0.56, depending on which fuel property is most important. This result agrees with the rescaling factor of one half obtained from the ammonia/hydrocarbon and ammonia/hydrogen open flame experiments.

REFERENCES

ASTM, 1956 *ASTM Manual for Rating Motor Fuels by Motor and Research Methods.* American Society for Testing Materials, Philadelphia.

Bro, K. and Pedersen, P. S., 1977 "Alternative Diesel Engine Fuels: an Experimental Investigation of Methanol, Ethanol, Methane, and Ammonia in a DI Diesel Engine with Pilot Injection," SAE Paper 770794.

Camp, J. and Rachel, T., 1975 "Closed Loop Electronic Fuel and Air Control of Internal Combustion Engines," SAE Paper 750369.

Caris, D. F. and Nelson, E. E., 1959 "A New Look At High Compression Ratio Engines," *SAE Transactions*, Vol. 67, pp. 112-124.

Cooper, J.R., Crookes, R.J., Mozafari, A., and Rose, J.W., 1991 "Ammonia as a Fuel for the IC Engine," *Proc. International Conference on Environmental Pollution*, Lisbon.

Cornelius, W., Huelmantel, W.L., and Mitchell, H.R., 1965 "Ammonia as an Engine Fuel," SAE Paper 650052.

Dale, J.D. and Oppenheim, A.K., 1981 "Enhanced Ignition for I.C. Engines with Premixed Gases," SAE Paper 810146.

Graves, R.L., Hodgeson, J.W., and Tennant, J.S., 1974 "Ammonia as a Hydrogen Carrier and its Application in a Vehicle". *Hydrogen Economy Miami Conference*, pp 755-764.

Graves, R.L. and Hodgeson, J.W., 1975 "Emissions from an Ammonia Fueled Spark Ignition Engine," *American Society of Mechanical Engineers*. 75-WA/DGP-2.

Gray, Jr. J.T., Dimitroff, E., Meckel, N.T., and Quillian, Jr. R.D., 1966 "Ammonia Fuel-Engine Compatibility and Combustion", SAE Paper 660156.

Hodgeson, J.W., 1973 "Is Ammonia a Transportation Fuel for the Future?" *American Society of Mechanical Engineers*. 73-ICT-65.

Hu, X. and Lawless, P.B., 2001 "Predictions of On-Engine Efficiency for the Radial Turbine of a Pulse Turbocharged Engine," SAE Technical Paper 2001-01-1238.

Kattwinkel, Thomas, Weiss, Robert, and Boeschlin, Jean-Philippe., 2003 "Mechatronic Solution for Electronic Turbocharger," SAE Technical Paper 2003-01-0712.

Kroch, E., 1945 "Ammonia, A Fuel for Motor Buses," *J. Petroleum Institute* Vol 31, pp. 213-223.

Kroch, E. and Restieau, J.L., Mar. 14, 1945 French Patent FR897181.

Liu, Rui, Ting, David S.-K., and Checkel, M. David, 2003 "Ammonia as a fuel for SI Engine" SAE Paper 2003-01-3095.

Luthra, S.P., Mathur, H.B., Narasimhan, T.N., and Natarajan, B., 1971 "Experimental Investigation into the Suitability of Ammonia as a Spark Ignition Engine Fuel," *Journal of the Institution of Engineers* (India) Vol. 51 Mechanical Engineering 6 pp.235-241.

Mozafari, A.V., 1988 *Prediction and Measurement of Spark Ignition Engine Characteristics using Ammonia and other Fuels*. Ph.D. Thesis, U. of London.

Pearsall, T.J. and Garabedian, C.G., 1967 "Combustion of Anhydrous Ammonia in Diesel Engines," SAE Paper 670947.

Sawyer, R.F., Starkman, E.S., Muzio, L., and Schmidt, W.L., 1968 "Oxides of Nitrogen in the Combustion Products of an Ammonia Fueled Reciprocating Engine". SAE Paper 680401.

Shand, R., Thomas, W., Reese, G. and Kristiansen, C., May 10, 1985 *Experimental Development of and Ammonia Fueled Engine* (Final Report) prepared for: National Research Council of Canada. Winnipeg, Manitoba.

Shores, R. C., Walker, J. T. Jr., Jones, L. G., Rodgers, M. O., Pearson, J. R., and McCulloch, R. B., 2001 "Ammonia Emissions from the EPA's Light Duty Test Vehicle" SAE Paper 2001-01-3538

Smith, D.S. and Starkman, E.S., February 1966 "Performance of Anhydrous Ammonia as a Spark Ignition Engine Fuel," Technical Report #6. University of California Dept. of Mechanical Engineering Thermal Systems Division. Reproduced by: The Clearinghouse for Federal Scientific and Technical Information. Springfield, Va. 22151.

Starkman, E.S., Newhall, H.K., Sutton, R., Maguire, T., and Farbar, L., 1966 "Ammonia as a Spark Ignition Engine Fuel: Theory and Application," SAE Paper 660155.

Starkman, E.S. and Samuelsen, G.S., 1967 "Flame Propagation Rates in Ammonia-Air Combustion at High Pressure," *Eleventh Symposium on Combustion*. pp. 1037-1045.

US EPA, 24 May, 2006 "Non-CO2 Gases Economic Analysis and Inventory: Global Warming Potentials and Atmospheric Lifetimes".

Verkamp, F.J., Hardin, M.C., and Williams, J.R., 1967 "Ammonia Combustion Properties and Performance in Gas Turbine Engines," *Eleventh Symposium on Combustion*. pp. 985-992.

Zavka, M. and Massagno, L., Dec. 13, 1938 U.S. Patent 2,140,254.